

**OPTIMIZATION OF ENERGY DETECTION IN  
COGNITIVE RADIO NETWORKS**

BY

**ALI ABDULLAH AL-SAIHATI**

A Thesis Presented to the  
DEANSHIP OF GRADUATE STUDIES

**KING FAHD UNIVERSITY OF PETROLEUM & MINERALS**

DHAHRAN, SAUDI ARABIA

In Partial Fulfillment of the  
Requirements for the Degree of

**MASTER OF SCIENCE**

In

**ELECTRICAL ENGINEERING**

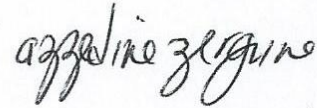
**MAY 2014**

KING FAHD UNIVERSITY OF PETROLEUM & MINERALS

DHAHRAN- 31261, SAUDI ARABIA

**DEANSHIP OF GRADUATE STUDIES**

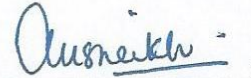
This thesis, written by **Ali Abdullah Al-Saihati** under the direction his thesis advisor and approved by his thesis committee, has been presented and accepted by the Dean of Graduate Studies, in partial fulfillment of the requirements for the degree of **MASTER OF SCIENCE IN ELECTRICAL ENGINEERING**.



Dr. Azzedine Zerguine  
(Advisor)



Dr. Ali Al-Shaikhi  
Department Chairman



Dr. Asrar U. H. Sheikh  
(Co-Advisor)



Dr. Salam A. Zummo  
Dean of Graduate Studies



Dr. Wessam Mesbah  
(Member)

Date

29/5/14



Dr. Abdelmalek Zidouri  
(Member)



Dr. Wajih Abu-Al-Saud  
(Member)

©Ali Abdullah Al-Saihati

2014

To my mother, father, brothers and sisters with love

## **ACKNOWLEDGMENTS**

I would like to thank KFUPM for giving me the opportunity to obtain the master degree and their support in the research work.

I would like to thank my thesis advisors Dr. Azzedine Zerguine and Dr. Asrar U. H. Sheikh for their hard work to achieve this thesis.

I would like to thank my thesis committee members for their encouragement and insightful comments to improve the quality of the thesis.

I would like to thank my friend Raza Umer for his support in my research work.

I would like to thank everyone who supported me in my research work.

# TABLE OF CONTENTS

<b>ACKNOWLEDGMENTS</b> .....	<b>V</b>
<b>TABLE OF CONTENTS</b> .....	<b>VI</b>
<b>LIST OF TABLES</b> .....	<b>X</b>
<b>LIST OF FIGURES</b> .....	<b>XI</b>
<b>LIST OF ABBREVIATIONS</b> .....	<b>XV</b>
<b>ABSTRACT</b> .....	<b>XVII</b>
<b>CHAPTER 1 INTRODUCTION</b> .....	<b>1</b>
<b>1.1 Cognitive Radio</b> .....	<b>1</b>
<b>1.2 Thesis Objectives</b> .....	<b>3</b>
<b>1.3 Contribution</b> .....	<b>4</b>
<b>1.4 Thesis Outline</b> .....	<b>4</b>
<b>CHAPTER 2 LITERATURE REVIEW</b> .....	<b>5</b>
<b>2.1 Spectrum Sensing Methods</b> .....	<b>5</b>
<b>2.1.1 Energy Detection</b> .....	<b>6</b>
<b>2.1.2 Filter Bank Power Spectrum</b> .....	<b>10</b>
<b>2.1.3 Multitaper Spectrum Estimation</b> .....	<b>11</b>
<b>2.1.4 Wavelet Based Spread Spectrum</b> .....	<b>12</b>
<b>2.1.5 Compressed Sensing</b> .....	<b>13</b>
<b>2.2 Signal Model</b> .....	<b>13</b>
<b>2.2.1 Rayleigh</b> .....	<b>16</b>
<b>2.2.2 Nakagami</b> .....	<b>16</b>

2.2.3	Lognormal .....	17
2.2.4	Nakagami – Lognormal .....	17
2.2.5	Nakagami – Gamma .....	19
2.3	Simulation Results for Single Secondary User .....	22
2.3.1	AWGN and Rayleigh Fading Channels .....	23
2.3.2	Nakagami Fading Channels.....	26
2.3.3	Lognormal Shadowing Channel .....	28
2.3.4	Gamma Fading Channel.....	30
2.3.5	Nakagami – Lognormal Composite Fading Channel .....	32
2.3.6	Nakagami – Gamma Composite Fading Channel.....	34
2.4	Methods for Improving Pd .....	36
2.4.1	Cooperative Spectrum Sensing.....	36
2.4.2	Spatial Correlation .....	39
2.4.3	Heuristic Algorithms.....	39
2.5	Simulation Results for Cooperative Secondary Users .....	40
2.5.1	AWGN Channel.....	41
2.5.2	Rayleigh Fading Channel.....	42
2.5.3	Nakagami Fading Channel .....	43
2.5.4	Lognormal Shadowing Channel .....	45
2.5.5	Gamma Fading Channel.....	46
2.5.6	Nakagami – Lognormal Composite Fading Channel .....	49
2.5.7	Nakagami – Gamma Composite Fading Channel.....	50
<b>CHAPTER 3 PARTICLE SWARM OPTIMIZATION .....</b>		<b>53</b>
3.1	Introduction .....	53
3.2	PSO for CR networks .....	56

3.3	Simulation Results for PSO .....	62
3.3.1	AWGN and Rayleigh Fading Channels .....	63
3.3.2	Nakagami Fading Channel .....	64
3.3.3	Lognormal Shadowing Channel .....	65
3.3.4	Gamma Fading Channel.....	66
3.3.5	Nakagami – Lognormal Composite Fading Channel .....	67
3.3.6	Nakagami – Gamma Composite Fading Channel .....	68
<b>CHAPTER 4 PARTICLE SWARM OPTIMIZATION-HILL CLIMBING HYBRID .....</b>		<b>69</b>
4.1	Introduction .....	69
4.2	PSO-HC for CR networks.....	71
4.3	Simulation Results for PSO-HC Fixed SNR.....	75
4.3.1	AWGN Channel.....	76
4.3.2	Rayleigh Fading Channel.....	77
4.3.3	Nakagami Fading Channel .....	78
4.3.4	Lognormal Shadowing Channel .....	80
4.3.5	Gamma Fading Channel.....	81
4.3.6	Nakagami – Lognormal Composite Fading Channel .....	82
4.3.7	Nakagami – Gamma Composite Fading Channel.....	83
4.4	Simulation Results for PSO-HC Fixed Pf .....	85
4.4.1	AWGN Channel.....	86
4.4.2	Rayleigh Fading Channel.....	87
4.4.3	Nakagami Fading Channel .....	88
4.4.4	Lognormal Shadowing Channel .....	91
4.4.5	Gamma Fading Channel.....	92
4.4.6	Nakagami – Lognormal Composite Fading Channel .....	94



4.4.7 Nakagami – Gamma Composite Fading Channel.....	95
4.5 Simulation Results for PSO-HC Fixed SNR.....	97
<b>CHAPTER 5 CONCLUSION.....</b>	<b>99</b>
5.1 Conclusion .....	99
5.2 Future Work .....	100
<b>REFERENCES.....</b>	<b>101</b>

## LIST OF TABLES

Table 2.1: Relationship values between $\sigma_{dB}$ and $m_0$ .....	20
Table 4.1: performance analysis of detection probability summary for four cooperating SUs using OR, AND and Majority rules .....	97
Table 4.2: performance analysis of detection probability summary for four cooperating SUs using OR, AND and Majority rules .....	97
Table 4.3: performance analysis of detection probability summary for three cooperating SUs using PSO.....	97
Table 4.4: performance analysis of detection probability summary for three cooperating SUs using PSO-HC hybrid.....	98

## LIST OF FIGURES

Figure 1.1: Spectrum usage Across time and frequency.....	3
Figure 2.1: Several sensing method in accordance to their sensing accuracy and complexity.....	6
Figure 2.2: Energy detector block diagram.....	8
Figure 2.3: Energy detector using FFT.....	8
Figure 2.4: Filter bank power spectrum estimation .....	11
Figure 2.5: Complementary ROC curves for ED under AWGN and Rayleigh channels with SNRs= 5, 10 dB .....	23
Figure 2.6: Probability of detection vs. SNR curves for ED under AWGN channel with false alarm probabilities of [0.01, 0.1, 0.2].....	24
Figure 2.7: Probability of detection vs. SNR curves for ED under Rayleigh channel with false alarm probabilities of [0.01, 0.1, 0.2].....	25
Figure 2.8: Complementary ROC curves for ED under Nakagami channel with $m=2$ and $m=3$ .....	26
Figure 2.9: Probability of detection vs. SNR curves for ED under Nakagami channel with $m=2, 3, 4$ and false alarm probabilities of [0.01, 0.1, 0.2].....	27
Figure 2.10: Complementary ROC curves for ED under Lognormal channel with $\sigma dB=2$ dB.....	28
Figure 2.11: Probability of detection vs. SNR curves for ED under Lognormal channel with $\sigma dB=2$ dB and false alarm probabilities of [0.01, 0.1, 0.2].....	29
Figure 2.12: Complementary ROC curves for ED under Gamma channel with $\sigma dB=2$ dB.....	30
Figure 2.13: Probability of detection vs. SNR curves for ED under Gamma channel with $\sigma dB=2, 6, 12$ dB and false alarm probabilities of [0.01, 0.1, 0.2].....	31
Figure 2.14: Complementary ROC curves for ED under Nakagami-Lognormal composite fading channel with $m=2$ and $\sigma dB=2$ dB.....	32
Figure 2.15: Probability of detection vs. SNR curves for ED under Nakagami-Lognormal composite fading channel with $m=2$ , $\sigma dB=2$ dB and false alarm probabilities of [0.01, 0.1, 0.2].....	33
Figure 2.16: Complementary ROC curves for ED under Nakagami-Gamma composite fading channel with $m=2$ and $\sigma dB=2, 6, 12$ dB .....	34
Figure 2.17: Probability of detection vs. SNR curves for ED under Nakagami-Gamma composite fading channel with $m=2$ , $\sigma dB=2, 6, 12$ dB and false alarm probabilities of [0.01, 0.1, 0.2].....	35
Figure 2.18: Cooperative spectrum sensing in shadowed environment .....	37
Figure 2.19: Complementary ROC curves for ED under AWGN channel with four cooperating users using AND, OR and Majority techniques.....	41
Figure 2.20: Complementary ROC curves for ED under Rayleigh channel with four cooperating users using AND, OR and Majority techniques.....	42

Figure 2.21: Complementary ROC curves for ED under Nakagami channel with $m=2$ and four cooperating users using AND, OR and Majority techniques .....	43
Figure 2.22: Complementary ROC curves for ED under Nakagami channel with $m=3$ and four cooperating users using AND, OR and Majority techniques .....	44
Figure 2.23: Complementary ROC curves for ED under Lognormal channel with $\sigma dB=2$ dB and four cooperating users using AND, OR and Majority techniques.....	45
Figure 2.24: Complementary ROC curves for ED under Gamma channel with $\sigma dB=2$ dB and four cooperating users using AND, OR and Majority techniques.....	46
Figure 2.25: Complementary ROC curves for ED under Gamma channel with $\sigma dB=6$ dB and four cooperating users using AND, OR and Majority techniques.....	47
Figure 2.26: Complementary ROC curves for ED under Gamma channel with $\sigma dB=12$ dB and four cooperating users using AND, OR and Majority techniques.....	48
Figure 2.27: Complementary ROC curves for ED under Nakagami-Lognormal channel with $m=2$ , $\sigma dB=2$ dB and four cooperating users using AND, OR and Majority techniques .....	49
Figure 2.28: Complementary ROC curve for ED under Nakagami-Gamma channel with $m=2$ , $\sigma dB=2$ dB and four cooperating users using AND, OR and Majority techniques.	50
Figure 2.29: Complementary ROC curves for ED under Nakagami-Gamma channel with $m=2$ , $\sigma dB=6$ dB and four cooperating users using AND, OR and Majority techniques .....	51
Figure 2.30: Complementary ROC curves for ED under Nakagami-Gamma channel with $m=2$ , $\sigma dB=12$ dB and four cooperating users using AND, OR and Majority techniques .....	52
Figure 3.1: Cooperative spectrum sensing using PSO.....	57
Figure 3.2: Flowchart of the PSO algorithm.....	61
Figure 3.3: ROC curves for ED under AWGN and Rayleigh channels with three cooperating SUs.....	63
Figure 3.4: ROC curves for ED under Nakagami channel with three cooperating SUs and $m=2$ .....	64
Figure 3.5: ROC curves for ED under Lognormal channel with three cooperating SUs and $\sigma dB=2$ dB .....	65
Figure 3.6: ROC curves for ED under Gamma channel with three cooperating SUs and $\sigma dB=2$ dB .....	66
Figure 3.7: ROC curves for ED under Nakagami-Lognormal channel with three cooperating SUs, $\sigma dB=2$ dB and $m=2$ .....	67
Figure 3.8: ROC curves for ED under Gamma-Lognormal channel with three cooperating SUs, $\sigma dB=6$ dB and $m=2$ .....	68
Figure 4.1: Hill climbing model.....	71
Figure 4.2: Flowchart of PSO-HC hybrid.....	74

Figure 4.3: ROC curves for ED under AWGN channel with three cooperating SUs using PSO and PSO-HC.....	76
Figure 4.4: ROC curves for ED under Rayleigh channel with three cooperating SUs using PSO and PSO-HC.....	77
Figure 4.5: ROC curves for ED under Nakagami channel with three cooperating SUs and $m=2$ using PSO and PSO-HC.....	78
Figure 4.6: ROC curves for ED under Nakagami channel with three cooperating SUs and $m=3$ using PSO and PSO-HC.....	79
Figure 4.7: ROC curves for ED under Lognormal channel with three cooperating SUs and $\sigma dB= 2$ dB using PSO and PSO-HC .....	80
Figure 4.8: ROC curves for ED under Gamma channel with three cooperating SUs and $\sigma dB= 6$ dB using PSO and PSO-HC .....	81
Figure 4.9: ROC curves for ED under Nakagami-Lognormal channel with three cooperating SUs, $m= 2$ and $\sigma dB= 2$ dB using PSO and PSO-HC.....	82
Figure 4.10: ROC curves for ED under Nakagami-Gamma channel with three cooperating SUs, $m= 2$ and $\sigma dB= 2$ dB using PSO and PSO-HC.....	83
Figure 4.11: ROC curves for ED under Nakagami-Gamma channel with three cooperating SUs, $m= 2$ and $\sigma dB= 6$ dB using PSO and PSO-HC.....	84
Figure 4.12: Probability of detection vs. SNR curves for ED under AWGN channel with three cooperating SUs and false alarm probability of 0.1 using PSO and PSO-HC.....	86
Figure 4.13: Probability of detection vs. SNR curves for ED under Rayleigh channel with three cooperating SUs and false alarm probability of 0.1 using PSO and PSO-HC.	87
Figure 4.14: Probability of detection vs. SNR curves for ED under Nakagami channel with three cooperating SUs, $m= 2$ and false alarm probability of 0.1 using PSO and PSO-HC .....	88
Figure 4.15: Probability of detection vs. SNR curves for ED under Nakagami channel with three cooperating SUs, $m= 3$ and false alarm probability of 0.1 using PSO and PSO-HC .....	89
Figure 4.16: Probability of detection vs. SNR curves for ED under Nakagami channel with three cooperating SUs, $m= 4$ and false alarm probability of 0.1 using PSO and PSO-HC .....	90
Figure 4.17: Probability of detection vs. SNR curves for ED under Lognormal channel with three cooperating SUs, $\sigma dB= 2$ dB and false alarm probability of 0.1 using PSO and PSO-HC .....	91
Figure 4.18: Probability of detection vs. SNR curves for ED under Gamma channel with three cooperating SUs, $\sigma dB= 2$ dB and false alarm probability of 0.1 using PSO and PSO-HC .....	92
Figure 4.19: Probability of detection vs. SNR curves for ED under Gamma channel with three cooperating SUs, $\sigma dB= 6$ dB and false alarm probability of 0.1 using PSO and PSO-HC .....	93

Figure 4.20: Probability of detection vs. SNR curves for ED under Nakagami-Lognormal channel with three cooperating SUs,  $m=2$ ,  $\sigma dB= 2$  dB and false alarm probability of 0.1 using PSO and PSO-HC..... 94

Figure 4.21: Probability of detection vs. SNR curves for ED under Nakagami-Gamma channel with three cooperating SUs,  $m=2$ ,  $\sigma dB= 2$  dB and false alarm probability of 0.1 using PSO and PSO-HC..... 95

Figure 4.22: Probability of detection vs. SNR curves for ED under Nakagami-Gamma channel with three cooperating SUs,  $m=2$ ,  $\sigma dB= 6$  dB and false alarm probability of 0.1 using PSO and PSO-HC..... 96

## LIST OF ABBREVIATIONS

<b>CR</b>	:	Cognitive Radio
<b>ED</b>	:	Energy Detection
<b>PU</b>	:	Primary User
<b>SU</b>	:	Secondary User
<b>FCC</b>	:	Federal Communications Commission
<b>SPTF</b>	:	Spectrum Policy Task Force
<b>IEEE</b>	:	Institute of Electrical and Electronics Engineers
<b>WRAN</b>	:	Wireless Regional Area Network.
<b>VHF</b>	:	Very High Frequency
<b>UHF</b>	:	Ultra High Frequency
<b>SNR</b>	:	Signal to Noise Ratio
<b>IID</b>	:	Independent and Identically Distributed
<b>BPF</b>	:	Band Pass Filter
<b>PSD</b>	:	Power Spectral Density
<b>FFT</b>	:	Fast Fourier Transform

<b>SDR</b>	:	Spectral Dynamic Range
<b>TS-CSS</b>	:	Two Step Compressed Spectrum Sensing
<b>AWGN</b>	:	Additive White Gaussian Noise
<b>ROC</b>	:	Receiver Operating Characteristics
<b>PDF</b>	:	Probability Density Function
<b>WLAN</b>	:	Wireless Local area Network
<b>EGC</b>	:	Equal Gain Combining
<b>MRC</b>	:	Maximum Ratio Combining
<b>LO</b>	:	Logical OR
<b>LA</b>	:	Logical AND
<b>PSO</b>	:	Particle Swarm Optimization
<b>PSO-HC</b>	:	Particle Swarm Optimization-Hill Climbing



## **ABSTRACT**

Full Name : Ali Abdullah Al-Saihati  
Thesis Title : Optimization of Energy Detection in Cognitive Radio Networks  
Major Field : Electrical Engineering  
Date of Degree : May 2014

The emergence of wireless services demands an efficient use of the radio spectrum due to its scarcity. This problem can be addressed by using Cognitive radio (CR) technology that uses the spectrum in an opportunistic manner. Spectral reuse is one application of cognitive radio that permits secondary users/networks to use the licensed spectrum of the primary users when they are not active. Different types of spectrum sensing methods will be explained. The signal model for CR networks under AWGN channel as well as CR networks experiencing Rayleigh, Nakagami, Lognormal, Gamma, Nakagami-Lognormal composite and Nakagami-Gamma composite fading will be discussed. The achievable average probability of detection is presented for different types of channels. Simulation results will be presented for the detection performance of CR networks under different channels for a single SU. After that, suggested methods for improving the detection performance such as cooperative spectrum sensing, spatial correlation and heuristic methods will be investigated. The detection performance of cooperating secondary users (SU) will be shown through simulation results for different fading channels. Particle Swarm Optimization (PSO) is a heuristic technique which achieves optimum value by mimicking the natural behavior of individual knowledge of communicating group of a swarm flock. PSO is implemented to maximize an objective function for a given problem

with set of parameters by exploring its search space. The implementation of PSO in CR networks is discussed. Simulation results of detection performance using PSO technique are produced among different fading channels. The new proposed method, PSO-HC hybrid is explained how it is implemented in CR networks. Results obtained from using PSO-HC hybrid method under different fading channels are compared to the conventional PSO method. While the PSO-HC hybrid performance shows little improvements in non-fading/ low fading channels, it gives good performance in deep fading channels compared to the conventional PSO method.

## ملخص الرسالة

الاسم الكامل: علي عبدالله السيهاتي

عنوان الرسالة: تعظيم كشف الطاقة في شبكات الراديو المعرفي

التخصص: الهندسة الكهربائية

تاريخ الدرجة العلمية: مايو 2014

ظهور الخدمات اللاسلكية يتطلب الاستخدام الفعال للطيف الراديوي بسبب ندرتها . ويمكن معالجة هذه المشكلة عن طريق استخدامات تكنولوجيا الإذاعة المعرفية ( CR ) التي تستخدم الطيف بطريقة انتهازية . إعادة استخدام الطيفية هو أحد تطبيقات من الراديو المعرفية التي تسمح للمستخدمين الثانويين / شبكات لاستخدام الطيف المرخص من المستخدمين الأوليين عندما تكون غير نشطة. وسيتم شرح أنواع مختلفة من أساليب الاستشعار عن الطيف. وسوف تناقش نموذج الإشارة لشبكات CR تحت قناة AWGN وكذلك شبكات CR التي تعاني تلاشي من نوع رايلي ، ناكاجامي ، اللوغاريتمي الطبيعي ، غاما ، مركب ناكاجامي - اللوغاريتمي الطبيعي و مركب ناكاجامي - غاما. وسوف يعرض متوسط احتمال الكشف عن الإشارة بأنواع مختلفة من القنوات. وستعرض نتائج المحاكاة لأداء الكشف عن شبكات CR تحت قنوات مختلفة لمستخدم واحد من SU. بعد ذلك، اقترح سيتم التحقيق من أساليب لتحسين أداء الكشف مثل التعاونية لاستشعار الطيف ، والارتباط المكاني وطرق الكشف عن مجريات الأمور . سيتم عرض أداء الكشف عن تعاون المستخدمين الثانويين ( SU ) من خلال نتائج المحاكاة لقنوات مختلفة. سرب الجسيمات الأمثل ( PSO ) هو أسلوب ارشادي الذي يحقق القيمة المثلى عن طريق محاكاة السلوك الطبيعي للمعرفة الفردية من مجموعة من قطع سرب التواصل. ويتم تنفيذ PSO لتعظيم دالة الهدف لمشكلة معينة مع مجموعة من المعلومات من خلال استكشاف فضاء البحث. وسيتم مناقشة تنفيذ PSO في شبكات CR . ويتم إنتاج نتائج المحاكاة لأداء الكشف باستخدام تقنية PSO بين القنوات المختلفة. ستوضح الطريقة الجديدة المقترحة هجين PSO-HC كيفية تنفيذها في شبكات CR . ستتم مقارنة النتائج التي تم الحصول عليها من هجين PSO-HC تحت قنوات مختلفة

بطريقة PSO التقليدية. في حين يظهر هجين PSO-HC تحسينات صغيرة في قنوات الغير متلاشية / قنوات المنخفضة التلاشي، وأنه يعطي أداء جيد في قنوات عميقة التلاشي بالمقارنة مع الطريقة التقليدية PSO .

# CHAPTER 1

## INTRODUCTION

### 1.1 Cognitive Radio

Nowadays, the demand for radio spectrum has increased significantly which is a result of the increase of consumers' interest in wireless services. Also, the emergence of new applications and mobile internet access requires a huge amount of spectrum usage. The spectrum is a limited resource that is regulated by government agencies like the Federal Communications Commission (FCC) in the US. Frequency bands are licensed exclusively to users to operate their communications. Today, it is hard to find vacant bands since they are mostly occupied. Recent measurements conducted by Spectrum Policy Task Force (SPTF) within FCC show the spectrum usage from 0 to 6 GHz bands varies between 15% and 85%. This led the FCC to propose the opening of licensed bands to unlicensed users. This posts a new challenge to find new ways to utilize the spectrum efficiently. Cognitive Radio (CR) can be used to effectively increase the spectrum usage [1, 2, 3, 4, 5, 6,7].

CR is a new technology that uses the spectrum in an opportunistic manner. Spectral reuse is one application of cognitive radio that permits secondary users (SUs)/networks to use

the licensed spectrum of the primary users (PUs) when they are not active. This is done by performing frequent channel sensing by SUs to detect the presence of PUs. SUs can use the spectrum for communication while primary users are not using the spectrum. However, detecting the presence of PUs must be accurate since SUs need to vacate the channel within certain time duration. This will permit PUs to utilize the spectrum when they become active. The spectrum usage for different frequencies along time can be seen in Figure 1.1. IEEE 802.22 wireless regional area network WRAN communication system implements spectrum reuse concept. It operates in the VHF/UHF bands which are used for TV broadcasting services and wireless microphone [4,9].

In practice, channel sensing is challenging matter because of some aspects. The SNR of the PUs might be very low. Also, it is difficult to sense the wireless channel because of the presence of multipath fading and time dispersion. The signal power could fluctuate by 30 dB resulted from multipath fading. Also, when the time dispersion of the channel is unknown, the coherent detection may not be reliable [4].

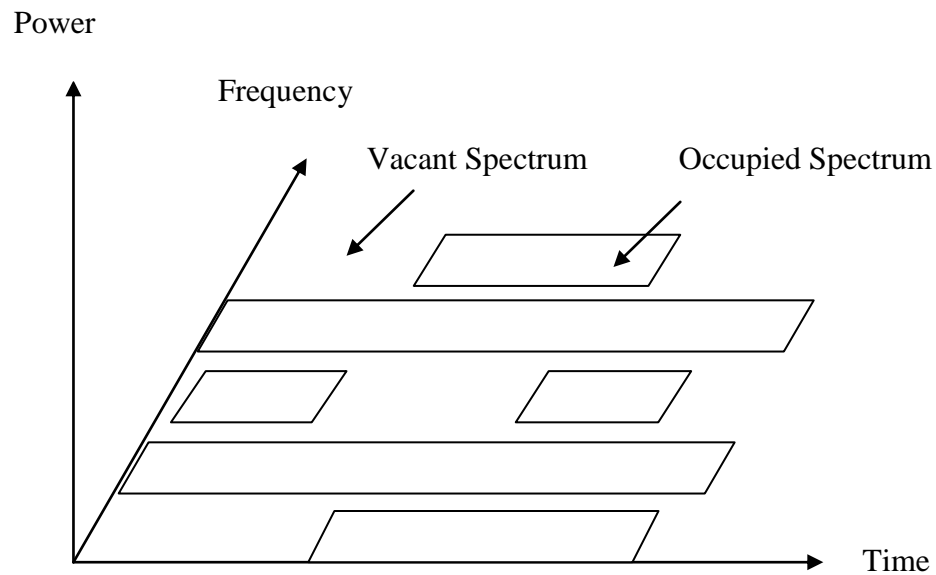


Figure 1.1: Spectrum usage Across time and frequency

## 1.2 Thesis Objectives

The thesis objectives are:

- Survey spectrum sensing techniques for cognitive radio.
- Study spectrum sensing in different radio environments.
- Evaluate the impact of channel fading and shadowing in cognitive radio network (Rayleigh, Nakagami, Lognormal, Gamma, Nakagami-Lognormal composite, Nakagami-Gamma composite).
- Look at methods of improving probability of detection and lowering probability of miss (Diversity, Correlation techniques, Heuristic algorithms).
- Implement Particle Swarm Optimization and Particle Swarm Optimization- Hill Climbing Hybrid to improve probability of detection.

### **1.3 Contribution**

The main contribution of the thesis is implementing PSO-HC hybrid technique to improve the detection performance of the CR network. PSO-HC hybrid method will be applied to seven different types of channels: AWGN, Rayleigh, Nakagami, Lognormal, Gamma, Nakagami-Lognormal composite and Nakagami-Gamma composite.

### **1.4 Thesis Outline**

The thesis is organized as follows. Chapter 2 discusses different types of spectrum sensing methods. The signal model for CR networks under AWGN channel as well as CR networks experiencing Rayleigh, Nakagami, Lognormal, Gamma, Nakagami-Lognormal composite and Nakagami-Gamma composite fading will be explained. Simulation results will be presented for the detection performance of CR networks under different channels for a single SU. After that, suggested methods for improving the detection performance such as cooperative spectrum sensing, spatial correlation and heuristic methods will be investigated. The detection performance of cooperating SU will be shown through simulation results for different fading channels. Chapter 3 talks about PSO and gives an introduction of this technique. Then, the implementation of PSO in CR networks is discussed. Simulation results of detection performance using PSO technique are produced among different fading channels. Chapter 4 discusses the new proposed method, PSO-HC hybrid and how it is implemented in CR networks. Results obtained from using PSO-HC hybrid method under different fading channels are discussed and compared to the conventional PSO method. Finally, Chapter 5 summarizes the thesis and the obtained new results.



## **CHAPTER 2**

### **LITERATURE REVIEW**

#### **2.1 Spectrum Sensing Methods**

There are different methods for channel or spectrum sensing. Energy detection (ED), cyclostationary detection, matched filtering detection and waveform based detection are some types of sensing methods which are used to identify the signal transmission method. Some methods can obtain the characteristics of the detected signal. The choice of a sensing method depends on the required computational complexity, sensing duration, network requirements and accuracy required to achieve. Several sensing methods are shown in terms of accuracy and complexity in Figure 2.1 [4,10].

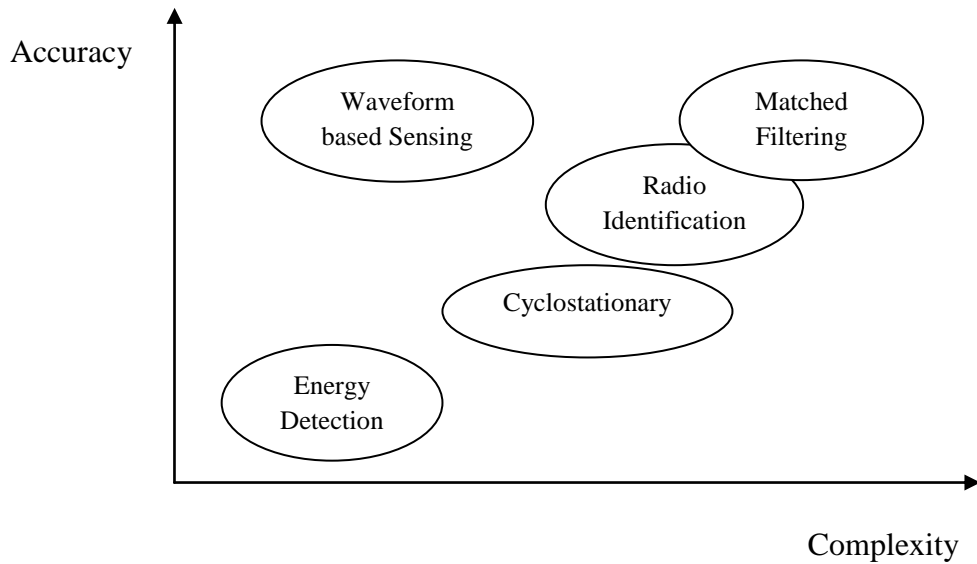


Figure 2.1: Several sensing method in accordance to their sensing accuracy and complexity

### 2.1.1 Energy Detection

In ED (known also as radiometry), a priori information of the source signal is not needed [10, 3]. It performs well in unknown dispersed channels and fading environments. ED has a good accuracy with low complexity implementation. As the averaging time increases, the SNR is improved which, in turn, decreases the noise power. In order to achieve certain detection probability, on the other hand, the required number of samples is of  $O(1/\text{SNR}^2)$  so it suffers from long detection time [5,12, 24]. This is because the detection is non-coherent. Although ED is simple to implement, it has many disadvantages. Unknown or changing noise level has a great impact on the threshold used for primary user signal detection. Moreover, it is difficult to set a threshold in frequency

selective fading environment. Another issue of the ED is that it can't cancel the interference using adaptive signal processing due to the inability to distinguish among modulated signals, noise and interference. So, it is up to CR users to take into account the other SUs as well as noise [3,12]. ED is not optimal for detecting correlated signals although it is optimal for independent and identically distributed (i.i.d.) signals.

The block diagram of ED is shown in Figure 2.2. Let the output of the integrator be  $Y$  which is given by:

$$Y = \frac{1}{T} \int_{t-T}^t |x(\tau)|^2 d\tau \quad (2.1)$$

and has the following distribution:

$$Y \sim \begin{cases} \chi_{2TW}^2, & H_0 \\ \chi_{2TW}^2(2\gamma), & H_1 \end{cases} \quad (2.2)$$

where  $\chi_{2TW}^2$  and  $\chi_{2TW}^2(2\gamma)$  represent the central and non-central chi-square distributions respectively,  $H_0$  is a signal hypothesis which represents the non existence of the primary signal and  $H_1$  is a signal hypothesis which represents the existence of the primary signal . They both have  $2TW$  degrees of freedom. For the non-central chi-square distribution, the distribution is not central by  $2\gamma$  where  $\gamma$  is the instantaneous SNR.  $TW$  is the time-bandwidth product (or time delay bandwidth product) and is assumed to be integer for simplicity. It will be denoted by  $m$ . The signal is passed through a band pass filter (BPF). Then it is passed to a squaring device until it is averaged over a period  $T$ . For the narrowband signals and sinewaves signals, the implementation of this method becomes inflexible. Another implementation of ED method can be done in frequency

domain where the spectrum is estimated by using fast Fourier Transform (FFT). This method is known as periodogram. Figure 2.3 shows implementation of ED using FFT. Multiple signals can be sensed simultaneously since the power spectral density (PSD) can be found to realize group of sub-bands [13, 14].

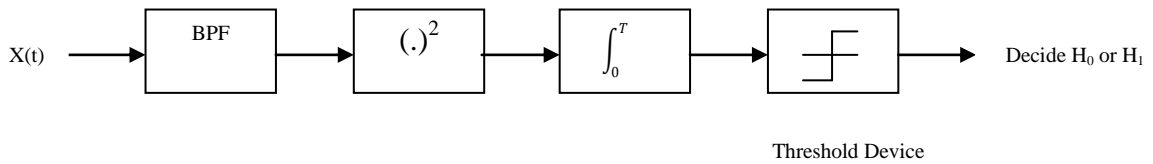


**Figure 2.2: Energy detector block diagram**

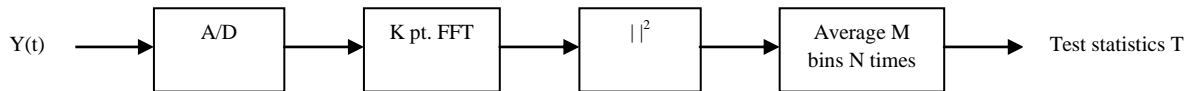


**Figure 2-3: Energy detector using FFT**

ED performs well in wideband spread spectrum. The signal detection can be improved in two ways: either increasing the FFT frequency resolution by increasing the number of points  $K$  or increasing the number of averages  $N$ . If  $K$  increases, the sensing time increases while if the number of averages increases, the signal energy estimation improves [14]. A fixed FFT size is chosen in order to get the required resolution at moderate complexity and low latency in practice. Hence, the number of averages becomes a variable parameter [14]. Practically, the wideband spectrum sensing can be done in two stages: ED with low complexity is used to find vacant or idle sub-bands then next a more complex advanced spectrum sensing technique is used for another usage of

sub-bands [14]. Examples of advanced spectrum sensing techniques are filter banks power spectrum estimation, multitaper spectrum estimator, wavelet based spectrum sensing and spectrum detection based on compressed sampling [14]. Because the transmitted powers may be different for licensed sub-bands and the random noise is present in unoccupied sub-bands, the power spectrum estimator must be accurate. The spectral dynamic range (SDR) which is the ratio of maximum to minimum spectral power is used in power spectrum estimator to determine the accuracy. A higher accuracy is achieved with higher SDR values.

When the SNR of the signal is very low, the signal during detection might be indistinguishable. This is known as noise uncertainty and it severely degrades the performance of the energy detector. The noise comes from the local thermal noise and the environmental noise. The former is generated because of the variations of temperature over time while the latter comes from the aggregate random signals from different sources. Let  $x$  dB,  $\sigma_n^2$  and  $\sigma_e^2$  be the uncertainty noise for estimation, noise power and interference power respectively.  $\sigma_n^2$  varies between  $\sigma_n^2 10^{-(x/10)}$  and  $\sigma_n^2 10^{(x/10)}$ , ( $\sigma_n^2 \in [10^{-(x/10)}\sigma_n^2, 10^{(x/10)}\sigma_n^2]$ ). For the primary signal to be always detected, the received signal power must be greater than the threshold  $\sigma_T^2 = 10^{-(x/10)}\sigma_e^2$  and for the worst case of  $\sigma_e^2 = 10^{(x/10)}\sigma_n^2$ ,  $\sigma_T^2 = 10^{(2x/10)}\sigma_n^2$ . Therefore, the received primary signal power must be greater than  $(\sigma_T^2 - \sigma_n^2)$  for energy detection to succeed in signal detection [13]. This defines the SNR wall which implies that the signal cannot be detected below the minimum value. The SNR wall is given by [15]:

$$\gamma_w = \frac{\sigma_T^2 - \sigma_n^2}{\sigma_n^2} = 10^{\frac{2x}{10}} - 1 \quad (2.3)$$

To illustrate, when the noise variance uncertainty is 0.5 dB the signal cannot be detected at  $-21$  dB using ED.

### 2.1.2 Filter Bank Power Spectrum

In filter bank power spectrum, the whole wide spectrum of interest is divided into  $N$  sub-bands. Each sub-band has a sub-filter which can be expressed as:

$$h_i(n) = h(n)e^{j2\pi f_i n} \quad (2.4)$$

where  $h_i(n)$  indicates the  $i^{\text{th}}$  sub-band filter,  $h(n)$  represents the zeroth sub-band which is a low pass filter of the filter bank also known as prototype filter and  $f_i$  is the normalized center frequency given by  $f_i = i/N$ . The spectral components extraction is done through each sub-band filter. Figure 2.4 shows the filter bank power spectrum estimation. The performance of spectral estimation depends on the selection of the prototype filter. The frequency response should be designed such that the power leakage coming from the side lobes of neighboring sub-bands is minimum. The side lobes also determine the power spectrum estimator SDR. The  $i^{\text{th}}$  sub-band signal energy can be estimated as:

$$\hat{S}(f_i) = \left| \sum_{n=0}^{N-1} y(n)w(n)e^{-j2\pi f_i n} \right|^2$$

$$= \left| \sum_{n=0}^{N-1} w(n) e^{-j2\pi f_i n} y(N-1-n) \right|^2 \quad (2.5)$$

where  $w(n)$  is a symmetric window function which is given by:

$$w(n) = w(N-1-n)$$

The window function  $w(n)$  is actually the prototype filter bank [14]. It is used to suppress side lobes in which cut-off frequencies are tapered [13]. For example, to apply simple FFT energy detection, a rectangular window is applied. Because of the simplicity of the prototype filter, however, the SDR is limited due to the large lobe generated [14]. The performance of the periodogram as spectral estimator can be further improved by implementing several window functions designed to generate less side lobes.

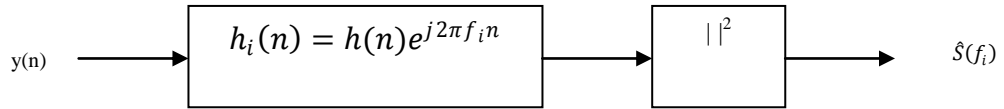


**Figure 2.4: Filter bank power spectrum estimation**

### 2.1.3 Multitaper Spectrum Estimation

When the received signal is processed before the FFT operation, the process is called tapering. Although tapering decreases the leaked power coming from neighboring subbands, there will be a loss in information due to the truncation in time domain window [12,14]. The variance of the power spectrum estimate increases as the information loss increases which, in turn, decreases the accuracy [12,14]. To solve the problem, a

multitaper power spectral estimator is applied where multitapers of prototype of filters are used. Tapers are implemented using Slepian sequences which are a special family of sequences [13]. The leakage power is minimum because the main lobe energy concentration of the Fourier transforms is maximum. Moreover, each sequence is orthogonal to others which results in generating outputs estimate from the tapers which are uncorrelated given the signal variation is negligible for each sub-band in the spectrum. Therefore, a minimum variance is obtained from averaging the estimates. The multitaper spectral estimation has a nearly optimal performance since the Cramer-Rao bound for a nonparametric is almost achieved. However, this can be achieved at high implementation complexities [13].

#### **2.1.4 Wavelet Based Spread Spectrum**

The whole wide spectrum is treated as a consecutive frequency sub-bands in which the adjacent sub-bands have discontinuous power [13]. In wavelet based detection, estimated PSD irregularities with wavelet transformed are analyzed to determine spectral holes. For the wavelet based detection, CR network knows the entire spectrum band except for the number of licensed spectrum bands. Each occupied band PSD is assumed to be smooth and almost flat. Also, the noise PSD is assumed to be flat for the entire bandwidth [13].



### 2.1.5 Compressed Sensing

Sub-Nyquist sampling has been used to find the sparsity of wireless signals in frequency domain. When the primary user occupancy is low, it will have some sparsity. The fundamental limit on the sampling rate can be found using maximum sparsity order. However, high sampling is required in this method which results in wasted sensing resources. The performance can be improved by using a two step compressed spectrum sensing (TS-CSS) scheme. The actual sparsity order is estimated in the first step which can be determined from the number of zero elements of the primary signal vector. After that, the additional number of samples required to reconstruct the wideband spectrum and find spectrum hole is decided by the number of estimated sparsity order that can be done adaptively in the second step. Although this method requires a complex clocking system due to the random sampling, it has a lower average sampling rate with good sensing performance [13].

## 2.2 Signal Model

There are two hypotheses for signal detection:  $H_0$  and  $H_1$ .  $H_0$  indicates signal does not exist while  $H_1$  indicates signal is present. The received signal samples for the given hypotheses are given by [3]:

$$x(t) = \begin{cases} n(t), & H_0 \\ h s(t) + n(t), & H_1 \end{cases} \quad (2.6)$$

where  $x(t)$  is the SU received signal,  $s(t)$  is the primary user transmitted signal,  $n(t)$  is the additive white Gaussian noise (AWGN) and  $h$  is the channel response. Errors can be made in two ways. Either deciding  $H_0$  while  $H_1$  is sent and this is called error of the first kind or false alarm or deciding  $H_1$  while  $H_0$  is sent and this is called error of the second kind or miss. Probability of miss detection equals to  $P_m = 1 - P_d$  where  $P_d$  is the probability of detection [9]. There is a tradeoff between false alarm and miss detection probabilities. Probability of miss detection determines how much interference is caused by SUs. False alarm probability, however, determines how efficiently the spectrum is used by SUs. So, the higher the miss probability, the higher the interference will become. A higher false alarm probability will result in a lot of missed opportunities [4].

$h$  is deterministic in a non fading environment and detection and false alarm probabilities could be computed by [3]:

$$P_d = P\{Y > \lambda | H_1\} = Q_m(\sqrt{2\lambda}, \sqrt{\lambda}) \quad (2.7)$$

$$P_f = P\{Y > \lambda | H_0\} = \frac{\Gamma(m, \lambda/2)}{\Gamma(m)} \quad (2.8)$$

Where  $\lambda$ ,  $m$ ,  $\Gamma(\cdot)$ ,  $\Gamma(\cdot, \cdot)$  and  $Q_m(\cdot, \cdot)$  are the detection threshold, time bandwidth product, complete gamma function, incomplete gamma function and the generalized Marcum Q-function respectively. The upper incomplete gamma function and the generalized Marcum Q-function are given respectively by [2,8]:

$$\Gamma(m, n) = \int_n^\infty t^{m-1} e^{-t} dt \quad (2.9)$$

$$Q_m(a, b) = \int_b^{\infty} \frac{x^m}{a^{m-1}} e^{-\frac{x^2+a^2}{2}} I_{m-1}(ax) dx \quad (2.10)$$

where  $I_{m-1}(\cdot)$  is the modified Bessel function with  $(m-1)^{\text{th}}$  order.

To achieve high probability of detection, false alarm probability should be as low as possible. Neyman-Pearson Criterion will be used in the detection process since it maximizes the detection probability on the constraint that the false alarm probability [10, 16, 17, 25, 31, 37]. The determination of  $P_d$  is tied by the threshold and  $P_f$ . Since it is hard to choose the threshold using detection probability, false alarm probability is used to find the threshold. The advantage of finding the threshold using  $P_f$  is that  $P_f$  does not depend on the SNR [2,9]. In the presence of fading, the detection probability is conditioned on the instantaneous SNR.  $P_d$  can be found by averaging (2.7) over fading statistics which gives:

$$P_d = \int_x Q_m(\sqrt{2\gamma}, \sqrt{\lambda}) f_\gamma(x) dx \quad (2.11)$$

where  $f_\gamma(x)$  is the SNR probability density function (pdf) under fading environment. The receiver performance can be examined as a function of threshold setting. This can be represented using receiver operating characteristic (ROC) where it is a plot of probability of detection against probability of false alarm for different set of thresholds. Moreover, when the miss probability is plotted against false alarm probability, the plot becomes complementary ROC. The plot indicates what is the optimal value of detection probability or miss detection probability that can be achieved for certain false alarm probability at a particular SNR [4,9].

### 2.2.1 Rayleigh

The instantaneous SNR of Rayleigh distribution follows an exponential distribution. After substituting  $f_\gamma(x)$  by exponential distribution in (2.11) and calculating the integration, a closed form solution can be found as:

$$P_d = e^{-\frac{\lambda}{2}} \sum_{k=0}^{m-2} \frac{1}{k!} \left(\frac{\lambda}{2}\right)^k + \left(\frac{1+\bar{\gamma}}{\bar{\gamma}}\right)^{m-1} \left( e^{-\frac{\lambda}{2(1+\bar{\gamma})}} - e^{-\frac{\lambda}{2}} \sum_{k=0}^{m-2} \frac{1}{k!} \left(\frac{\lambda\bar{\gamma}}{2(1+\bar{\gamma})}\right)^k \right) \quad (2.12)$$

where  $\bar{\gamma}$  is the average SNR and  $\lambda$  is the threshold [3, 36].

### 2.2.2 Nakagami

The instantaneous SNR of Nakagami distribution has the following distribution [3, 28]:

$$f_\gamma(\gamma, m) = \frac{m^m \gamma^{m-1}}{\bar{\gamma}^m \Gamma(m)} e^{-\frac{m\gamma}{\bar{\gamma}}}, \gamma \geq 0 \quad (2.13)$$

Where  $m$  is the nakagami fading parameter,  $\gamma$  is the instantaneous SNR and  $\bar{\gamma}$  is the average SNR.  $P_d$  can be calculated after substituting  $f_\gamma(x)$  in (2.11) which gives:

$$\begin{aligned} P_d(\bar{\gamma}, m, M, \lambda) &= \int_0^{+\infty} P_d(M, \lambda, \gamma) f_\gamma(\gamma, m) d\gamma \\ &= \int_0^{+\infty} e^{-\frac{\lambda}{2(1+\gamma)}} \sum_{k=0}^{M/2-1} \frac{1}{k!} \left(\frac{\lambda}{2(1+\gamma)}\right)^k f_\gamma(\gamma, m) d\gamma \\ &= \frac{\lambda}{2(1+\bar{\gamma})} \frac{\lambda m^m e^{\frac{m}{\bar{\gamma}}}}{2\Gamma(m)\bar{\gamma}^m} \sum_{k=0}^{M/2-1} \frac{1}{k!} \int_0^{\frac{\lambda}{2}} \left(\frac{\lambda}{2t} - 1\right)^{m-1} t^{k-2} e^{-\left(t+\frac{m\lambda}{2\bar{\gamma}t}\right)} dt \quad (2.14) \end{aligned}$$

### 2.2.3 Lognormal

The received power variation of the medium scale has a normal distribution if it is presented in dB which has been shown in [11] from empirical measurements. A lognormal random variable can be modeled from the linear channel gain as  $e^X$  where  $X$  is a Gaussian random variable with zero mean and variance  $\sigma^2$ . The dB-spread  $\sigma_{dB}$  is used to represent the Lognormal distribution. The relation between  $\sigma$  and  $\sigma_{dB}$  is given by:  $\sigma = \sigma_{dB}/8.686$ .  $\sigma_{dB}$  indicates the shadowing level or intensity which occurred in the channel. The shadowing intensity is proportional to the dB-spread so the higher the dB-spread, the higher the shadowing intensity. The instantaneous SNR has a lognormal distribution because of the shadowing.  $P_d$  does not have a closed form so it is calculated numerically after substituting  $f_y(x)$  in (2.11) [3, 30].

### 2.2.4 Nakagami – Lognormal

The Nakagami distribution is used to model the fading while Lognormal distribution is used to model the shadowing that occurs in the channel. The Nakagami-Lognormal model is used to model both fading and shadowing occurring simultaneously at the same time. The Nakagami and Lognormal pdfs are given by, respectively:

$$f_x(x) = \frac{2m^m x^{2m-1} e^{-(m/p)x^2}}{\Gamma(m)p^m}, x \geq 0.5 \quad (2.15)$$

$$f_p(p) = \frac{1}{p\sqrt{2\pi\sigma^2}} \exp\left(-\frac{(20 \log p - \mu_{dBm})^2}{2\sigma^2}\right), p > 0 \quad (2.16)$$

where the  $p$  in (2.15) is the mean power of the received signal i.e.  $p = E[x^2]$ ,  $\sigma$  is the shadowing standard deviation and  $\mu_{dBm}$  is the constant area mean power where the local mean power  $p$  fluctuates around it. The value of  $\mu_{dBm}$  can be calculated as:  $\mu_{dBm} = 30 + 10 E[\text{Log}_{10} p]$ . The shadowing disappears as  $\sigma$  approaches zero. When the shadowing is not present, the average power becomes deterministic. On the other hand, the received signal average power becomes random in the presence of shadowing. Therefore, the received envelope becomes conditioned by the average power  $p$  which can be written as:

$$f_{X|P}(x|p) = \frac{2m^m x^{2m-1} e^{-(m/p)x^2}}{\Gamma(m)p^m}, x, p > 0 \quad (2.17)$$

In general, the composite fading and shadowing pdf can be found as:

$$f_X(x) = \int_0^\infty f_{X|P}(x|p) f_p(p) dp \quad (2.18)$$

where  $f_p(p)$  is the shadowing average power pdf. In case we have  $f_{X|P}(x|p)$  a Nakagami distribution and a Lognormal distribution, computing (2.18) will give a Nakagami-Lognormal composite distribution.

However, the Nakagami-Lognormal composite will be approximated to a Nakagami-Gamma distribution because the computation of Nakagami-Lognormal pdf as well as the average probability of detection involves complicated integral form. Neither the Nakagami-Lognormal pdf nor the probability of detection have a closed form expression. A two-parameter gamma distribution will be used to approximate the Lognormal

distribution. Also, it can be used to approximate many pdfs which has been tested using theoretical and empirical measurements[8, 27, 29, 33].

### 2.2.5 Nakagami – Gamma

For small values of  $\sigma_{dB}$ , Lognormal and Gamma pdfs are for data simulation interchangeably. For  $\sigma_{dB} < 6$ , Gamma has a good approximation to Lognormal. The Gamma distribution is given by:

$$f_p(p) = \frac{p^{m_0-1}}{\Gamma(m_0)p_0^{m_0}} \exp\left(-\frac{p}{p_0}\right) \quad (2.19)$$

where  $p_0$  is the average power and  $m_0$  is the Gamma pdf order. The relationships between  $p_0$  and  $m_0$  and Lognormal mean and variance are:

$$m_0 = \frac{1}{(e^{\sigma^2} - 1)} \quad (2.20)$$

$$p_0 = \mu\sqrt{(m_0 + 1)/m_0} \quad (2.21)$$

where  $\sigma$  and  $\mu$  are standard deviation and mean power. Table 2.1 shows  $m_0$  values for different  $\sigma_{dB}$ . The Nakagami-Gamma composite pdf can be computed as [8]:

$$\begin{aligned} f_X(x) &= \int_0^\infty f_{X|P}(x|p)f_p(p)dp \\ &= \frac{2c}{\Gamma(m_0)\Gamma(m)} \left(\frac{cx}{2}\right)^{m_0+m-1} K_{m_0-m}(cx), x > 0 \end{aligned} \quad (2.22)$$

**Table 2.1: Relationship values between  $\sigma_{dB}$  and  $m_0$**

$\sigma_{dB}$	2	4	6	12
$m_0$	18.37	4.23	1.64	0.174

where  $c = 2\sqrt{(m/p_0)}$  and  $K_{m_0-m}(\cdot)$  is the modified Bessel function with  $(m_0 - m)^{\text{th}}$  order. The Nakagami-Gamma composite moments is given by:

$$E_c[X^t] = \frac{\Gamma(m_0 + t/2)\Gamma(m + t/2)}{\Gamma(m_0)\Gamma(m)} \left(\frac{2}{c}\right)^t \quad (2.23)$$

The amount of fading (AF) can be found from the moments:

$$\begin{aligned} A_f &= \frac{\text{variance}[X^2]}{E[X^2]^2} \\ &= \frac{mm_0 + m^2m_0 + mm_0^2}{m^2m_0^2} > 0 \end{aligned} \quad (2.24)$$

Again, to find  $P_d$  we need to use (2.11). In the case of the Nakagami-Gamma composite [34, 35],  $f_\gamma(\gamma)$  experiencing fading and shadowing becomes conditioned on the average SNR. The SNR pdf of the Nakagami distribution can be expressed in terms of Gamma distribution, i.e.:

$$f_{\gamma|\bar{\gamma}}(\gamma) = \frac{m^m \gamma^{m-1}}{\Gamma(m) \bar{\gamma}^m} \exp\left(-\frac{m\gamma}{\bar{\gamma}}\right), \gamma \geq 0, m \geq 0.5 \quad (2.25)$$



The average SNR  $\bar{\gamma}$  equals to  $\bar{\gamma} = E[h^2 E_b/N_0]$ . The two-parameter Gamma distribution is modeled as:

$$f_{\bar{\gamma}_0}(\gamma) = \frac{m_0^{m_0} \gamma^{m_0-1}}{\Gamma(m_0) \bar{\gamma}_0^{m_0}} \exp\left(-\frac{\gamma}{\bar{\gamma}_0}\right) \quad (2.26)$$

where  $\gamma_0$  is the mean power related to average SNR  $\bar{\gamma}$  and  $m_0$  is the Gamma pdf order and it measures the channel shadowing. The instantaneous SNR pdf under fading and shadowing is found as:

$$f_\gamma(\gamma) = \int_0^\infty f(\gamma|\bar{\gamma}) f_P(p) \quad (2.27)$$

Therefore  $f_\gamma(\gamma)$  becomes after using (2.25) and (2.26):

$$f_\gamma(\gamma) = \frac{2}{\Gamma(m)\Gamma(m_0)} \left(\frac{c_0}{2}\right)^{m_0+m} \gamma^{\left(\frac{m_0+m}{2}\right)-1} K_{m_0-m}(c_0\sqrt{\gamma}), \gamma > 0 \quad (2.28)$$

where  $c_0 = \sqrt{mm_0/\bar{\gamma}_0}$  is the scaling parameter which has a relation with average SNR  $\bar{\gamma}$ . Since the computation of  $P_d$  involves integration over Marcum-Q function which is a complex process, another representation of the Marcum-Q function which has a series expansion can be used. It is expressed as:

$$Q_u(\sqrt{2\gamma}, \sqrt{\lambda}) = 1 - e^{\left(-\frac{2\gamma+\lambda}{2}\right)} \sum_{n=u}^{\infty} \left(\frac{\lambda}{2\gamma}\right)^{\frac{n}{2}} I_n(\sqrt{2\lambda\gamma}) \quad (2.29)$$

where  $I_n(\cdot)$  is the nth order modified Bessel function of the first kind.  $P_d$  is obtained after using (2.28) and (2.29) in (2.11) as:

$$P_d = \int_0^\infty \left( 1 - e^{\left(-\frac{2\gamma+\lambda}{2}\right)} \sum_{n=u}^\infty \left(\frac{\lambda}{2\gamma}\right)^{n/2} I_n(\sqrt{2\lambda\gamma}) \right) \times \frac{2}{\Gamma(m_0)\Gamma(m)} \left(\frac{c_0}{2}\right)^{m_0+m} \gamma^{\left(\frac{m_0+m}{2}\right)-1} K_{m_0-m}(c_0\sqrt{\gamma}) d\gamma \quad (2.30)$$

This can be simplified after using  $\int_0^\infty f_\gamma(y) dy = 1$  which becomes:

$$P_d = 1 - \frac{2e^{-\lambda/2}}{\Gamma(m_0)\Gamma(m)} \left(\frac{c_0}{2}\right)^{m_0+m} \sum_{n=u}^\infty \left(\frac{\lambda}{2}\right)^{n/2} \times \int_0^\infty e^{-\gamma} \gamma^{\left(\frac{-n+m_0+m}{2}\right)-1} I_n(\sqrt{2\lambda\gamma}) K_{m_0-m}(c_0\sqrt{\gamma}) d\gamma \quad (2.31)$$

The expression does not have a closed form because of the product  $I_n(\cdot)$ ,  $K_{m_0-m}(\cdot)$  and the exponential, so  $P_d$  can be evaluated numerically [8].

### 2.3 Simulation Results for Single Secondary User

The energy detector performance is simulated for a single SU with various channels including AWGN, Rayleigh, Nakagami, Gamma, Lognormal, Nakagami-Lognormal composite and Nakagami-Gamma composite using complementary ROC and  $P_d$  vs. SNR curves. The time-bandwidth product is taken as  $m = 5$ , hence the number of samples become  $N = 10$ . For complementary ROC curves the fixed SNR is 10 dB. For  $P_d$  vs. SNR curves, false alarm probabilities are taken as 0.01, 0.1 and 0.2. The results are produced using 1000 Monte-Carlo simulations.

### 2.3.1 AWGN and Rayleigh Fading Channels

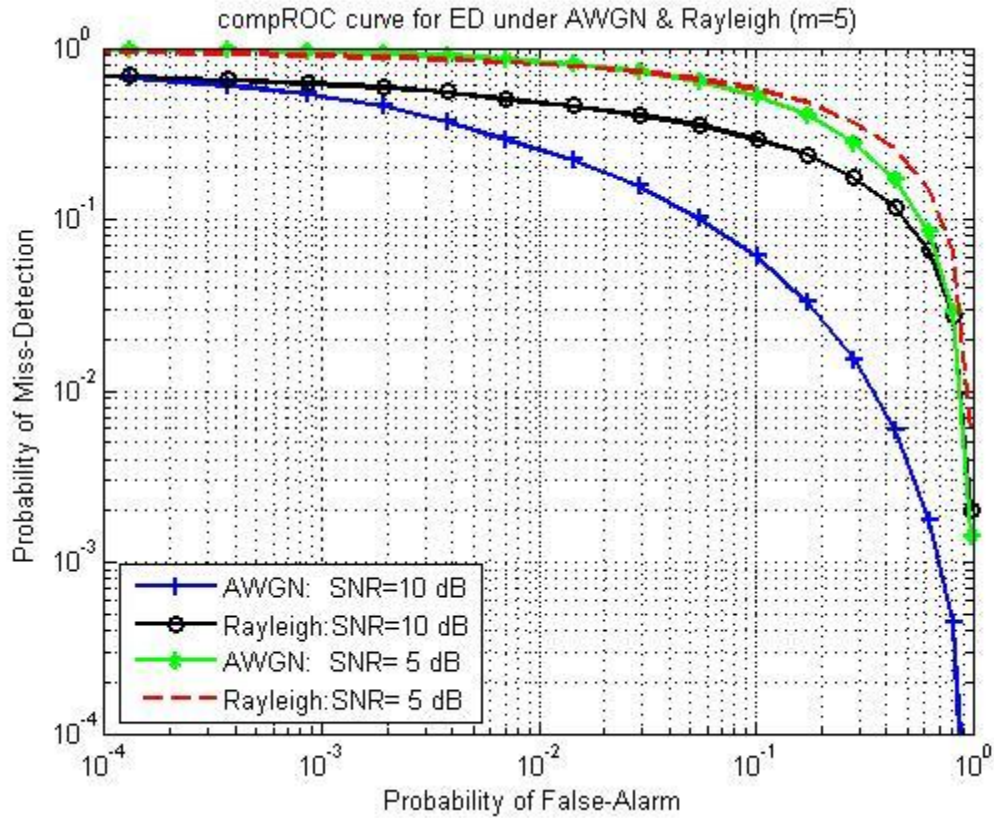


Figure 2-5: Complementary ROC curves for ED under AWGN and Rayleigh channels with SNRs= 5, 10 dB

Figure 2.5 shows the complementary ROC curve of a single SU for ED under AWGN and Rayleigh fading channels with SNR of 10 dB and 5 dB across different probability of false alarm values. The detection performance in AWGN channel is better than the performance when the experiences Rayleigh fading. When the probability of false alarm is 0.1, the probability of miss detection for AWGN channel is 0.06 while in Rayleigh fading channel is 0.30 in the case of SNR =10 dB.

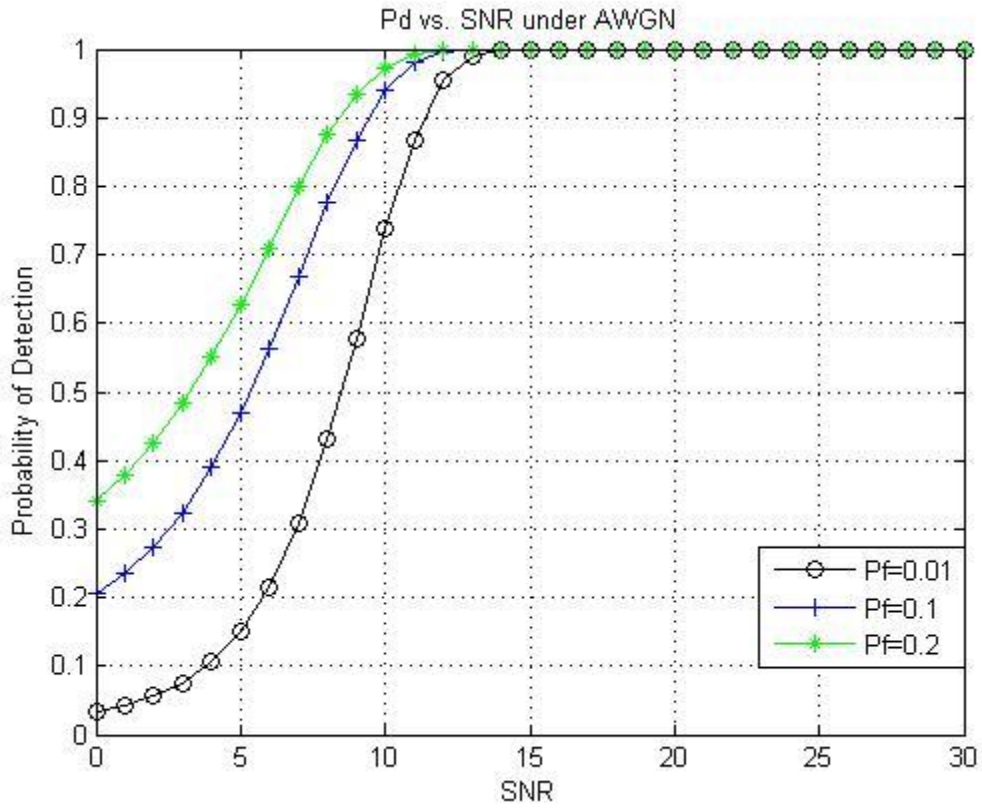
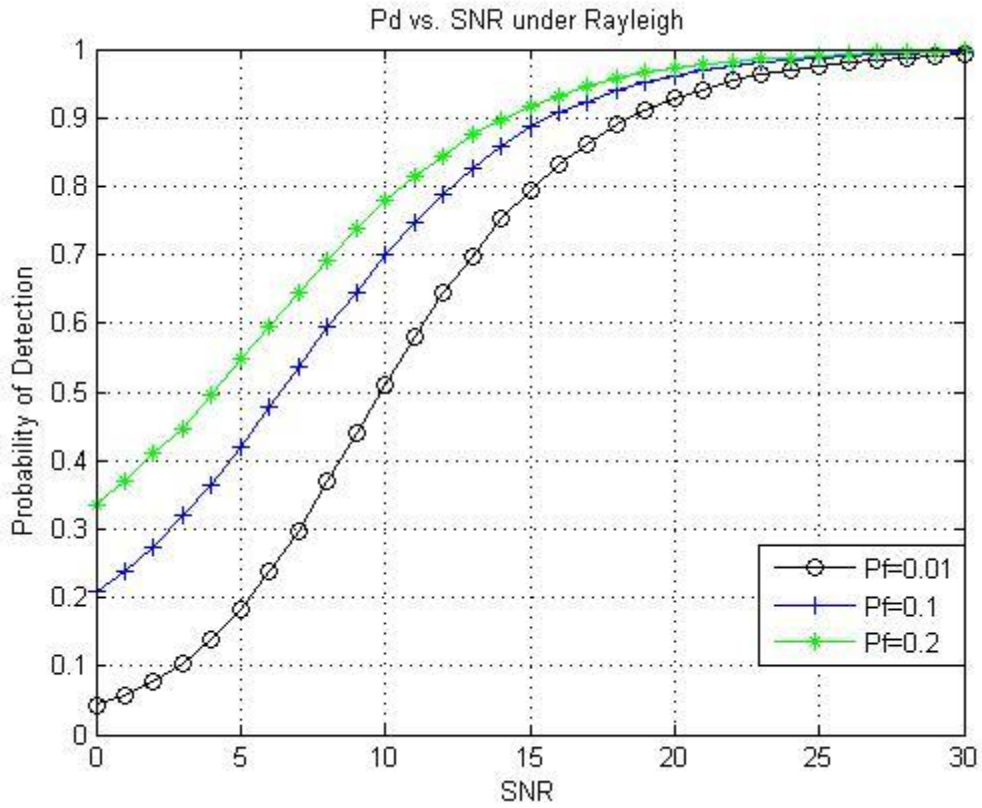


Figure 2-6: Probability of detection vs. SNR curves for ED under AWGN channel with false alarm probabilities of [0.01, 0.1, 0.2]

Figure 2.6 shows the ED performance of a single SU under AWGN channel for different SNR from [0-30] dB. When the SNR is 10 dB, the probabilities of detection with  $P_f = [0.01, 0.1, 0.2]$  are 0.74, 0.95 and 0.98 respectively.



**Figure 2-7: Probability of detection vs. SNR curves for ED under Rayleigh channel with false alarm probabilities of [0.01, 0.1, 0.2]**

Figure 2.7 shows the ED performance of a single SU under Rayleigh fading channel for different SNR from [0-30] dB. When the SNR is 10 dB, the probability of detections with  $P_f = [0.01, 0.1, 0.2]$  are 0.51, 0.70 and 0.78 respectively.

### 2.3.2 Nakagami Fading Channels

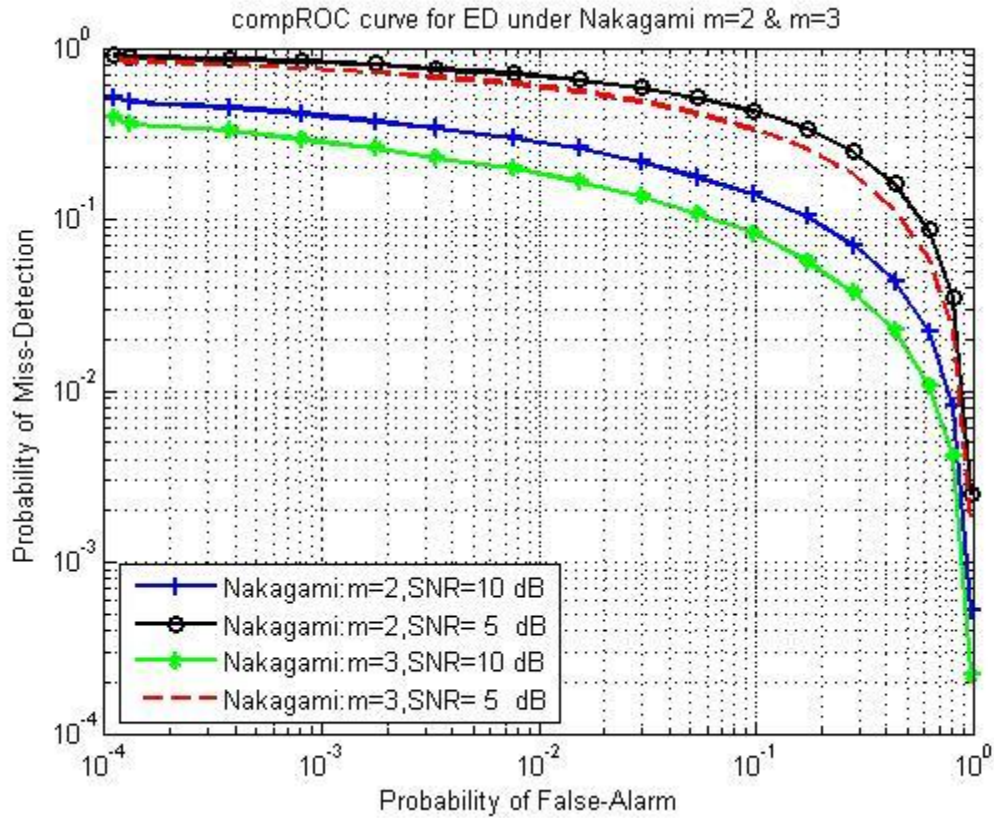
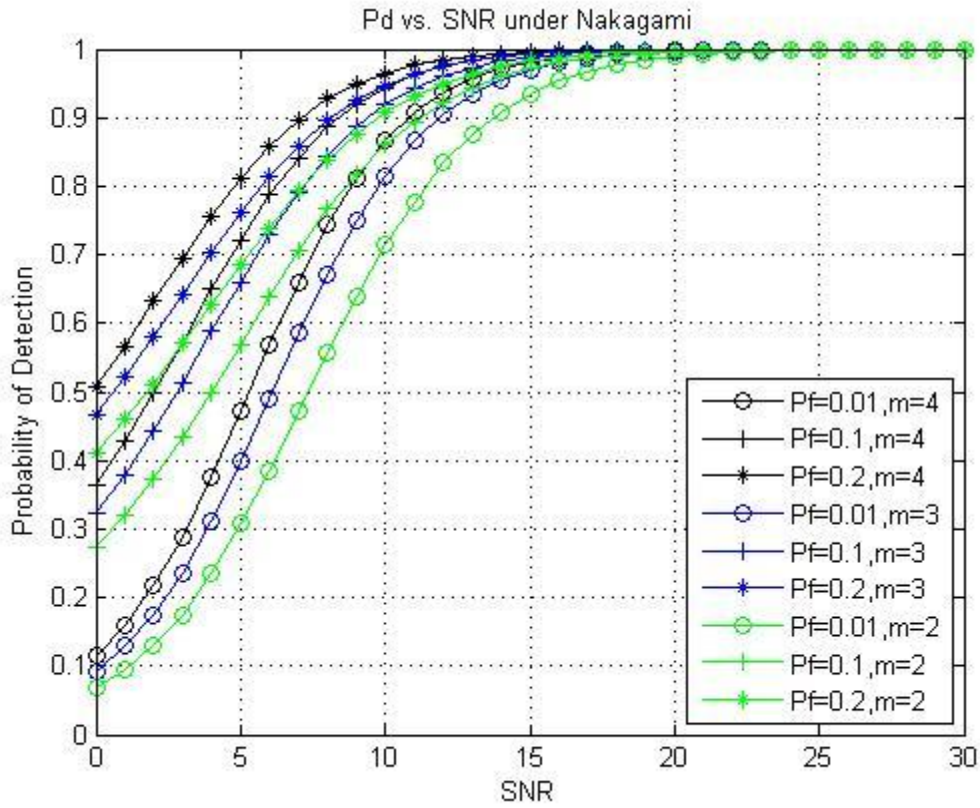


Figure 2-8: Complementary ROC curves for ED under Nakagami channel with  $m = 2$  and  $m = 3$

Figure 2.8 shows the complementary ROC curve of a single SU for ED under Nakagami fading channel with fading parameter  $m = 2$  and  $m = 3$  and SNR of 5 and 10 dB across different probability of false alarm values. For probability of false alarm of 0.1, the achieved miss detection probabilities at SNR= 10 dB are 0.15 and 0.08 for  $m = 2$  and  $m = 3$ , respectively while at SNR= 5 dB it will give 0.45 and 0.30 for  $m = 2$  and  $m = 3$ , respectively.



**Figure 2-9: Probability of detection vs. SNR curves for ED under Nakagami channel with  $m=2, 3, 4$  and false alarm probabilities of  $[0.01, 0.1, 0.2]$**

Figure 2.9 shows the ED performance of a single SU under Nakagami fading channel with  $m = 2, 3$  and  $4$  for different SNR from  $[0-30]$  dB. When the SNR is 10 dB, the probabilities of detection with  $P_f = [0.01, 0.1, 0.2]$  are 0.72, 0.87 and 0.91 respectively in the case of  $m = 2$ .

### 2.3.3 Lognormal Shadowing Channel

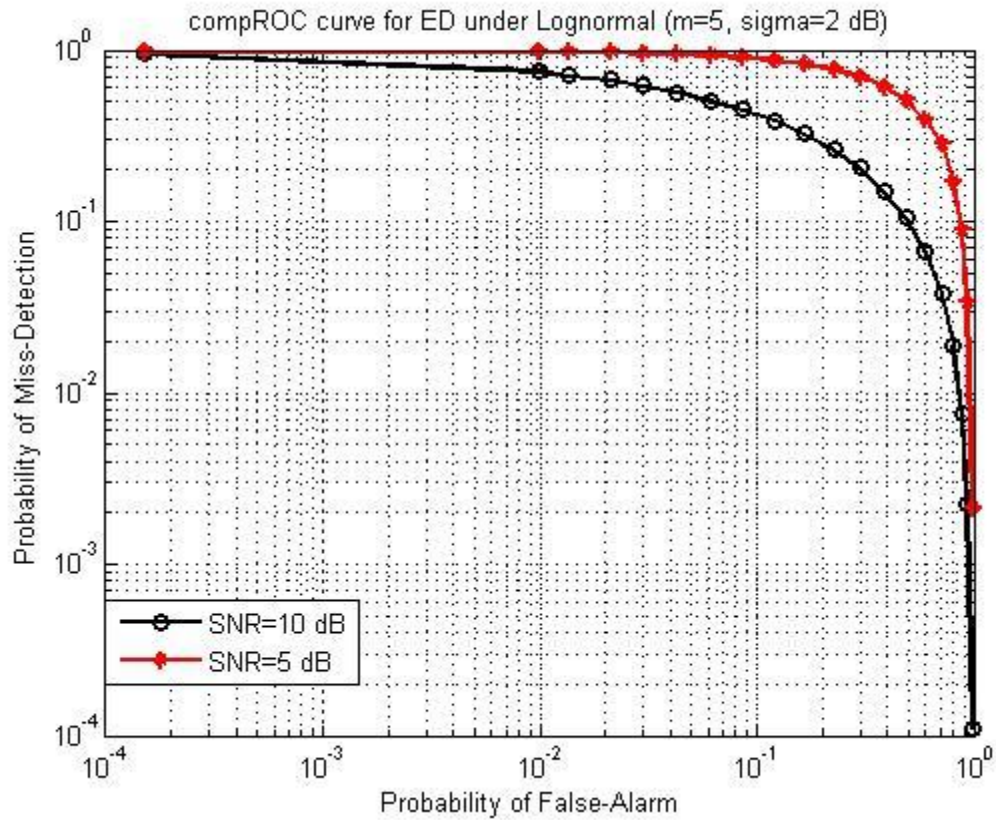


Figure 2-10: Complementary ROC curves for ED under Lognormal channel with  $\sigma_{dB} = 2$  dB

Figure 2.10 shows the complementary ROC curve of a single SU for ED under Lognormal channel with SNR of 5 and 10 dB across different probability of false alarm values. When the probability of false alarm is 0.1, the probabilities of miss detection are 0.90 and 0.40 for SNRs 5 and 10 dB respectively.



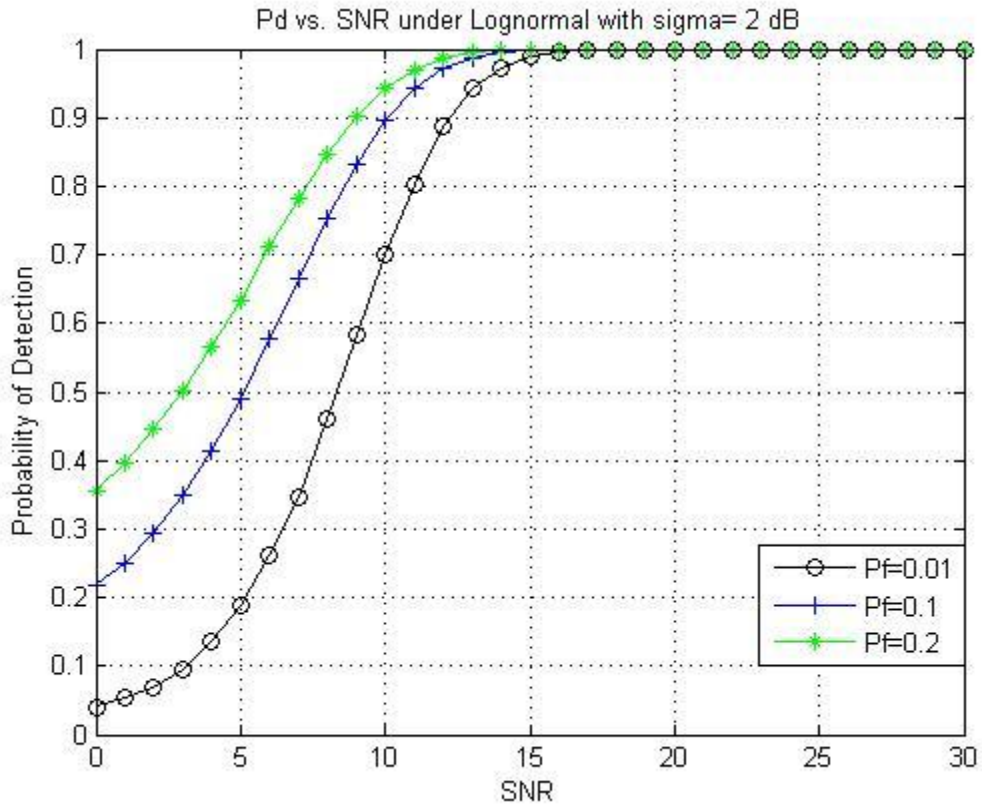


Figure 2-11: Probability of detection vs. SNR curves for ED under Lognormal channel with  $\sigma_{dB}= 2$  dB and false alarm probabilities of [0.01, 0.1, 0.2]

Figure 2.11 shows the ED performance of a single SU under Lognormal channel for different SNR from [0-30] dB. When the SNR is 10 dB, the probabilities of detection with  $P_f = [0.01, 0.1, 0.2]$  are 0.70, 0.90 and 0.94 respectively.

### 2.3.4 Gamma Fading Channel

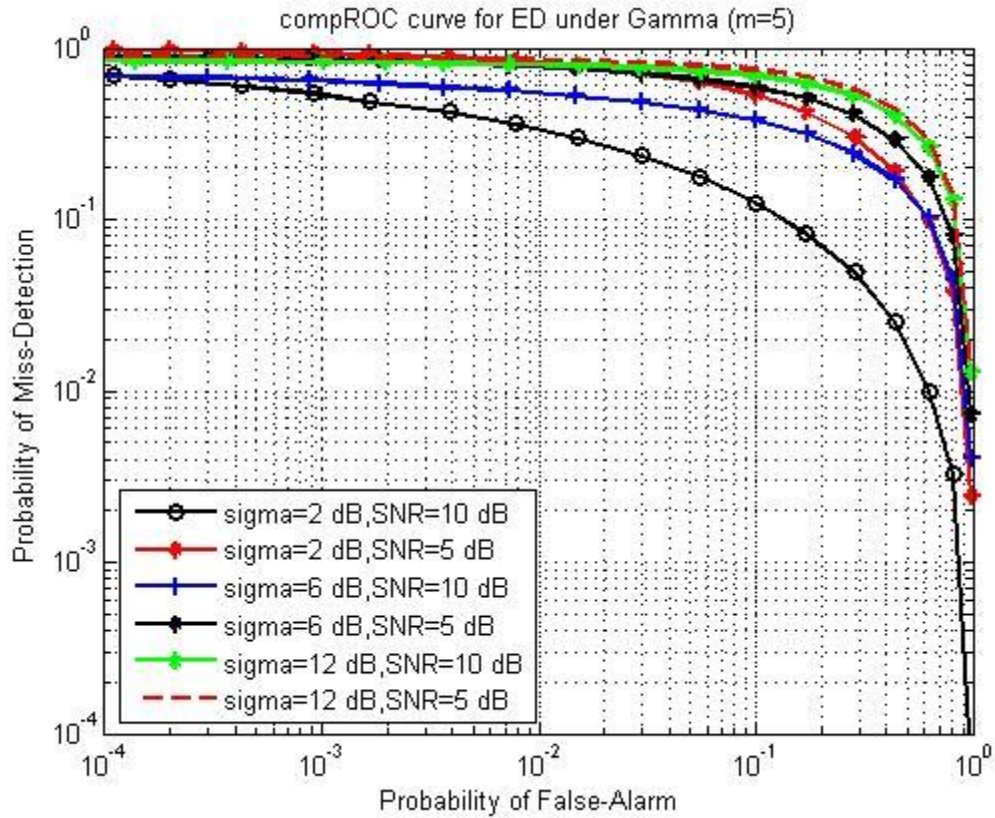


Figure 2-12: Complementary ROC curves for ED under Gamma channel with  $\sigma_{dB} = 2$  dB

Figure 2.12 shows the complementary ROC curve of a single user for ED under Gamma channel with  $\sigma_{dB} = 2, 6$  and  $12$  dB and SNR of  $5$  and  $10$  dB across different probability of false alarm values. When the probability of false alarm is  $0.1$ , the probabilities of miss detection are  $0.60$  and  $0.12$  for  $5$  and  $10$  dB respectively at  $\sigma_{dB} = 2$  dB.

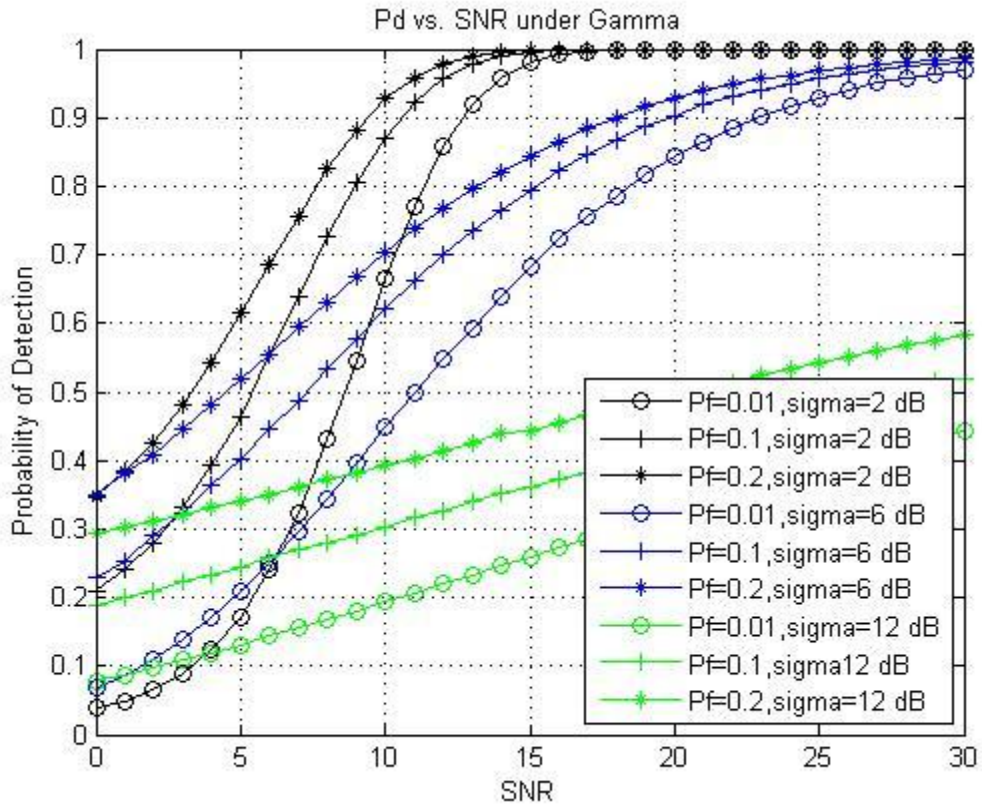


Figure 2-13: Probability of detection vs. SNR curves for ED under Gamma channel with  $\sigma_{dB} = 2, 6, 12$  dB and false alarm probabilities of [0.01, 0.1, 0.2]

Figure 2.13 shows the ED performance of a single SU under Gamma channel with  $\sigma_{dB} = 2$  dB for different SNR from [0-30] dB. When the SNR is 10 dB, the probabilities of detection with  $P_f = [0.01, 0.1, 0.2]$  are 0.66, 0.88 and 0.93 respectively.

### 2.3.5 Nakagami – Lognormal Composite Fading Channel

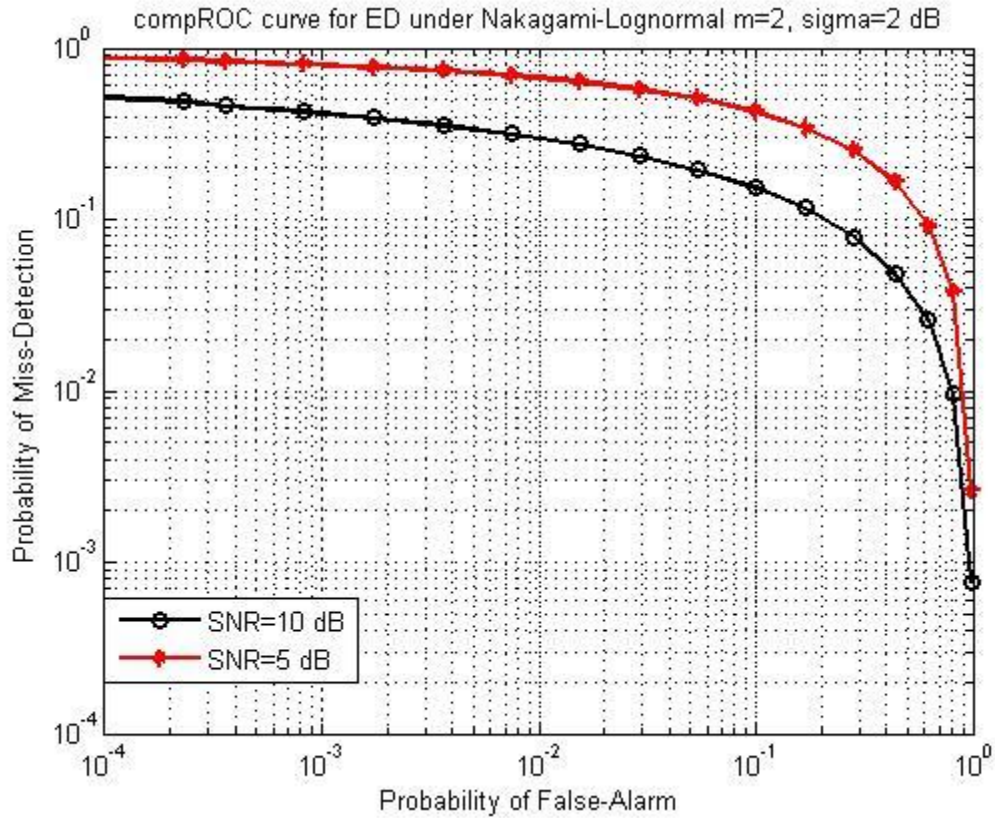
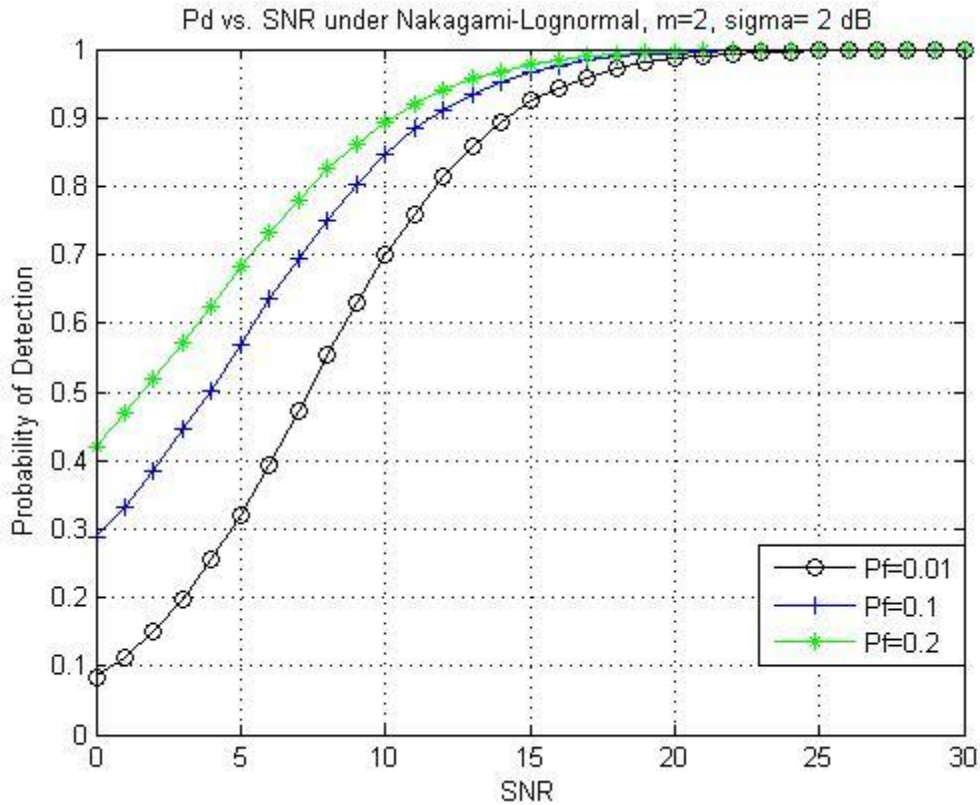


Figure 2-14: Complementary ROC curves for ED under Nakagami-Lognormal composite fading channel with  $m=2$  and  $\sigma_{dB}=2$  dB

Figure 2.14 shows the complementary ROC curve of a single SU for ED under Nakagami-Lognormal channel with  $\sigma_{dB} = 2$  dB,  $m = 2$  and SNR of 5 and 10 dB across different probability of false alarm values. When the probability of false alarm is 0.01, the probabilities of miss detection are 0.65 and 0.30 for 5 and 10 dB respectively.



**Figure 2-15: Probability of detection vs. SNR curves for ED under Nakagami-Lognormal composite fading channel with  $m= 2$ ,  $\sigma_{dB}= 2$  dB and false alarm probabilities of [0.01, 0.1, 0.2]**

Figure 2.15 shows the ED performance of a single user under Nakagami-Lognormal channel with  $\sigma_{dB} = 2$  dB and  $m = 2$  for different SNR from [0-30] dB. When the SNR is 10 dB, the probabilities of detection with  $P_f = [0.01, 0.1, 0.2]$  are 0.70, 0.85 and 0.89 respectively. This indicates that higher false alarm probability results in higher detection probability.

### 2.3.6 Nakagami – Gamma Composite Fading Channel

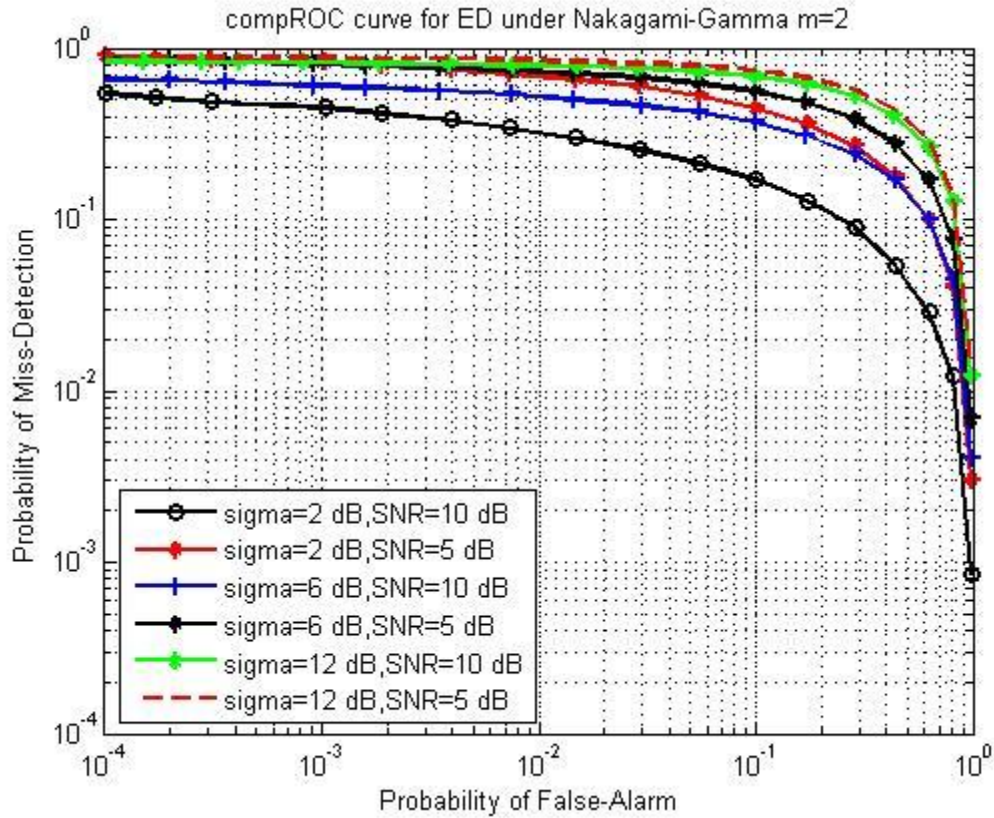
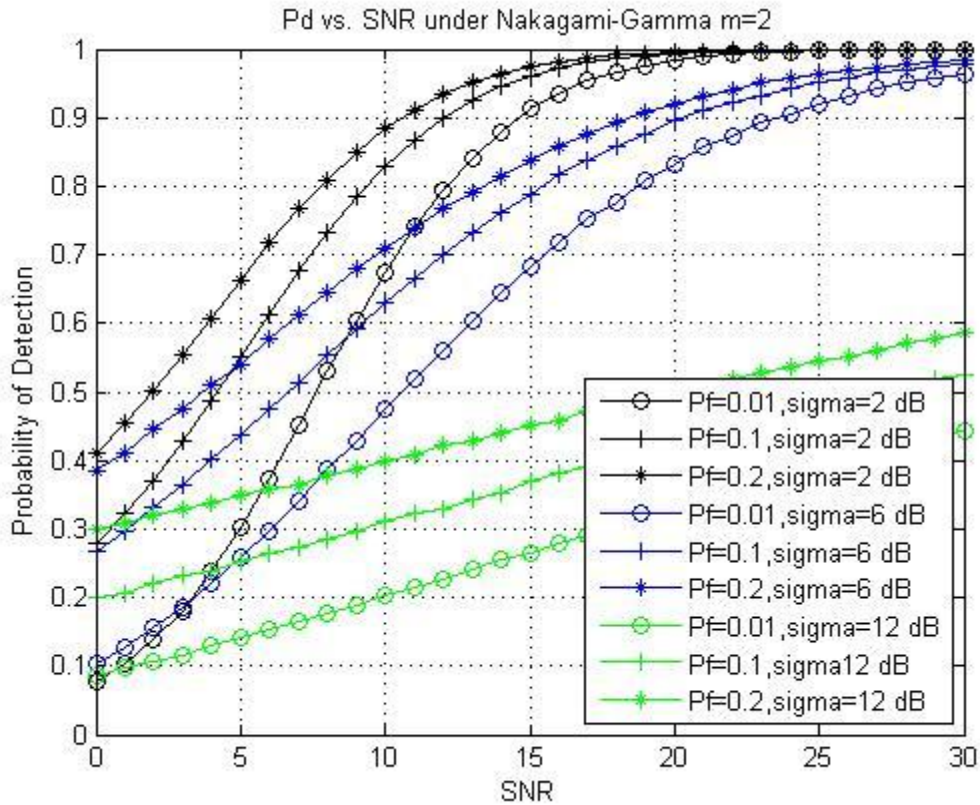


Figure 2-16: Complementary ROC curves for ED under Nakagami-Gamma composite fading channel with  $m=2$  and  $\sigma_{dB} = 2, 6, 12$  dB

Figure 2.16 shows the complementary ROC curve of a single SU for ED under Nakagami-Gamma channel with  $\sigma_{dB} = 2$  dB,  $m = 2$  and SNR of 5 and 10 dB across different probability of false alarm values. When the probability of false alarm is 0.01 and  $\sigma_{dB} = 2$  dB, the probabilities of miss detection are 0.70 and 0.30 for 5 and 10 dB respectively.



**Figure 2-17: Probability of detection vs. SNR curves for ED under Nakagami-Gamma composite fading channel with  $m=2$ ,  $\sigma_{dB}=2, 6, 12$  dB and false alarm probabilities of [0.01, 0.1, 0.2]**

Figure 2.17 shows the ED performance of a single SU under Nakagami-Gamma channel with  $\sigma_{dB} = 2$  dB and  $m = 2$  for different SNR from [0-30] dB. When the SNR is 10 dB, the probabilities of detection with  $P_f = [0.01, 0.1, 0.2]$  are 0.67, 0.82 and 0.88 respectively.

## **2.4 Methods for Improving Pd**

The performance of spectrum sensing is hindered by the multipath fading and shadowing which degrades the detection performance. The performance of spectrum sensing can be improved by increasing the diversity such as increasing the number of users or using spatial correlation of the received signals.

### **2.4.1 Cooperative Spectrum Sensing**

Reliable sensing can be achieved if multiple users setting in different locations cooperate in finding the primary signal [15]. Cooperative spectrum sensing enhances the detection performance. A CR network is shown in Figure 2.18 where three SUs sense the spectrum to look for spectrum holes. The primary signal is not detected by users one and three because the signal is obscured by a building and tree which is known as shadowing. Only user two detects the presence of primary user so cooperative sensing improves the detection performance in a sense that users with undetected signals do not use the spectrum and cause interference with primary user.



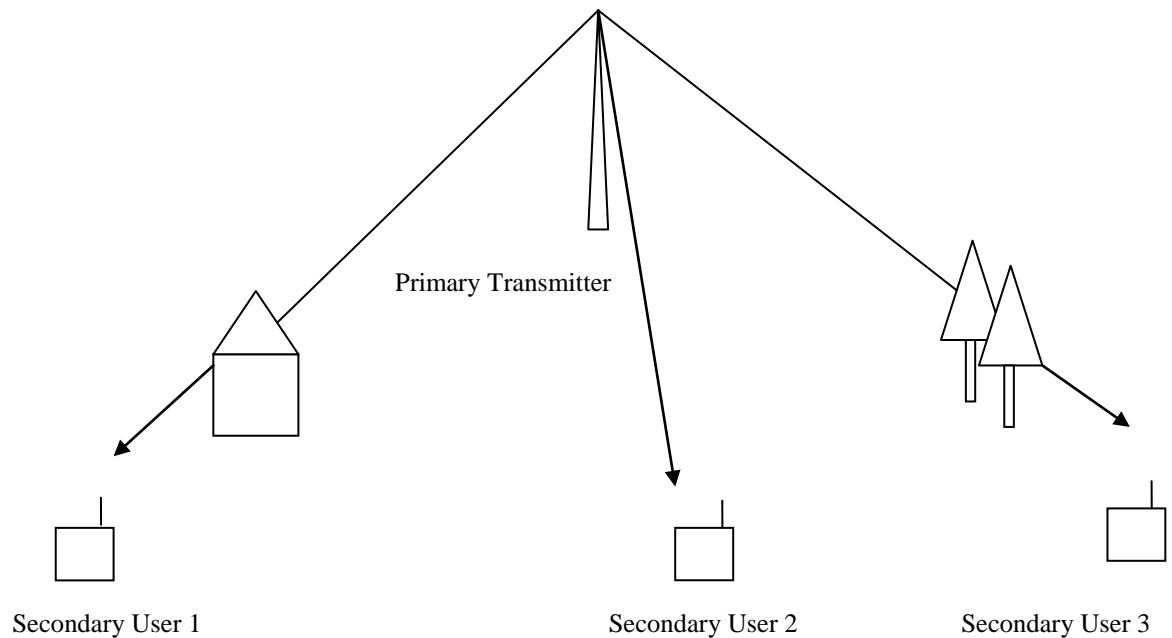


**Figure 2-18: Cooperative spectrum sensing in shadowed environment**

There are two ways to process the sensed data: either by observing data or processing data for all users together and send data for decision fusion or by processing data independently for each user to make decisions independently and send their decision for a final decision. The former is called data fusion while the latter is called decision fusion [15]. Also cooperative network can be centralized or distributed network. The centralized CR network consists of a central unit like base station in wireless local area network (WLAN) or access point in cellular network for cognitive radio ad hoc networks where it controls the CR network traffic regarding spectrum opportunity usage [15, 16]. The distributed CR network, on the other hand, does not need fusion center to make a decision for signal presence [13]. In data fusion, the entire data is sent to the fusion center to declare the status of the PU. Although it achieves accurate results, it has high

implementation cost due to the large overhead of the data. However, it can be further simplified by using combining schemes like equal gain combination (EGC) or maximal ratio combination (MRC) where the users data are weighted in terms of their significance [1,15, 31]. To minimize the data overhead, a hard combination scheme is used with 1-bit or multiple-bit for decision making. The hard combination is implemented in decision fusion. In 1-bit decision, 0 bit decides signal is not present and 1 decides signal is present. Different decision fusion rules like Logical-OR (LO), Logical-AND (LA) and K out of N rule are used to determine the final decision. In LO, the primary user will be declared present if only one user declares the signal is present, the probability of detection and probability of false alarm of the final decision are given by respectively:

$$P_d = 1 - \prod_{i=1}^M (1 - P_{d,i}) \quad (2.32)$$

$$P_{fa} = 1 - \prod_{i=1}^M (1 - P_{fa,i}) \quad (2.33)$$

where  $P_{d,i}$  and  $P_{fa,i}$  are the probability of detection and probability of false alarm of user  $i$  respectively and  $M$  is the total number of cooperating SUs. In contrast, the LA requires all users to declare the signal is present to determine signal presence. The  $P_d$  and  $P_{fa}$  are given by respectively:

$$P_d = \prod_{i=1}^M P_{d,i} \quad (2.34)$$

$$P_{fa} = \prod_{i=1}^M P_{fa,i} \quad (2.35)$$

The  $K$  out of  $N$  rule is more general rule where LO and LA can be obtained by letting  $K=1$  and  $K=N$  respectively. The majority rule is obtained by having  $K=N/2$ . The  $P_d$  and  $P_f$  are given by respectively [15]:

$$P_d = \sum_{i=0}^{M-K} \binom{M}{K+i} (1 - P_{d,i})^{M-K-i} (1 - P_{d,i})^{K+i} \quad (2.36)$$

$$P_{fa} = \sum_{i=0}^{M-K} \binom{M}{K+i} (1 - P_{fa,i})^{M-K-i} (1 - P_{fa,i})^{K+i} \quad (2.37)$$

## 2.4.2 Spatial Correlation

Usually the received signals are correlated because they are generated from the same source. Since the energy detection is not optimal for detecting correlated signals. The sample covariance matrix is used in the analysis. This method enhances the detection performance and also mitigates the noise uncertainty.

## 2.4.3 Heuristic Algorithms

Heuristic algorithms are inspired by natural behavior of living creatures. Some examples of heuristic techniques are genetic algorithm, ant colony algorithm and particle swarm algorithm. These algorithms are used to find the optimum solution to given problem.

## 2.5 Simulation Results for Cooperative Secondary Users

The energy detector performance is simulated for four cooperating SUs ( $M = 4$ ) with various channels including AWGN, Rayleigh, Nakagami, Gamma, Lognormal, Nakagami-Lognormal composite and Nakagami-Gamma composite using complementary ROC curves. The time-bandwidth product is taken as  $m = 5$ , hence the number of samples become  $N = 10$ . The fixed SNR is set at 10 dB. Three techniques are used in the system: OR rule, AND rule and Majority rule. The performance of different techniques is compared to each other. The results are produced using 1000 Monte-Carlo simulations. The threshold is calculated from (2.8) for each SU independently.

## 2.5.1 AWGN Channel

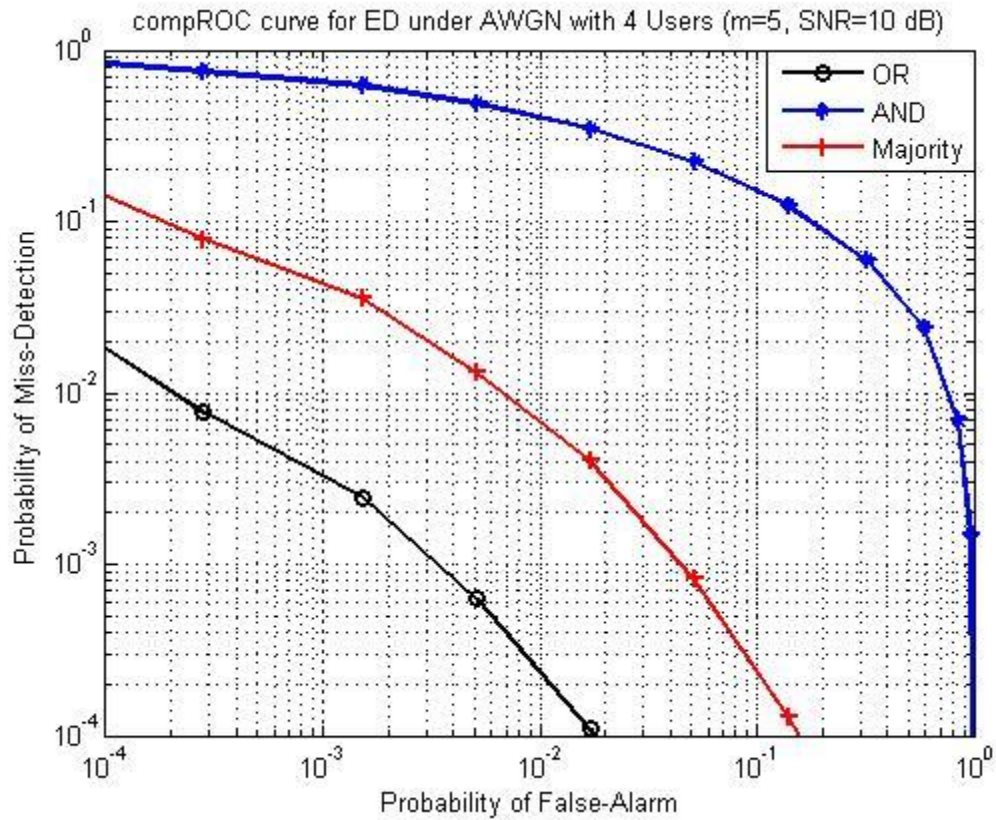


Figure 2-19: Complementary ROC curves for ED under AWGN channel with four cooperating users using AND, OR and Majority techniques

Figure 2.19 shows the complementary ROC curve of four cooperating SUs for ED under AWGN channel with SNR of 10 dB across different probability of false alarm values. When the probability of false alarm is 0.01, the probabilities of miss detection using OR, AND and Majority rules are  $2.3 \times 10^{-4}$ , 0.40 and 0.007 respectively.

## 2.5.2 Rayleigh Fading Channel

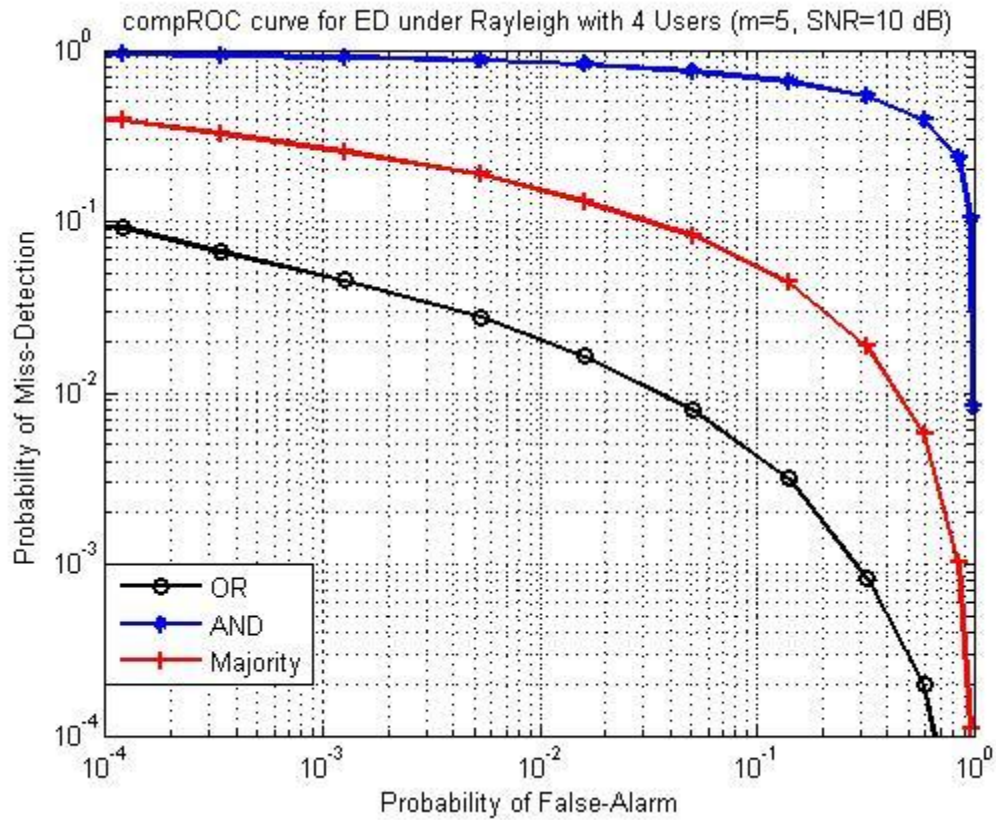


Figure 2-20: Complementary ROC curves for ED under Rayleigh channel with four cooperating users using AND, OR and Majority techniques

Figure 2.20 shows the complementary ROC curve of four cooperating SUs for ED under Rayleigh channel with SNR of 10 dB across different probability of false alarm values. When the probability of false alarm is 0.01, the probabilities of miss detection using OR, AND and Majority rules are 0.02, 0.80 and 0.16 respectively.

### 2.5.3 Nakagami Fading Channel

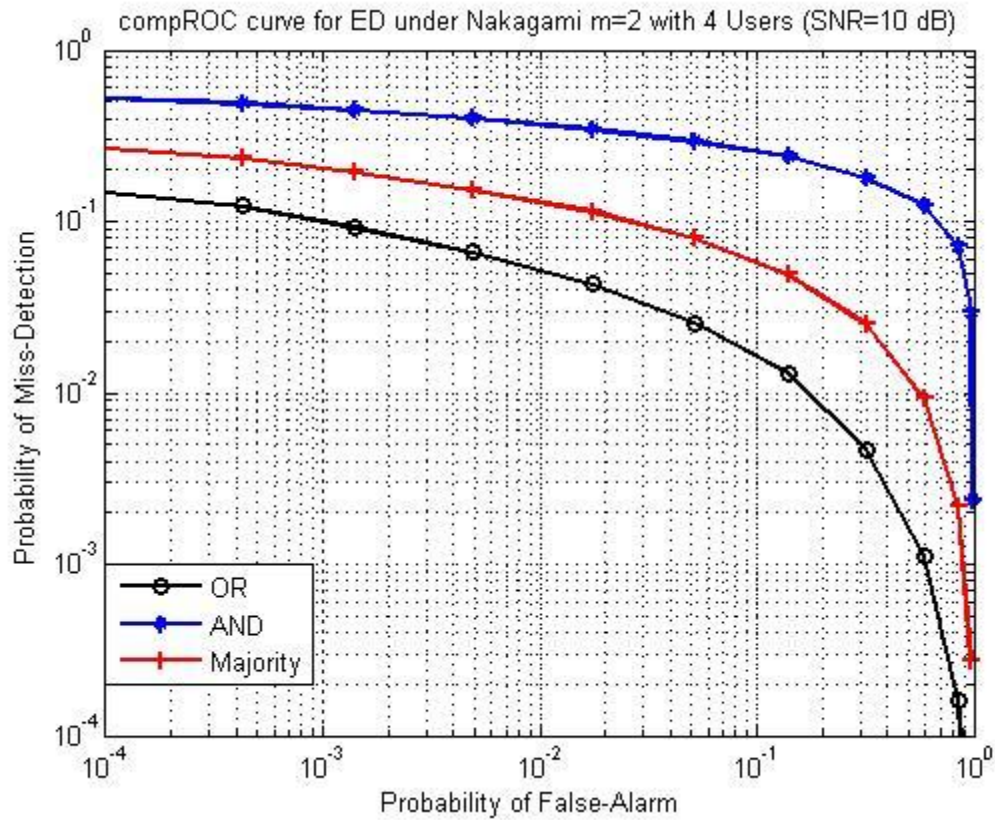


Figure 2-21: Complementary ROC curves for ED under Nakagami channel with  $m=2$  and four cooperating users using AND, OR and Majority techniques

Figure 2.21 shows the complementary ROC curve of four cooperating SUs for ED under Nakagami fading channel with  $m = 2$  and SNR of 10 dB across different probability of false alarm values. When the probability of false alarm is 0.01, the probabilities of miss detection using OR, AND and Majority rules are 0.05, 0.39 and 0.13 respectively.

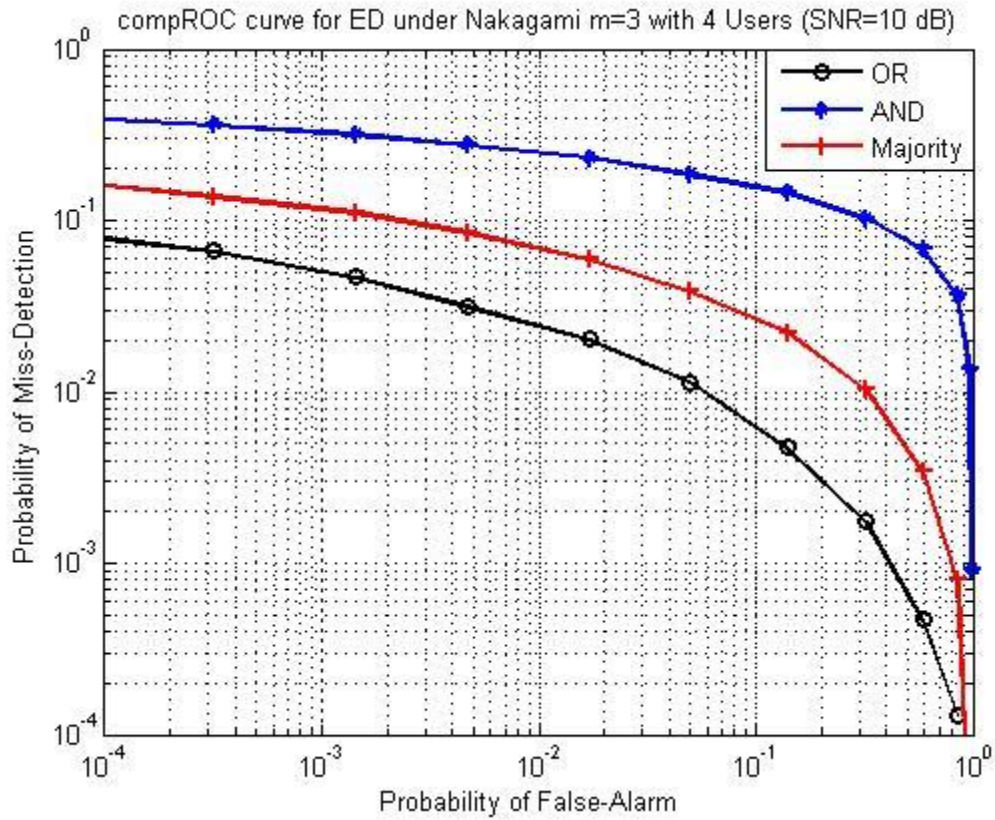


Figure 2-22: Complementary ROC curves for ED under Nakagami channel with  $m=3$  and four cooperating users using AND, OR and Majority techniques

Figure 2.22 shows the complementary ROC curve of four cooperating SUs for ED under Nakagami fading channel with  $m = 3$  and SNR of 10 dB across different probability of false alarm values. When the probability of false alarm is 0.01, the probabilities of miss detection using OR, AND and Majority rules are 0.024, 0.15 and 0.07 respectively.



## 2.5.4 Lognormal Shadowing Channel

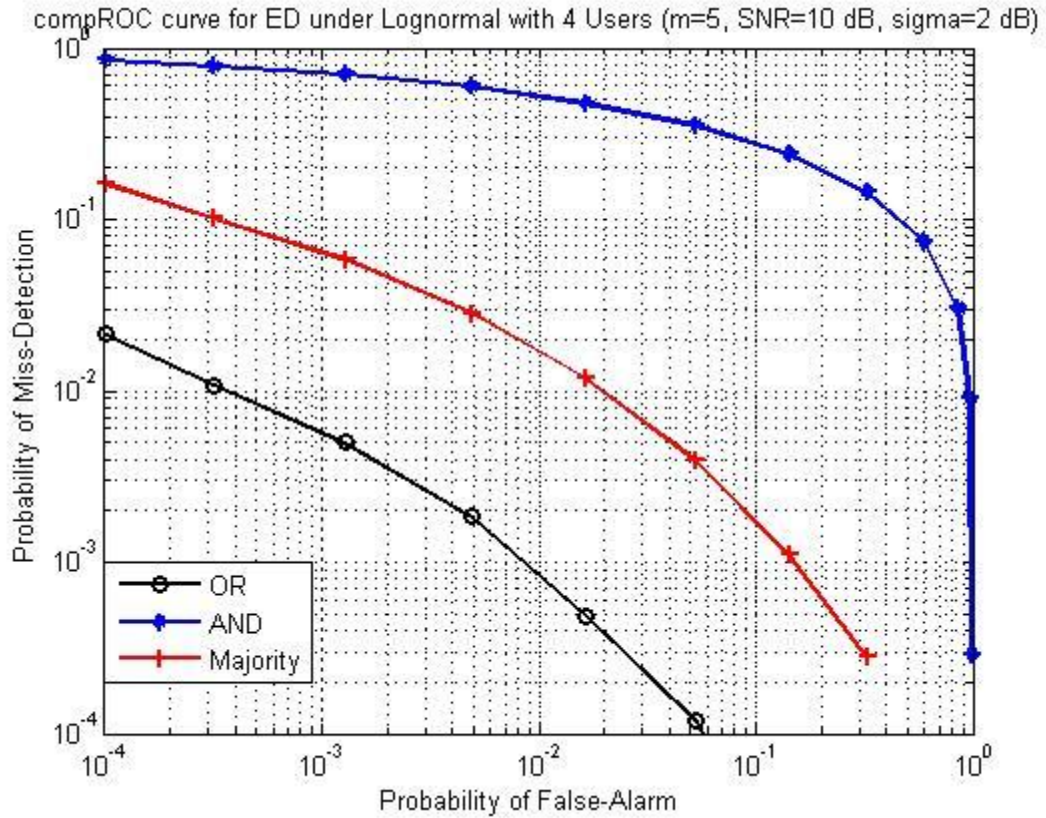


Figure 2-23: Complementary ROC curves for ED under Lognormal channel with  $\sigma_{dB} = 2$  dB and four cooperating users using AND, OR and Majority techniques

Figure 2.23 shows the complementary ROC curve of four cooperating SUs for ED under Lognormal channel with  $\sigma_{dB} = 2$  dB and SNR of 10 dB across different probability of false alarm values. When the probability of false alarm is 0.01, the probabilities of miss detection using OR, AND and Majority rules are  $8 \times 10^{-4}$ , 0.50 and 0.018 respectively.

## 2.5.5 Gamma Fading Channel

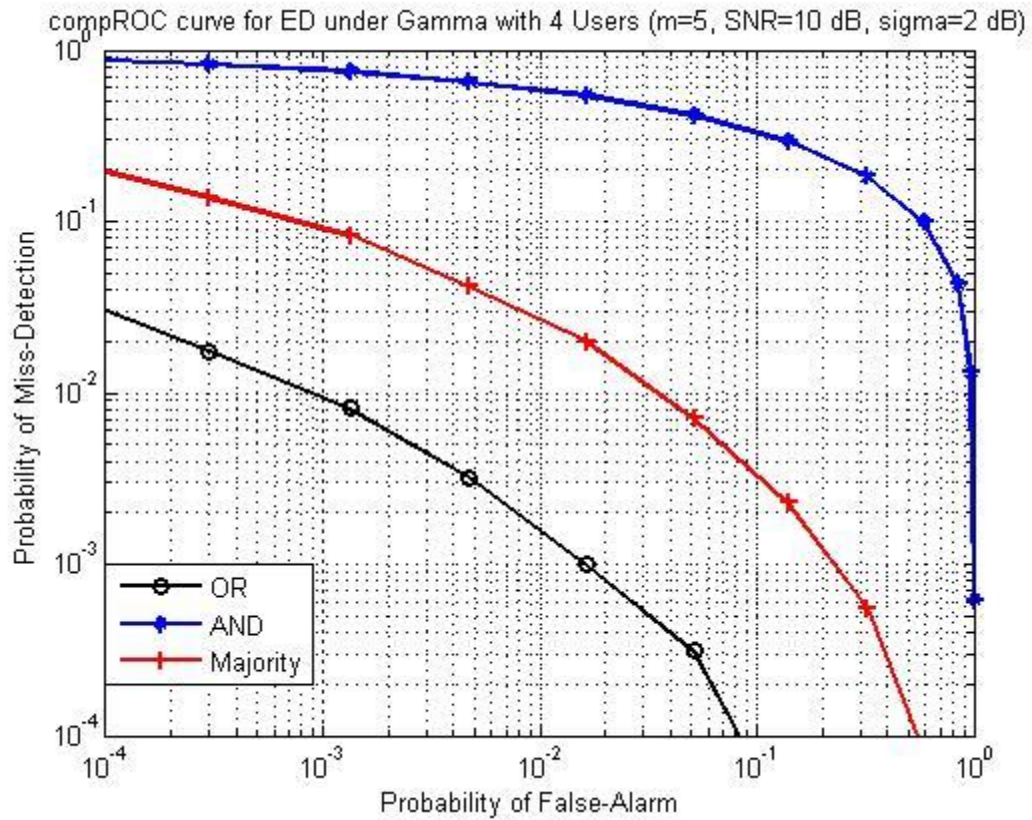


Figure 2-24: Complementary ROC curves for ED under Gamma channel with  $\sigma_{dB} = 2$  dB and four cooperating users using AND, OR and Majority techniques

Figure 2.24 shows the complementary ROC curve of four cooperating SUs for ED under Gamma channel with  $\sigma_{dB} = 2$  dB and SNR of 10 dB across different probability of false alarm values. When the probability of false alarm is 0.01, the probabilities of miss detection using OR, AND and Majority rules are  $1.6 \times 10^{-3}$ , 0.60 and 0.029 respectively.

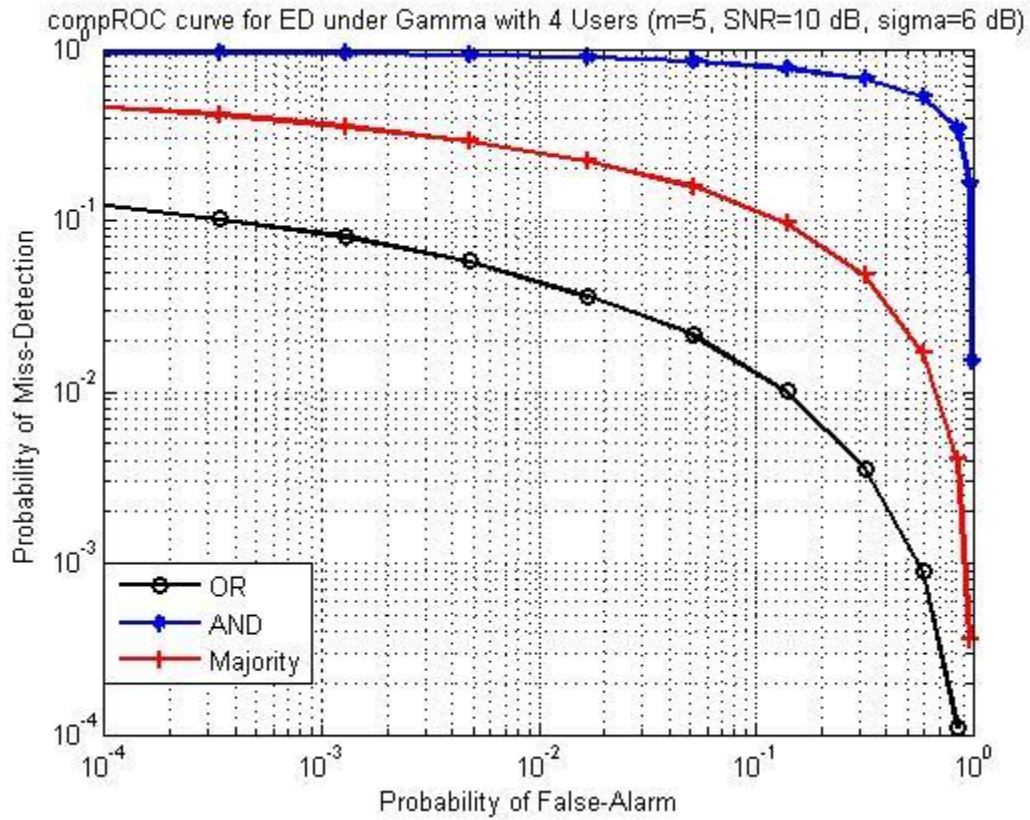


Figure 2-25: Complementary ROC curves for ED under Gamma channel with  $\sigma_{dB} = 6$  dB and four cooperating users using AND, OR and Majority techniques

Figure 2.25 shows the complementary ROC curve of four cooperating SUs for ED under Gamma channel with  $\sigma_{dB} = 6$  dB and SNR of 10 dB across different probability of false alarm values. When the probability of false alarm is 0.01, the probabilities of miss detection using OR, AND and Majority rules are 0.041, 0.90 and 0.25 respectively.

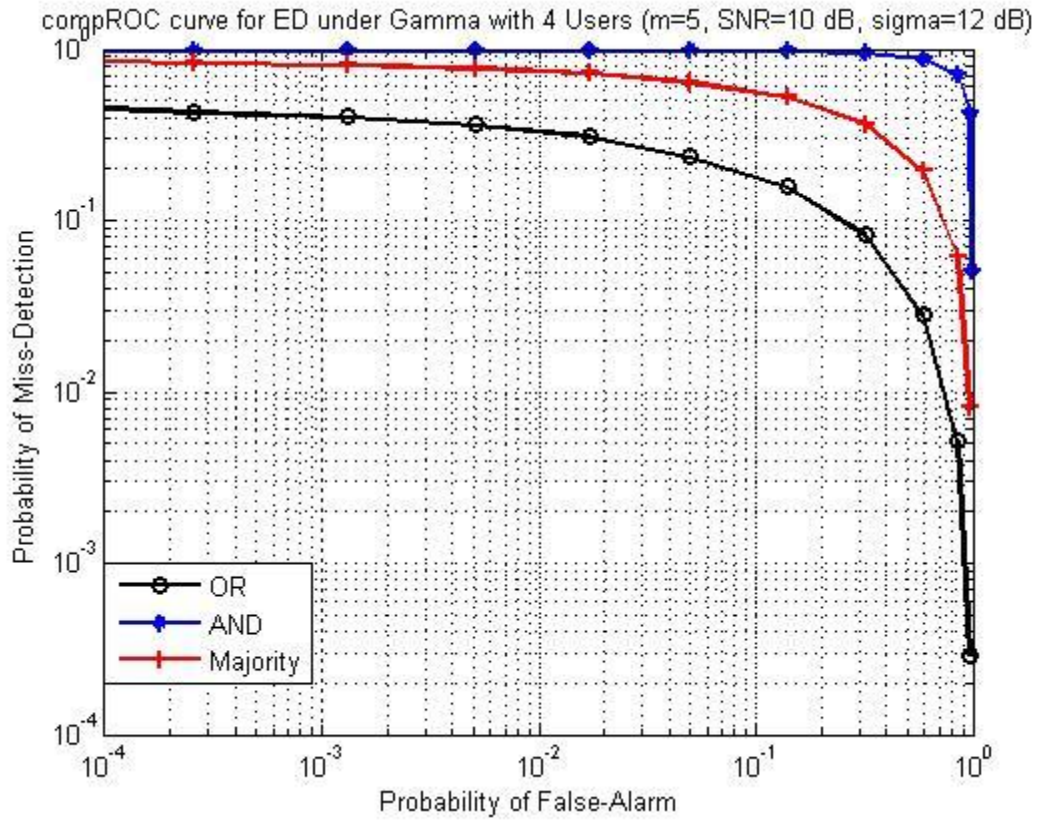


Figure 2-26: Complementary ROC curves for ED under Gamma channel with  $\sigma_{dB} = 12$  dB and four cooperating users using AND, OR and Majority techniques

Figure 2.26 shows the complementary ROC curve of four cooperating SUs for ED under Gamma channel with  $\sigma_{dB} = 12$  and SNR of 10 dB across different probability of false alarm values. When the probability of false alarm is 0.01, the probabilities of miss detection using OR, AND and Majority rules are 0.31, 0.99 and 0.07 respectively.

## 2.5.6 Nakagami – Lognormal Composite Fading Channel

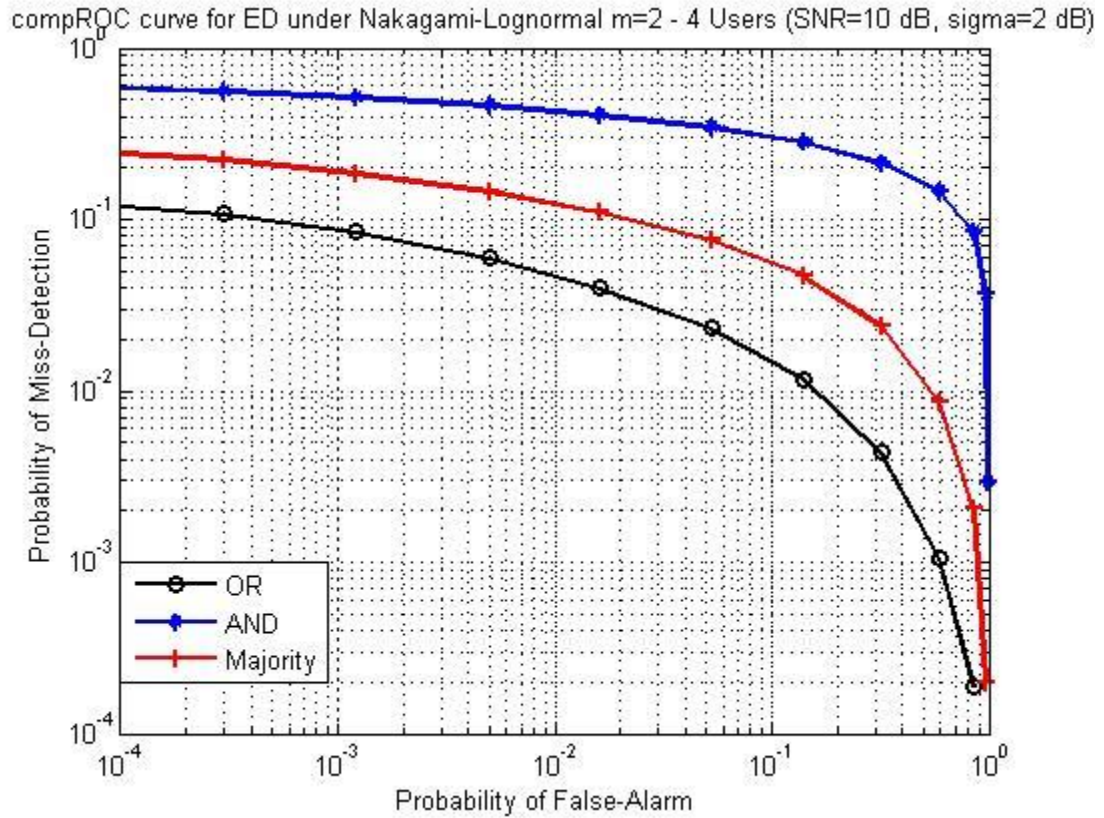


Figure 2-27: Complementary ROC curves for ED under Nakagami-Lognormal channel with  $m=2$ ,  $\sigma_{dB}=2$  dB and four cooperating users using AND, OR and Majority techniques

Figure 2.27 shows the complementary ROC curve of four cooperating SUs for ED under Nakagami-Lognormal channel with  $m = 2$ ,  $\sigma_{dB} = 2$  dB and SNR of 10 dB across different probability of false alarm values. When the probability of false alarm is 0.01, the probabilities of miss detection using OR, AND and Majority rules are 0.045, 0.42 and 0.12 respectively.

### 2.5.7 Nakagami – Gamma Composite Fading Channel

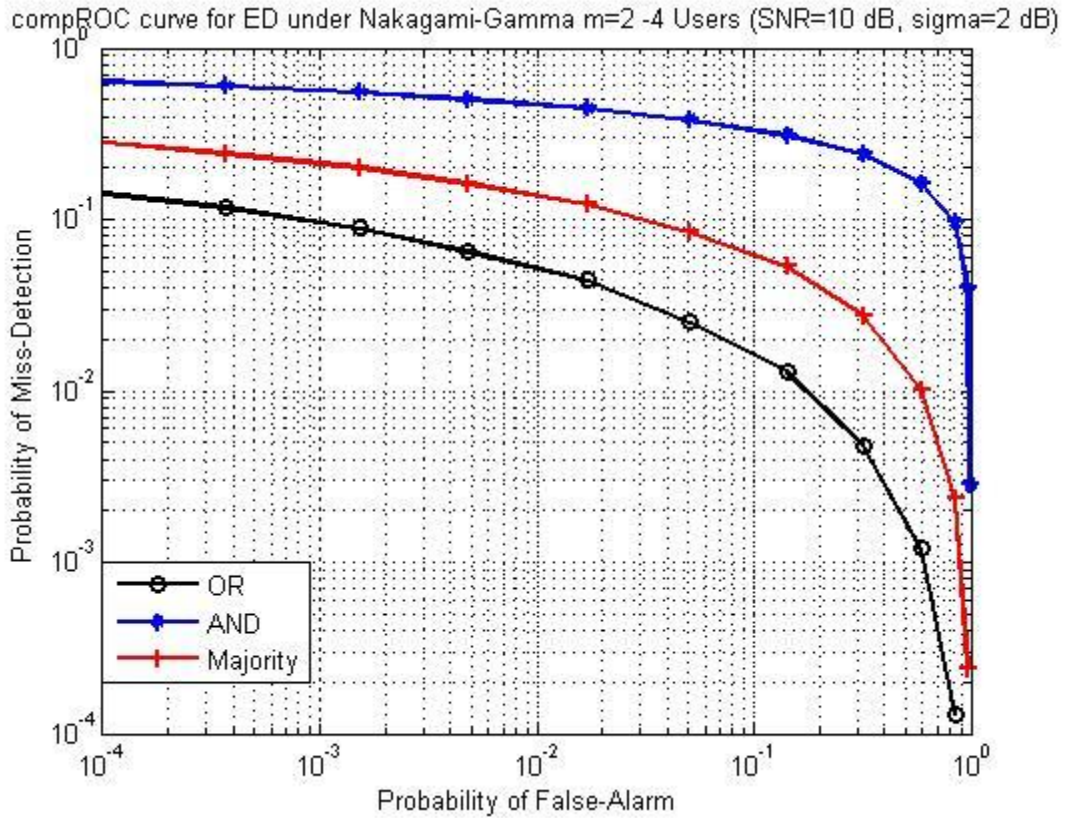


Figure 2-28: Complementary ROC curve for ED under Nakagami-Gamma channel with  $m=2$ ,  $\sigma_{dB}= 2$  dB and four cooperating users using AND, OR and Majority techniques

Figure 2.28 shows the complementary ROC curve of four cooperating SUs for ED under Nakagami-Gamma channel with  $m = 2$ ,  $\sigma_{dB} = 2$  dB and SNR of 10 dB across different probability of false alarm values. When the probability of false alarm is 0.01, the probabilities of miss detection using OR, AND and Majority rules are 0.05, 0.48 and 0.14 respectively.

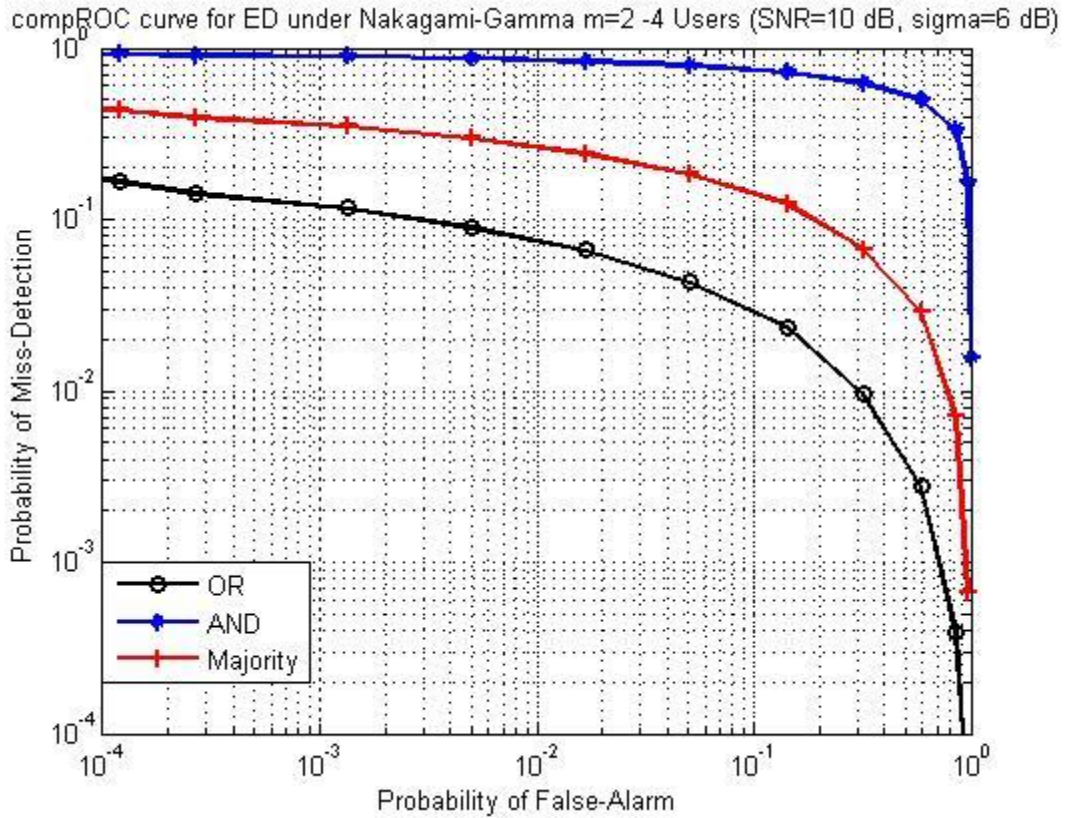


Figure 2-29: Complementary ROC curves for ED under Nakagami-Gamma channel with  $m=2$ ,  $\sigma_{dB}=6$  dB and four cooperating users using AND, OR and Majority techniques

Figure 2.29 shows the complementary ROC curve of four cooperating SUs for ED under Nakagami-Gamma channel with  $m = 2$ ,  $\sigma_{dB} = 6$  dB and SNR of 10 dB across different probability of false alarm values. When the probability of false alarm is 0.01, the probabilities of miss detection using OR, AND and Majority rules are 0.071, 0.85 and 0.28 respectively.

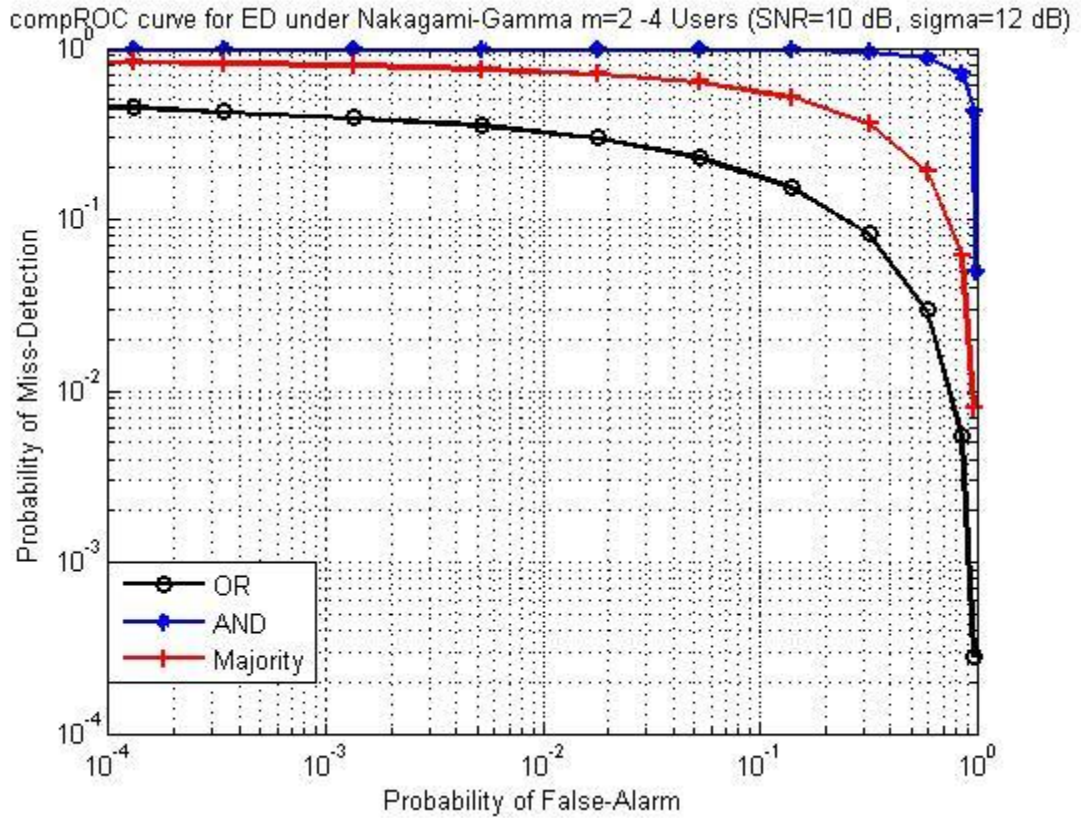


Figure 2-30: Complementary ROC curves for ED under Nakagami-Gamma channel with  $m=2$ ,  $\sigma_{dB}=12$  dB and four cooperating users using AND, OR and Majority techniques

Figure 2.30 shows the complementary ROC curve of four cooperating SUs for ED under Nakagami-Gamma channel with  $m = 2$ ,  $\sigma_{dB} = 12$  dB and SNR of 10 dB across different probability of false alarm values. When the probability of false alarm is 0.01, the probabilities of miss detection using OR, AND and Majority rules are 0.30, 0.99 and 0.70 respectively.



## CHAPTER 3

### PARTICLE SWARM OPTIMIZATION

#### 3.1 Introduction

PSO is a heuristic technique developed by James Kennedy and Russell C. Eberhart in 1995. The roots of PSO come from two main concepts: swarming theory and evolutionary computation. Swarming theory is related to the behavior of some kinds of animals. PSO achieves optimum value by mimicking the natural behavior of individual knowledge of communicating group of a swarm flock. PSO is implemented to maximize an objective function for a given problem with set of parameters by exploring its search space [39, 40, 41, 42, 43, 44].

Let  $f$  a function to be minimized within the search space  $R^n$  with  $n$  being the number of dimensions. The minimization process is defined as [50]:

$$\text{Given } f: R^n \longrightarrow R$$

$$\text{Find } \hat{x} \in R^n \text{ such that } f(\hat{x}) \leq f(x), x \in R^n \quad (3.1)$$

If a function to be maximized, the maximized process becomes [50]:

$$\text{Given } f: R^n \longrightarrow R$$

$$\text{Find } \hat{x} \in R^n \text{ such that } f(\hat{x}) \geq f(x), x \in R^n \quad (3.2)$$

A candidate solution is considered for each individual element in the search space.  $x$  represents the optimal solution in the search space. Here,  $f$  is called the objective function where the search space is mapped to the function space. The fitness value is obtained by mapping the function space to the fitness space. Sometimes candidate solution elements undergo certain constraints e.g. ( $x > 2$ ) if we have constrained optimization. The candidate solution and fitness values can be represented graphically through fitness landscape. The fitness landscape is a plot between  $n$ -dimensional parameter space and one dimensional fitness for each parameter [50].

A random swarm is used to initialize the conventional PSO algorithm the swarm has  $M$  particles each with dimension  $d$ . The fitness function is evaluated for each particle at each iteration. There are two sets which are stored and memorized by the algorithm: best particle solution and global best solution. These sets change whenever they achieve better values of fitness as the algorithm progresses. PSO consists of two equations: velocity equation and position equation. The velocity and position are adjusted for each particle as[45-55]:

$$v_{id}^t = \omega v_{id}^{t-1} + c_1 \xi (p_{id}^{t-1} - x_{id}^{t-1}) + c_2 \eta (p_{bd}^{t-1} - x_{id}^{t-1}) \quad (3.3)$$

$$x_{id}^t = x_{id}^{t-1} + v_{id}^t \quad (3.4)$$

where  $v_{id}^t$  is the velocity of the  $i^{\text{th}}$  particle in dimension  $d$  at iteration  $t$ ,  $\omega$  is the inertia weight,  $x_{id}^t$  is the position of the  $i^{\text{th}}$  particle in dimension  $d$  at iteration  $t$ ,  $p_{id}^{t-1}$  is the best global solution at iteration  $t-1$ ,  $p_{bd}^{t-1}$  is the best particle solution at iteration  $t-1$ ,  $c_1$  and  $c_2$  are constants which are called the cognitive coefficient and the social coefficient respectively.  $\eta$  and  $\xi$  are random numbers uniformly distributed between [0,1].

The velocity update consists of three components: inertia component, cognitive component and social component. The inertia weight keeps the moving particles toward the intended destination. The inertia weight can have values between 0.4 - 1.2. Higher values of inertia weight results in particle acceleration thus higher convergence. This is because the exploration in the whole search space is increased. Lower values of inertia weight, on the other hand, result in more accuracy in the solution. The cognitive component serves as the memory of the particles. It directs the particles toward the area of high fitness value within the search space. The social component directs the particle toward the swarm's best region. The social component and cognitive component have a stochastic influence resulted from the random values of  $\eta$  and  $\zeta$ . The stochastic process acts as a semi-random stochastic. Therefore, the particles movement is heavily affected by the best particle solution and global best solution. The velocity determines the speed of particles movement within the search space. A higher velocity would let the particles stray from the search space. Therefore, the velocity is limited to  $V_{max}$  for each particle [48-62].

The PSO advantages are listed as follows:

- 1) PSO provides an accurate solution with few iterations.
- 2) PSO maintains the cost per iteration and memory occupations for each iteration.
- 3) Derivatives of the objective function is not required for the algorithm to work.

PSO performance is affected by tuning parameters sometimes called exploration-exploitation tradeoff. Exploration is related to finding a good optimum solution by testing

various solution regions. On the other hand, exploitation is related to finding a good optimum solution by concentrating the search around a promising solution.

The PSO algorithm is given as:

- 1) Initiate PSO position and velocity.
- 2) Compute fitness value for each particle.
- 3) Update best particle and global best particle fitness by comparing current and previous values.
- 4) Update velocity and position for each particle.
- 5) Repeat step (2) until the maximum iteration is reached.

### 3.2 PSO for CR networks

PSO algorithm is implemented in CR network to find the weights of each SU in the fusion center. Figure 3.1 shows a CR network with cooperating SUs. An internal noise in control channel occurs during transmission of SUs energies to the fusion center which is denoted by  $n$  with zero mean Gaussian noise and variance  $\delta^2$ . At the fusion center, each SU energy is multiplied by a weight where they are summed and compared to a threshold to determine the presence or absence of PU signal. The global test statistics at the fusion center  $y_{fc}$  is calculated as:

$$y_{fc} = \sum_{l=1}^M w_l y_l = \mathbf{w}^T \mathbf{y} \quad (3.5)$$

where  $\mathbf{w}$  is the weight vector of assigned by the fusion center,  $\mathbf{y}$  is the sensed data vector of the SUs and  $T$  is the transpose of a matrix.  $\mathbf{w} = [w_1, w_2, \dots, w_M]^T$  with  $w_l \geq 0$  and  $\mathbf{y} = [y_1, y_2, \dots, y_M]^T$  [38, 63].

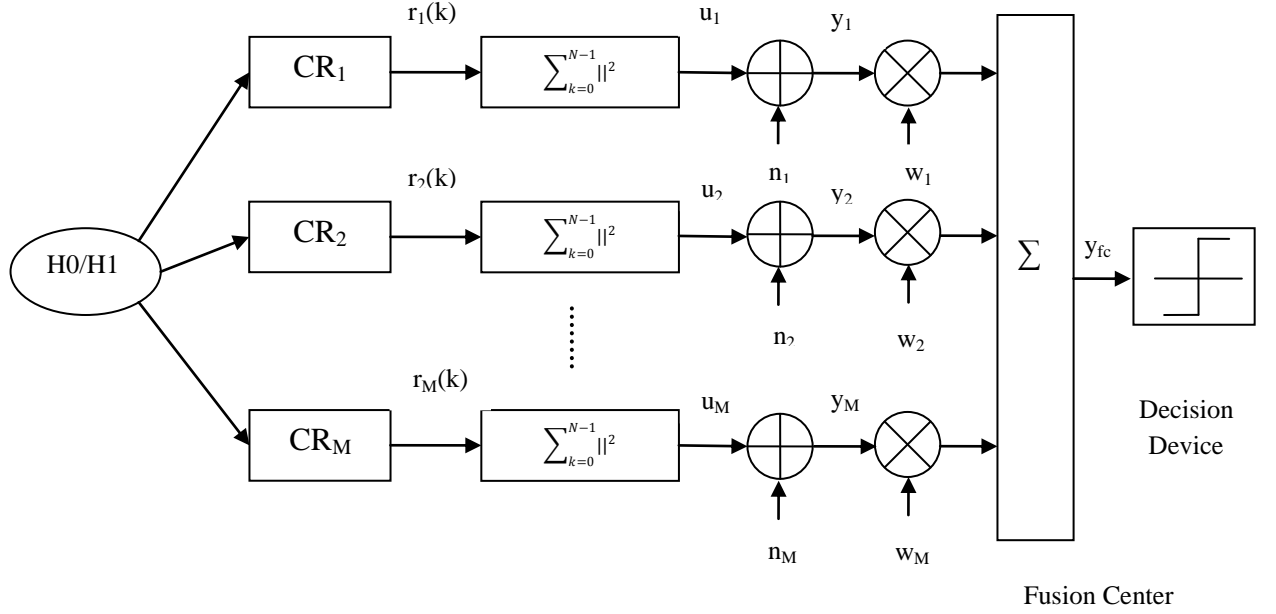


Figure 3-1: Cooperative spectrum sensing using PSO

The probability of detection is given by:

$$P_d = Q\left(\frac{Q^{-1}(P_f)\sqrt{\mathbf{w}^T \mathbf{A} \mathbf{w}} - E_s \mathbf{h}^T \mathbf{w}}{\sqrt{\mathbf{w}^T \mathbf{B} \mathbf{w}}}\right) \quad (3.6)$$

where  $Q(x)$  is the Q-function,  $E_s$  is the energy signal,  $\mathbf{h}$  is the channel gain vector,  $\mathbf{A}$  is a variable vector taken from the variance of the global test statistics  $y_{fc}$  under hypothesis  $H_0$ ,  $\mathbf{B}$  is a variable vector taken from the variance of the global test statistics  $y_{fc}$  under hypothesis  $H_1$  and  $P_f$  is false alarm probability.  $\sigma$  is the variance of the noise and  $\delta$  is the variance of the internal noise in the control channel.

$Q(x)$ ,  $E_s$ ,  $h$ ,  $A$ ,  $B$ ,  $\sigma$  and  $\delta$  are expressed as, respectively [38]:

$$Q(x) = \int_x^{+\infty} \frac{1}{\sqrt{2\pi}} e^{-t^2/2} dt \quad (3.7)$$

$$E_s = \sum_{k=0}^{N-1} |s(k)|^2 \quad (3.8)$$

$$A = 2N \text{diag}^2(\sigma) + \text{diag}(\delta) \quad (3.9)$$

$$B = 2N \text{diag}^2(\sigma) + \text{diag}(\delta) + 4E_s \text{diag}(h) + \text{diag}(\delta) \quad (3.10)$$

where  $s(k)$  is primary signal,  $N$  is the number of samples,  $\sigma$  is the variance of the noise channel and  $\delta$  is the variance of the internal noise in the control channel occurred during data transmission to the fusion center. The number of samples  $N$  can be obtained by multiplying the time bandwidth product  $m$  by 2 ( $N = 2m$ ). The ED threshold for the fusion center, where the combined energies from SUs are summed and compared to the threshold, is given by:

$$\lambda = N\sigma^T \mathbf{w} + Q^{-1}(P_f) \sqrt{\mathbf{w}^T \mathbf{A} \mathbf{w}} \quad (3.11)$$

where  $\lambda$  is the threshold,  $N$  is the number of samples,  $\sigma$  is the channel noise vector,  $Q^{-1}$  is the inverse q function,  $P_f$  is false alarm probability,  $\mathbf{w}$  is the weight vector and  $\mathbf{A}$  is a variable vector taken from the variance of the global test statistics  $y_{fc}$  under hypothesis  $H_0$ .

The objective function to be optimized by PSO algorithm is given as:

$$f(\mathbf{w}) = \frac{Q^{-1}(P_f) \sqrt{\mathbf{w}^T \mathbf{A} \mathbf{w}} - E_s \mathbf{h}^T \mathbf{w}}{\sqrt{\mathbf{w}^T \mathbf{B} \mathbf{w}}} \quad (3.12)$$

where PSO tries to maximize the detection probability by finding the weight values of each user. Since there are infinite optimal solutions which can be acquired from the function, a constraint is applied to limit the number of the optimal solution. So if  $w^o$  is an optimal solution, then  $\lambda w^o$  is also an optimal solution provided that  $\lambda$  is positive real number. The total weight sum of SUs is equal to one which can be expressed as:

$$\min_w f(w), \text{ st. } \sum_{l=1}^M w_l = 1, \quad 0 \leq w_l \leq 1, \quad l = 1, 2, \dots, M \quad (3.13)$$

Each particle's velocity and position in PSO can be expressed as [38, 63]:

$$v_{id}^t = \omega v_{id}^{t-1} + c_1 \xi (p_{id}^{t-1} - x_{id}^{t-1}) + c_2 \eta (p_{bd}^{t-1} - x_{id}^{t-1}) \quad (3.14)$$

$$x_{id}^t = x_{id}^{t-1} + v_{id}^t \quad (3.15)$$

where  $d$  represents the number of dimensions of the particle. In the case of the CR network, the number of dimensions  $d$  represents the number of cooperating users  $M$ . The fitness function  $f(w)$  will be multiplied by -1 i.e.,  $-f(w)$  since it is a minimization of the function  $f(w)$ . To satisfy the condition of the total weight sum equal to one, the position vector is divided by the total sum of position vector values i.e.,  $x_{id}^t / \sum_{d=1}^M x_{id}^t$ . The PSO algorithm for the CR network is given by [38]:

- 1) Generate the position and velocity vectors  $x_{id}^t$  and  $v_{id}^t$  randomly at  $t=0$ .  $x_{id}^t \in [0,1]$ ,  $v_{id}^t \in [-V_{max}, +V_{max}]$ ,  $1 \leq d \leq M$ ,  $1 \leq i \leq S$ , where  $S$  is the total number of particles.
- 2) Exchange  $x_{id}^t$  by  $x_{id}^t / \sum_{d=1}^M x_{id}^t$

- 3) Evaluate fitness value for each particle in population then set  $\mathbf{p}_i^t = [x_{i1}^t, x_{i2}^t, \dots, x_{iM}^t]^T$ ,  $\mathbf{p}_b^t = [x_{b1}^t, x_{b2}^t, \dots, x_{bM}^t]^T$ .  $b$  represents the index of the particle which has the highest fitness value.
- 4) Update  $v_{id}^t$  using equation (3.3) at  $t=t+1$ . If  $v_{id}^t > V_{max}$ , let  $v_{id}^t = V_{max}$ . If  $v_{id}^t < -V_{max}$ , let  $v_{id}^t = -V_{max}$ .
- 5) Update  $x_{id}^t$  using equation (3.4).
- 6) Exchange  $x_{id}^t$  by  $x_{id}^t / \sum_{d=1}^M x_{id}^t$ .
- 7) Evaluate fitness value for each particle in population. If the fitness value of particle  $i$  is larger than  $\mathbf{p}_i^{t-1}$  fitness value, let  $\mathbf{p}_i^t = [x_{i1}^t, x_{i2}^t, \dots, x_{iM}^t]^T$  otherwise let  $\mathbf{p}_i^t = \mathbf{p}_i^{t-1}$ . If the fitness value of particle  $i$  is larger than  $\mathbf{p}_b^{t-1}$  fitness value, let  $\mathbf{p}_b^t = [x_{i1}^t, x_{i2}^t, \dots, x_{iM}^t]^T$  otherwise let  $\mathbf{p}_b^t = \mathbf{p}_b^{t-1}$ .
- 8) Terminate the algorithm if the maximum number of iteration is reached, otherwise return to step 4.

The flowchart of the PSO algorithm is shown in Figure 3.2.



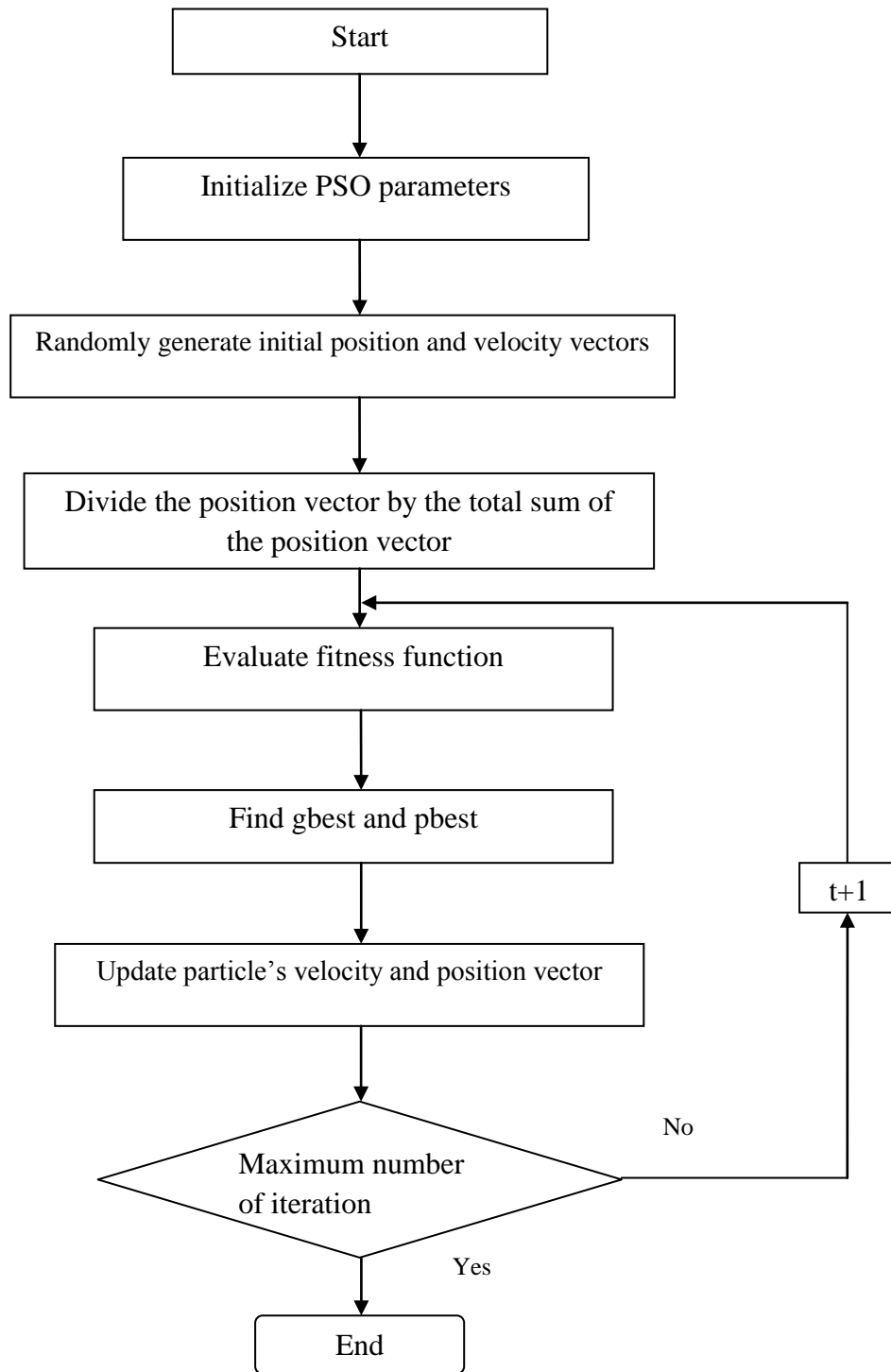


Figure 3-2: Flowchart of the PSO algorithm

### 3.3 Simulation Results for PSO

The energy detector performance is simulated for three cooperating SUs ( $M = 3$ ) with various channels including AWGN, Rayleigh, Nakagami, Gamma, Lognormal, Nakagami-Lognormal composite and Nakagami-Gamma composite using ROC curves. The time-bandwidth product is taken as  $m = 5$ , hence the number of samples become  $N = 10$ . The fixed SNR is set at 10 dB. The PSO parameters are taken as: the number of particles  $S = 60$ , the inertia weight  $\omega = 1$ , the cognitive coefficient  $c_1 = 2$ , the social coefficient  $c_2 = 2$  and the maximum number of iterations  $t = 30$ . The threshold at the fusion center is calculated from (3.11). The performance of PSO technique is plotted. The results are produced using 1000 Monte-Carlo simulations.

### 3.3.1 AWGN and Rayleigh Fading Channels

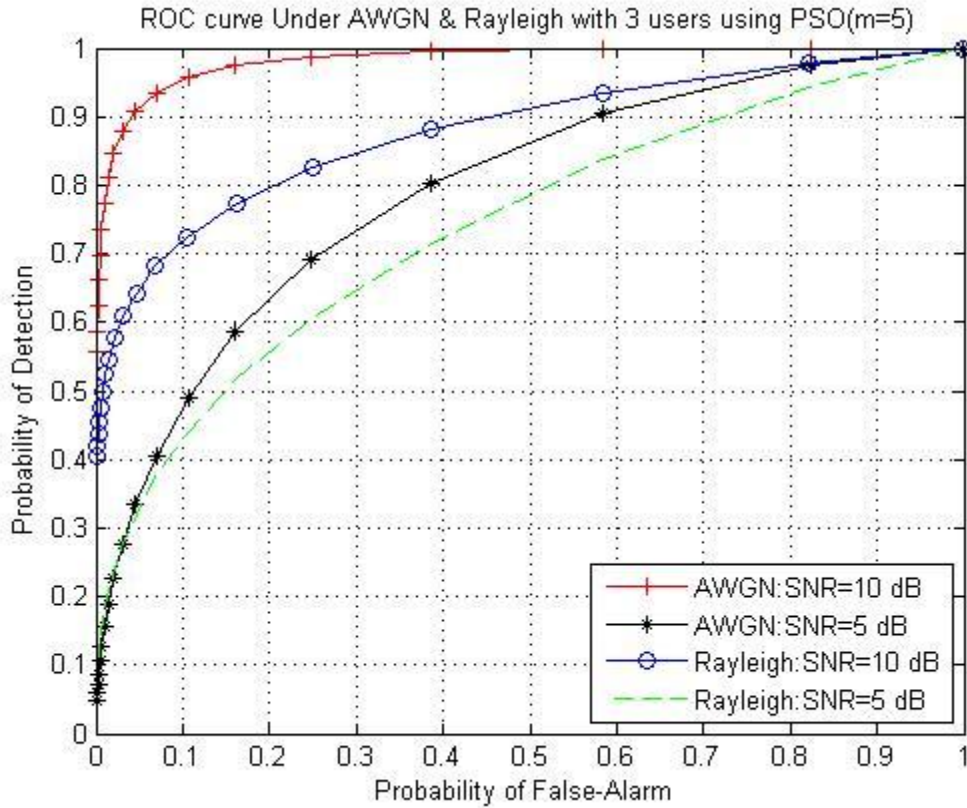


Figure 3-3: ROC curves for ED under AWGN and Rayleigh channels with three cooperating SUs

The ROC curve of three cooperating SUs for ED using PSO algorithm under AWGN and Rayleigh fading channels with SNRs of 10 dB and 5 dB across different probability of false alarm values is plotted in Figure 3.3. Given a probability of false alarm of 0.2, the probabilities of detection under AWGN at SNRs of 5 dB and 10 dB are 0.63 and 0.98, respectively. In the case of Rayleigh fading channel, the probabilities of detection at SNRs of 5 dB and 10 dB are 0.56 and 0.80, respectively.

### 3.3.2 Nakagami Fading Channel

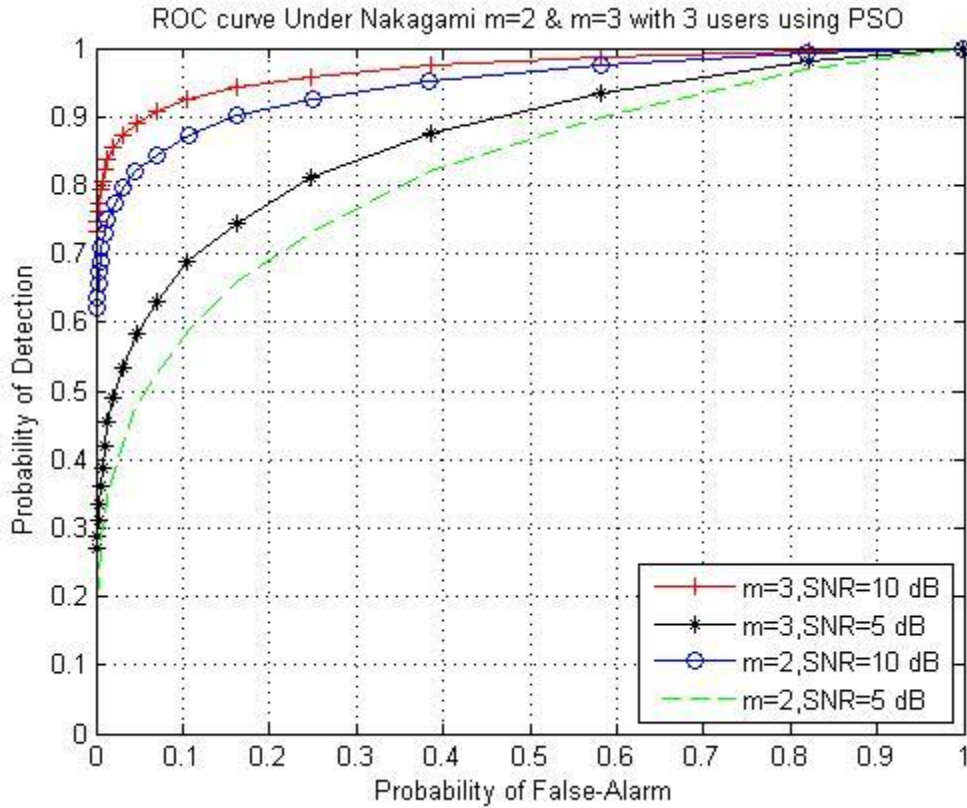


Figure 3-4 ROC curves for ED under Nakagami channel with three cooperating SUs and  $m=2$

The ROC curve of three cooperating SUs for ED using PSO algorithm under Nakagami fading channel with fading parameters  $m = 2$  and  $m = 3$  and SNRs of 10 dB and 5 dB across different probability of false alarm values is shown in Figure 3.4. When the probability of false alarm is 0.2, the probabilities of detection for  $m = 2$  at SNRs of 5 dB and 10 dB are 0.69 and 0.91, respectively. For  $m = 3$ , the probabilities of detection at SNRs of 5 dB and 10 dB are 0.77 and 0.95, respectively.

### 3.3.3 Lognormal Shadowing Channel

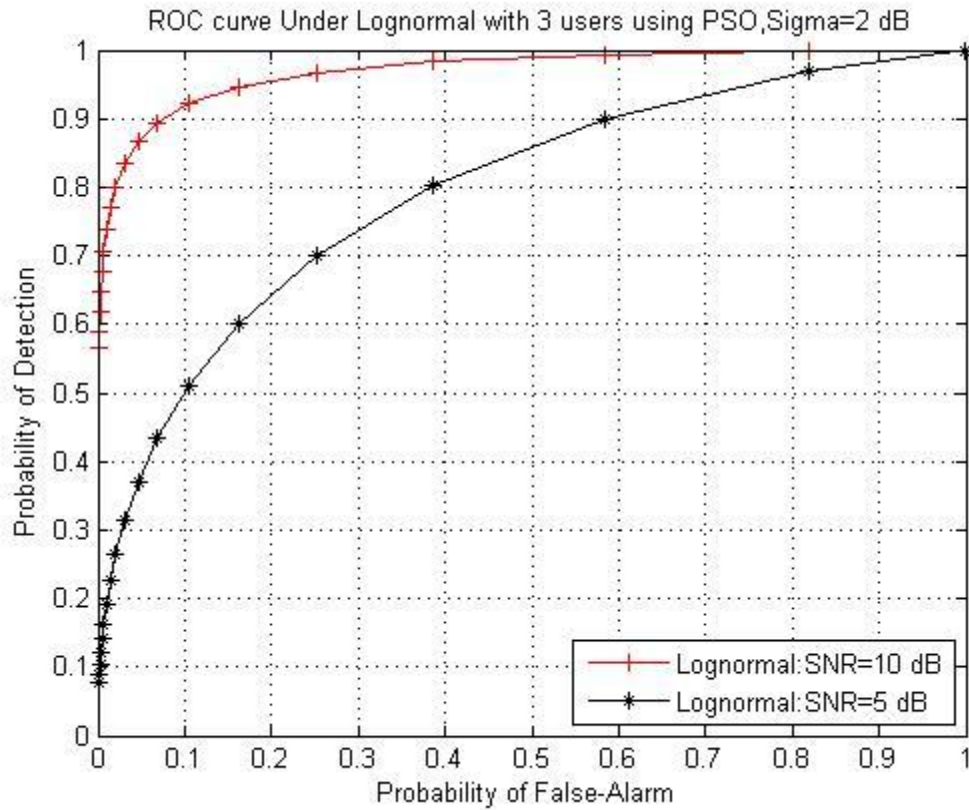


Figure 3-5: ROC curves for ED under Lognormal channel with three cooperating SUs and  $\sigma_{dB}=2$  dB

The ROC curve of three cooperating SUs for ED using PSO algorithm under Lognormal channel with  $\sigma_{dB} = 2$  dB and SNR of 5 dB across different probability of false alarm values is shown in Figure 3.5. When the probability of false alarm is 0.2, the probability of detection is 0.63 at SNR 5 dB while the probability of detection is 0.96 at SNR 10 dB.

### 3.3.4 Gamma Fading Channel

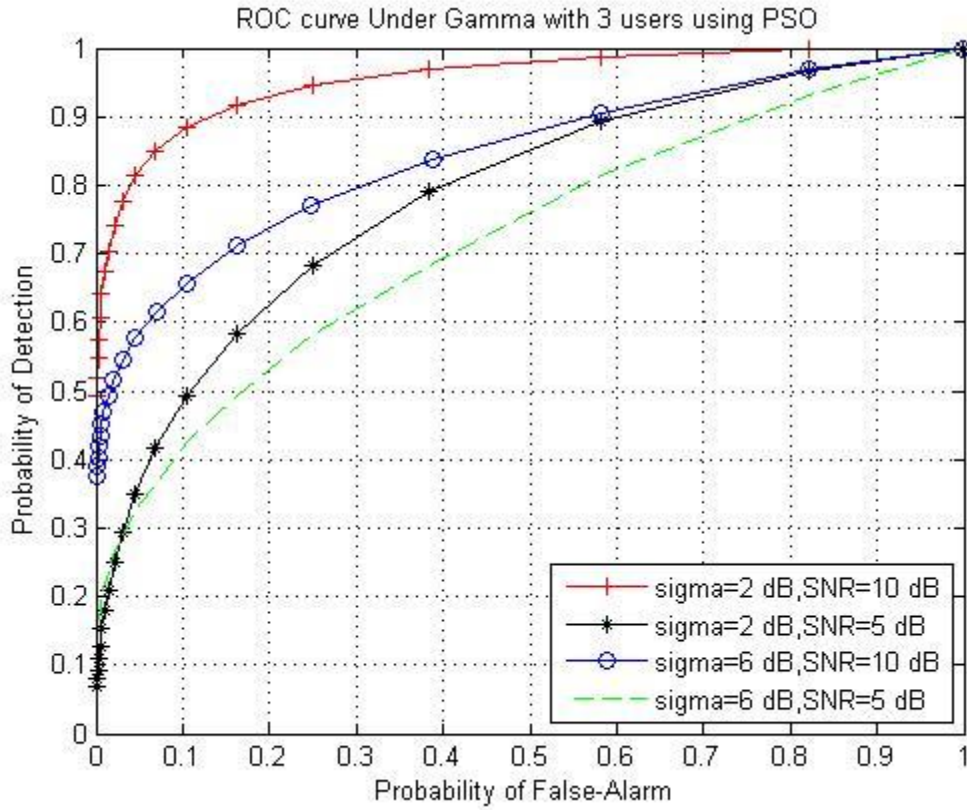


Figure 3-6: ROC curves for ED under Gamma channel with three cooperating SUs and  $\sigma_{dB} = 2$  dB

The ROC curve of three cooperating SUs for ED using PSO algorithm under Gamma channel with  $\sigma_{dB} = 2$  dB and SNR of 5 dB across different probability of false alarm values is plotted in Figure 3.6. When the probability of false alarm is 0.2, the probabilities of detection for  $\sigma_{dB} = 2$  at SNRs of 5 dB and 10 dB are 0.62 and 0.88, respectively. For  $\sigma_{dB} = 6$ , the probabilities of detection at SNRs of 5 dB and 10 dB are 0.53 and 0.73, respectively.

### 3.3.5 Nakagami – Lognormal Composite Fading Channel

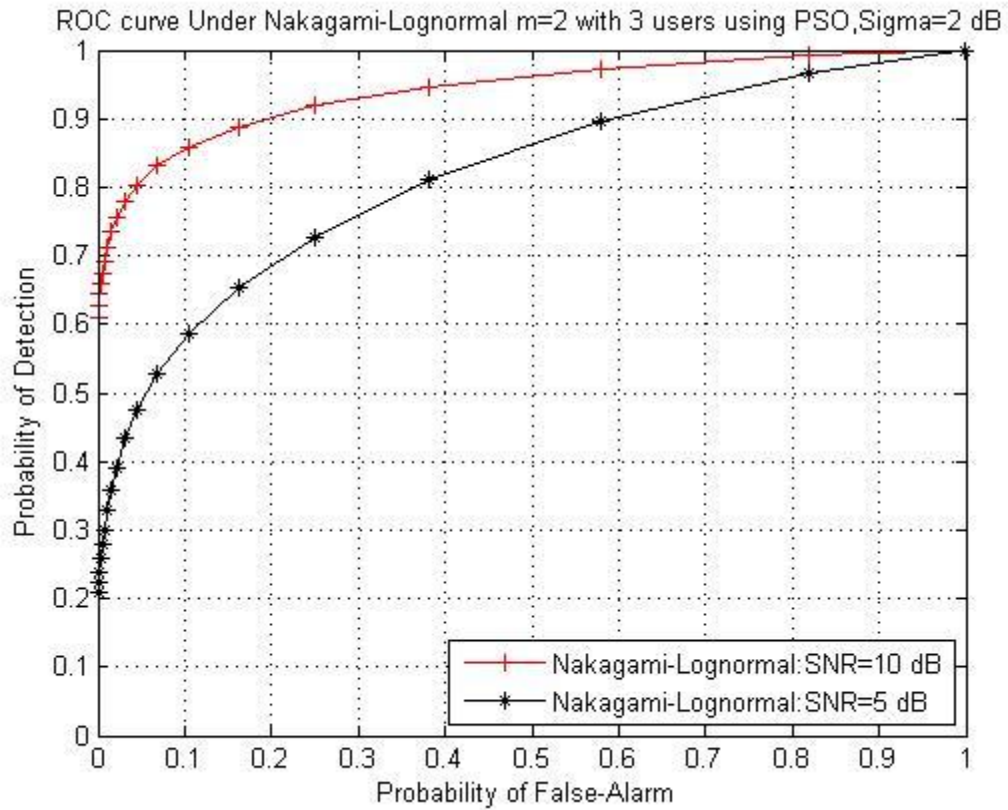


Figure 3-7: ROC curves for ED under Nakagami-Lognormal channel with three cooperating SUs,  $\sigma_{dB} = 2$  dB and  $m=2$

The ROC curve of three cooperating SUs for ED using PSO algorithm under Nakagami-Lognormal channel with  $m = 2$ ,  $\sigma_{dB} = 2$  dB and SNR of 5 dB across different probability of false alarm values is shown in Figure 3.7. When the probability of false alarm is 0.2, the probability of detection is 0.69 at SNR 5 dB while the probability of detection is 0.90 at SNR 10 dB.

### 3.3.6 Nakagami – Gamma Composite Fading Channel

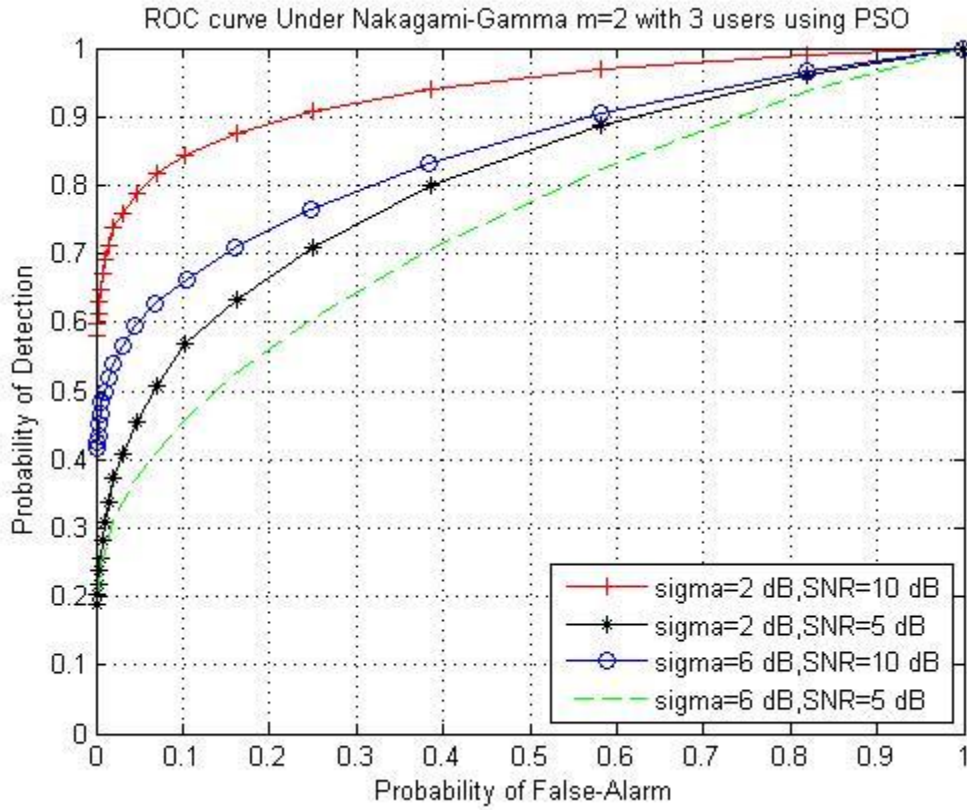


Figure 3-8: ROC curves for ED under Gamma-Lognormal channel with three cooperating SUs,  $\sigma_{dB} = 6$  dB and  $m=2$

The ROC curve of three cooperating SUs for ED using PSO algorithm under Nakagami-Gamma channel with  $m = 2$ ,  $\sigma_{dB} = 2$  dB and 6 dB and SNRs of 5 dB and 10 dB across different probability of false alarm values is shown in Figure 3.8. When the probability of false alarm is 0.2, the probabilities of detection for  $\sigma_{dB} = 2$  at SNRs of 5 dB and 10 dB are 0.66 and 0.89, respectively. For  $\sigma_{dB} = 6$ , the probabilities of detection at SNRs of 5 dB and 10 dB are 0.56 and 0.73, respectively.



## CHAPTER 4

### PARTICLE SWARM OPTIMIZATION-HILL CLIMBING

#### HYBRID

##### 4.1 Introduction

Hill climbing algorithm is a local search method used to make some improvement of the problem solution which is done by initiating a random solution to the problem. Based on the random chosen value, evaluation of the change of movement between neighborhood entities is selected. The change will become either positive or negative. Generation of a new individual is done if the move is positive. On the other hand, the individual is kept if the move is negative. The process is halted when there is no improvement to be found. Because of the simplicity of hill climbing algorithm, it is mostly chosen among other optimizing algorithms. Hill climbing algorithm is capable of giving better results than other algorithms when search time is limited [64, 65].

In terms of mathematical description, hill climbing algorithm tries to minimize a target function  $f(x)$  where  $x$  is a continuous or discrete vector. A single element in  $x$  is adjusted at each iteration. The change determines if it improves the value of  $f(x)$ . The process ends if there is no change found in to improve the value of  $f(x)$  and  $x$  becomes locally optimized [64, 65].

Local maximum and local minimum are encountered during optimizing problem solution. The problem real optimal solution cannot be found if the local optimum is not overcome. One of the effective methods to solve this problem is using hill climbing algorithm. The local optimum can be overcome by applying hill climbing algorithm to find the real global optimal value of the problem. However, hill climbing algorithm does not always converge to the global maximum since most problems are not convex but it can converge to a local maximum [70].

The hill climbing algorithm process is expressed as [65]:

- 1) Pick a random number in the search space.
- 2) Consider all current state's neighbors.
- 3) Choose the neighbor which has the best quality and move to that state.
- 4) Repeat steps (2-4) until all neighboring states have lower quality.
- 5) Return the current state as the solution state.

To illustrate how the hill climbing algorithm works, let's consider the hill climbing model shown in Figure 4.1. Here we have two current states: current state 'A' and current state 'B' at different time instances trying to find the global maximum using hill climbing algorithm. Each current state tries to find the best neighbor value in order to reach the global maximum. Current state 'A' will eventually reach a local maximum since it will move to the right based on the best neighbor to the right while current state 'B' will eventually reach a global maximum since it will move to the left based on the best neighbor to the left. This indicates that the hill climbing algorithm does not always guarantee a global maximum.

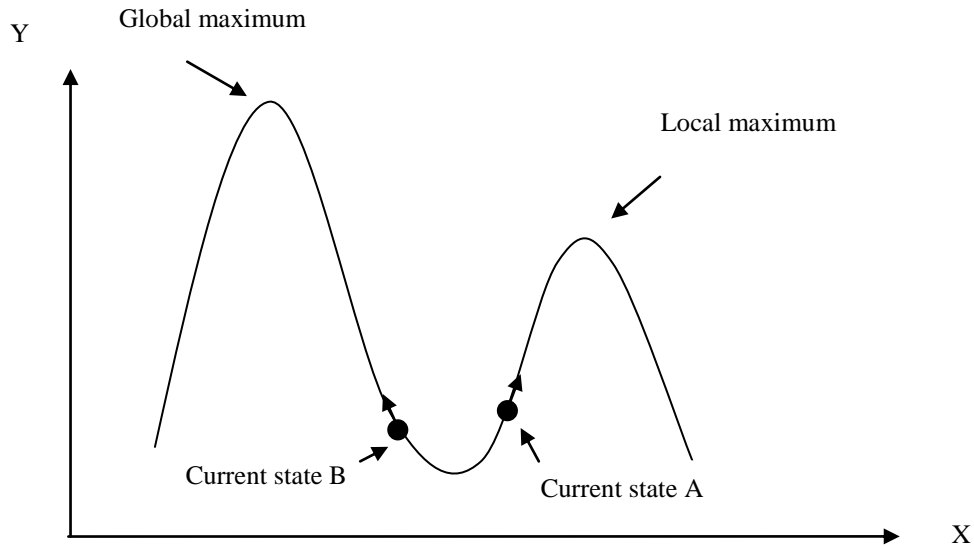


Figure 4-1: Hill climbing model

## 4.2 PSO-HC for CR networks

To improve the probability of detection in CR networks, a PSO-HC hybrid is proposed. The PSO-HC hybrid improves the global search and increases the accuracy. The optimal position and velocity vectors are obtained in one iteration operation. After that, the hill climbing algorithm is applied to further optimize the velocity vector. This is done by applying hill climbing algorithm to each particle velocity vector at iteration  $t$ . A random value is chosen from each particle velocity vector to compare between the neighbors of the chosen value. If one of the neighbors' value is greater than the current state value, then the current state will move to the next neighbor. The process is repeated whenever there is a higher value found between the neighbors until no further higher values encountered. The highest value found will be returned to the current state and replaced by

its newly found value. The results of PSO-HC give better improvement than the conventional PSO.

The hill climbing algorithm process applied to the PSO is expressed as:

- 1) Pick a random number in the particle velocity vector ( $v_{id}^t$ ) at iteration  $t$ .
- 2) Consider all current state's neighbors in the particle velocity vector ( $v_{id}^t$ ) at iteration  $t$ .
- 3) Choose the neighbor which has a higher value and move to that state.
- 4) Repeat steps (2-4) until all neighboring states have lower values in the same particle velocity vector ( $v_{id}^t$ ) at iteration  $t$ .
- 5) Return the current state as the solution state within the particle velocity vector ( $v_{id}^t$ ) at iteration  $t$  i.e., replace the current state value by the higher value found through the search.

The PSO-HC hybrid procedure can be described as:

- 1) Generate the position and velocity vectors  $x_{id}^t$  and  $v_{id}^t$  randomly at  $t=0$ .  $x_{id}^t \in [0,1]$  and  $v_{id}^t \in [-V_{max}, +V_{max}]$ ,  $1 \leq d \leq M$ ,  $1 \leq i \leq S$  where  $S$  is the total number of particles.
- 2) Exchange  $x_{id}^t$  by  $x_{id}^t / \sum_{d=1}^M x_{id}^t$
- 3) Evaluate fitness value for each particle in population then set  $\mathbf{p}_i^t = [x_{i1}^t, x_{i2}^t, \dots, x_{iM}^t]^T$ ,  $\mathbf{p}_b^t = [x_{b1}^t, x_{b2}^t, \dots, x_{bM}^t]^T$ .  $b$  represents the index of the particle which has the highest fitness value.
- 4) Update  $v_{id}^t$  using equation (3.3) at  $t=t+1$ . If  $v_{id}^t > V_{max}$ , let  $v_{id}^t = V_{max}$ . If  $v_{id}^t < -V_{max}$ , let  $v_{id}^t = -V_{max}$ .

- 5) Update  $x_{id}^t$  using equation (3.4).
- 6) Exchange  $x_{id}^t$  by  $x_{id}^t / \sum_{d=1}^M x_{id}^t$ .
- 7) Apply hill climbing algorithm on the velocity vector  $\mathbf{v}_i^t = [v_{i1}^t, v_{i2}^t, \dots, v_{iM}^t]^T$  at iteration  $t$  for each velocity particle to optimize it.
- 8) Evaluate fitness value for each particle in population. If the fitness value of particle  $i$  is larger than  $\mathbf{p}_i^{t-1}$  fitness value, let  $\mathbf{p}_i^t = [x_{i1}^t, x_{i2}^t, \dots, x_{iM}^t]^T$  otherwise let  $\mathbf{p}_i^t = \mathbf{p}_i^{t-1}$ . If the fitness value of particle  $i$  is larger than  $\mathbf{p}_b^{t-1}$  fitness value, let  $\mathbf{p}_b^t = [x_{i1}^t, x_{i2}^t, \dots, x_{iM}^t]^T$  otherwise let  $\mathbf{p}_b^t = \mathbf{p}_b^{t-1}$ .
- 9) Terminate the algorithm if the maximum number of iteration is reached, otherwise return to step 4.

Figure 4.2 shows the flowchart of PSO-HC hybrid:

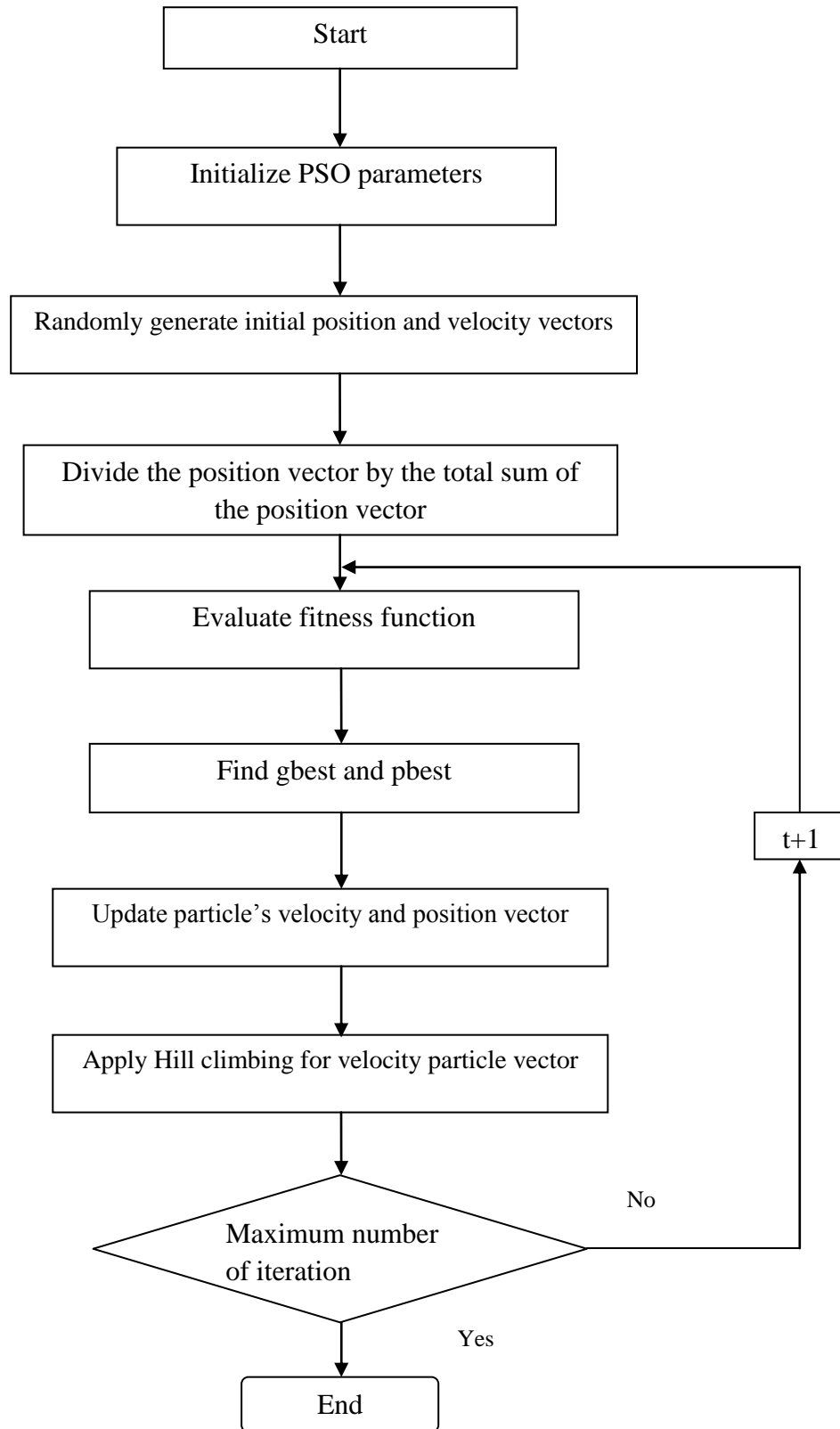


Figure 4-2: Flowchart of PSO-HC hybrid

### 4.3 Simulation Results for PSO-HC Fixed SNR

The energy detector performance is simulated for three cooperating SUs ( $M = 3$ ) with various channels including AWGN, Rayleigh, Nakagami, Gamma, Lognormal, Nakagami-Lognormal composite and Nakagami-Gamma composite using ROC curves. The time-bandwidth product is taken as  $m = 5$ , hence the number of samples become  $N = 10$ . The fixed SNR is set at 10 dB. The PSO parameters are taken as: the number of particles  $S = 60$ , the inertia weight  $\omega = 1$ , the cognitive coefficient  $c_1 = 2$ , the social coefficient  $c_2 = 2$  and the maximum number of iterations  $t = 30$ . The threshold at the fusion center is calculated from (3.). PSO-HC hybrid is applied among cooperating SUs to improve the detection performance. The performance of PSO and PSO-HC hybrid techniques are compared to each other. The results are produced using 1000 Monte-Carlo simulations.

### 4.3.1 AWGN Channel

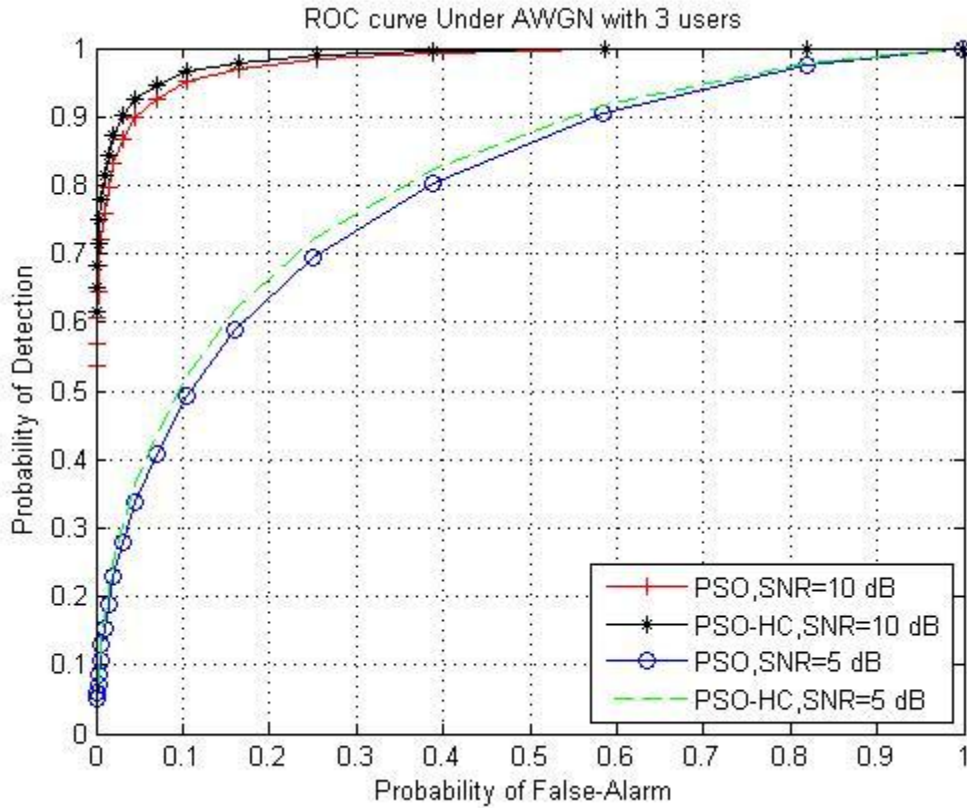


Figure 4-3: ROC curves for ED under AWGN channel with three cooperating SUs using PSO and PSO-HC

The performance of detection probabilities are compared between PSO and PSO-HC algorithms. Both ROC curves are plotted in Figure 4.3 each with three cooperating SUs under AWGN channel with SNRs of 5 dB and 10 dB across different probability of false alarm values. When the probability of false alarm is 0.2, the probabilities of detection using PSO algorithm and PSO-HC hybrid are 0.63 and 0.67 respectively at SNR of 10 dB. At SNR of 5 dB, the probabilities of detection are 0.63 and 0.67 for PSO algorithm and PSO-HC hybrid, respectively



### 4.3.2 Rayleigh Fading Channel

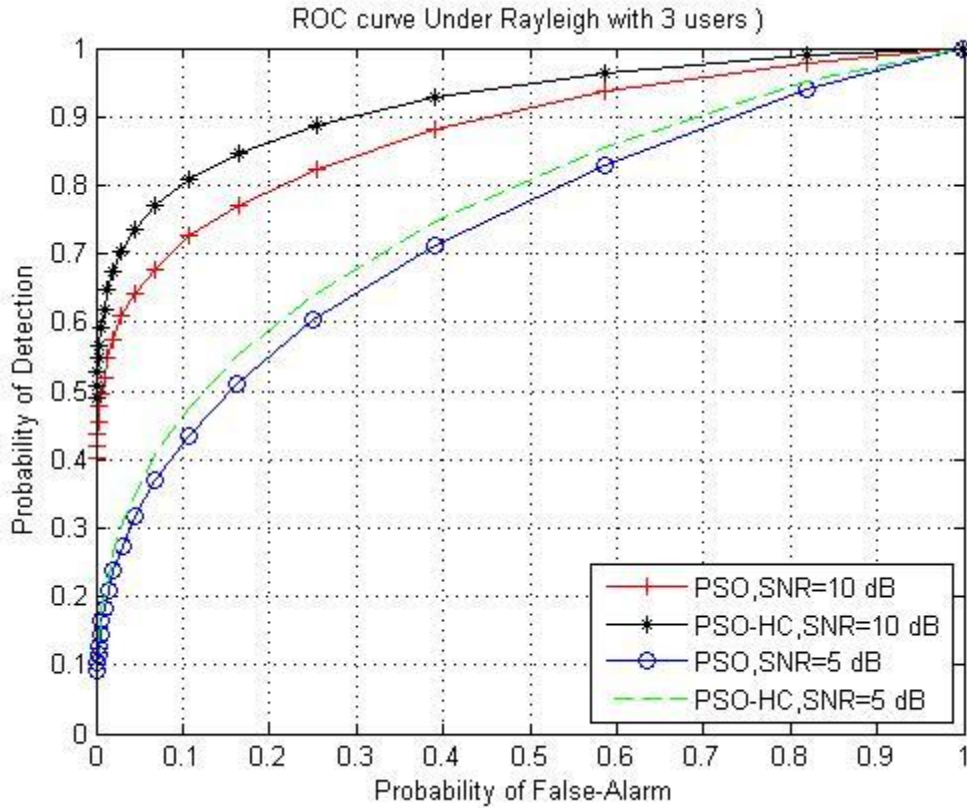


Figure 4-4: ROC curves for ED under Rayleigh channel with three cooperating SUs using PSO and PSO-HC

The performances of signal detection are compared between PSO and PSO-HC algorithms. Both ROC curves using PSO algorithm and PSO-HC hybrid are plotted in Figure 4.4 each with three cooperating SUs for under Rayleigh channel with SNRs of 5 dB and 10 dB across different probability of false alarm values. When the probability of false alarm is 0.1, the probabilities of detection for PSO-HC hybrid at SNRs of 5 dB and 10 dB are 0.46 and 0.80, respectively. For PSO, the probabilities of detection at SNRs of 5 dB and 10 dB are 0.43 and 0.72, respectively.

### 4.3.3 Nakagami Fading Channel

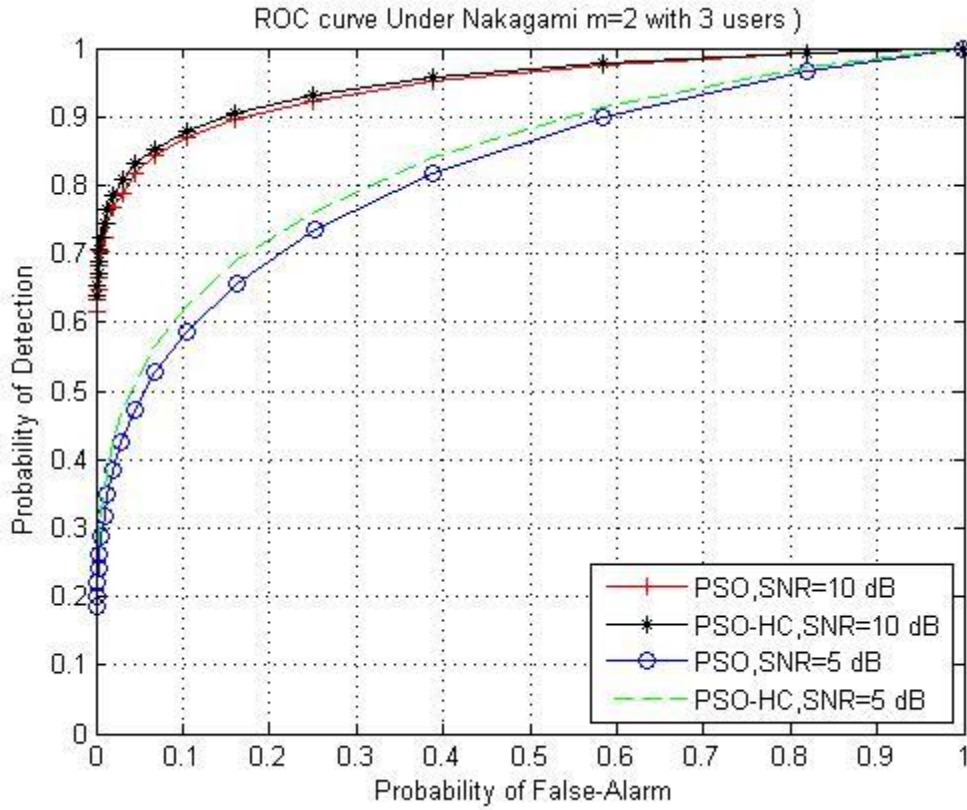
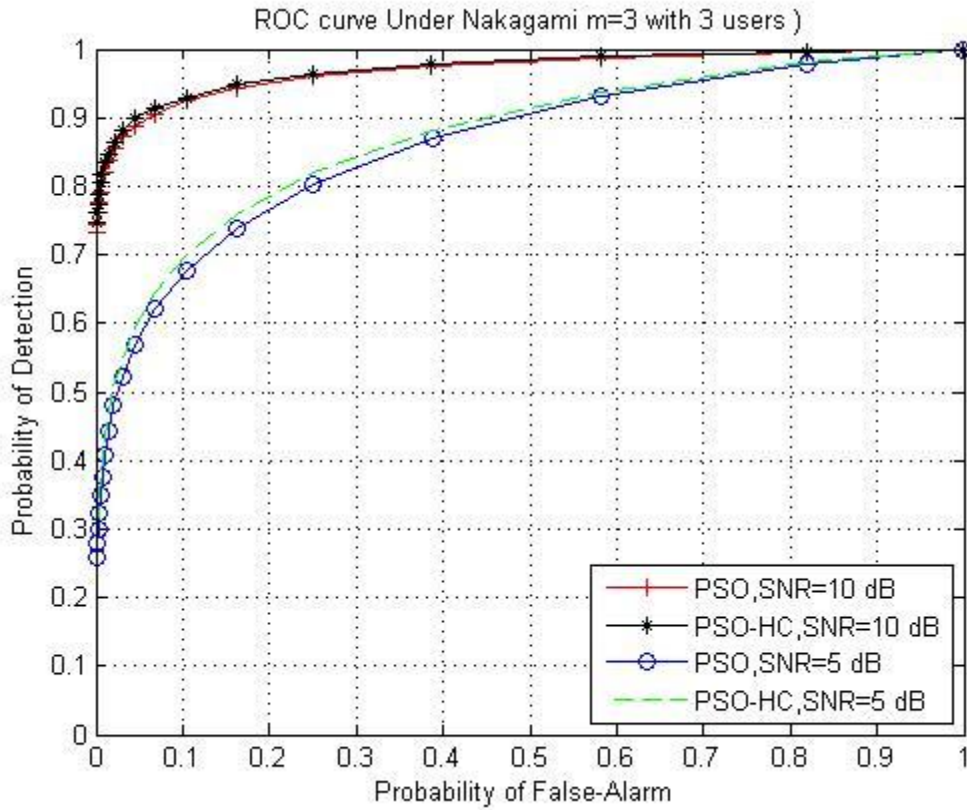


Figure 4-5: ROC curves for ED under Nakagami channel with three cooperating SUs and  $m=2$  using PSO and PSO-HC

The performance of detection probabilities are compared between PSO and PSO-HC algorithms. Both ROC curves are plotted in Figure 4.5 each with three cooperating SUs under Nakagami channel with  $m = 2$  and SNRs of 5 dB and 10 dB across different probability of false alarm values. When the probability of false alarm is 0.1, the probabilities of detection for PSO-HC hybrid at SNRs of 5 dB and 10 dB are 0.51 and 0.87, respectively. For PSO, the probabilities of detection at SNRs of 5 dB and 10 dB are 0.49 and 0.86, respectively.



**Figure 4-6: ROC curves for ED under Nakagami channel with three cooperating SUs and  $m=3$  using PSO and PSO-HC**

The performance of detection probabilities are compared between PSO and PSO-HC algorithms. Both ROC curves are plotted in Figure 4.6 each with three cooperating SUs under Nakagami channel with  $m = 2$  and SNRs of 5 dB and 10 dB across different probability of false alarm values. When the probability of false alarm is 0.1, the probabilities of detection for PSO-HC hybrid at SNRs of 5 dB and 10 dB are 0.70 and 0.93, respectively. For PSO, the probabilities of detection at SNRs of 5 dB and 10 dB are 0.67 and 0.93, respectively.

### 4.3.4 Lognormal Shadowing Channel

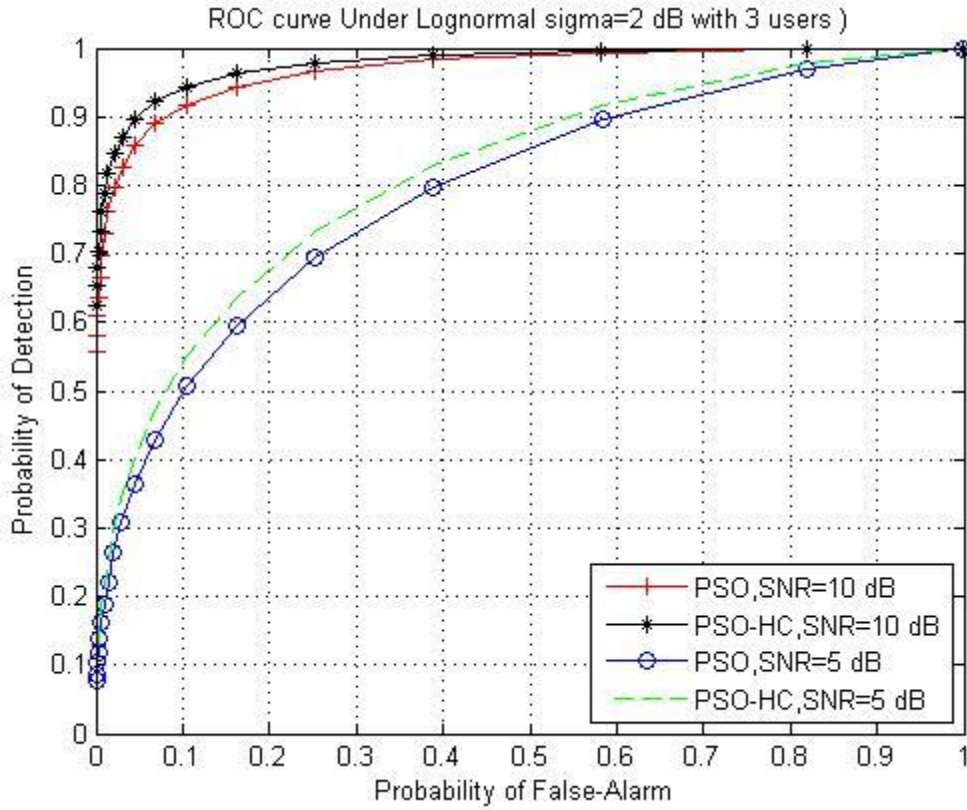


Figure 4-7: ROC curves for ED under Lognormal channel with three cooperating SUs and  $\sigma_{dB} = 2$  dB using PSO and PSO-HC

Figure 4.7 represents the ROC curves of three cooperating SUs for ED using PSO algorithm and PSO-HC hybrid under Lognormal channel with  $\sigma_{dB} = 2$  dB and SNR SNRs of 5 dB and 10 dB across different probability of false alarm values. When the probability of false alarm is 0.1, the probabilities of detection for PSO-HC hybrid at SNRs of 5 dB and 10 dB are 0.55 and 0.94, respectively. For PSO, the probabilities of detection at SNRs of 5 dB and 10 dB are 0.50 and 0.91, respectively.

### 4.3.5 Gamma Fading Channel

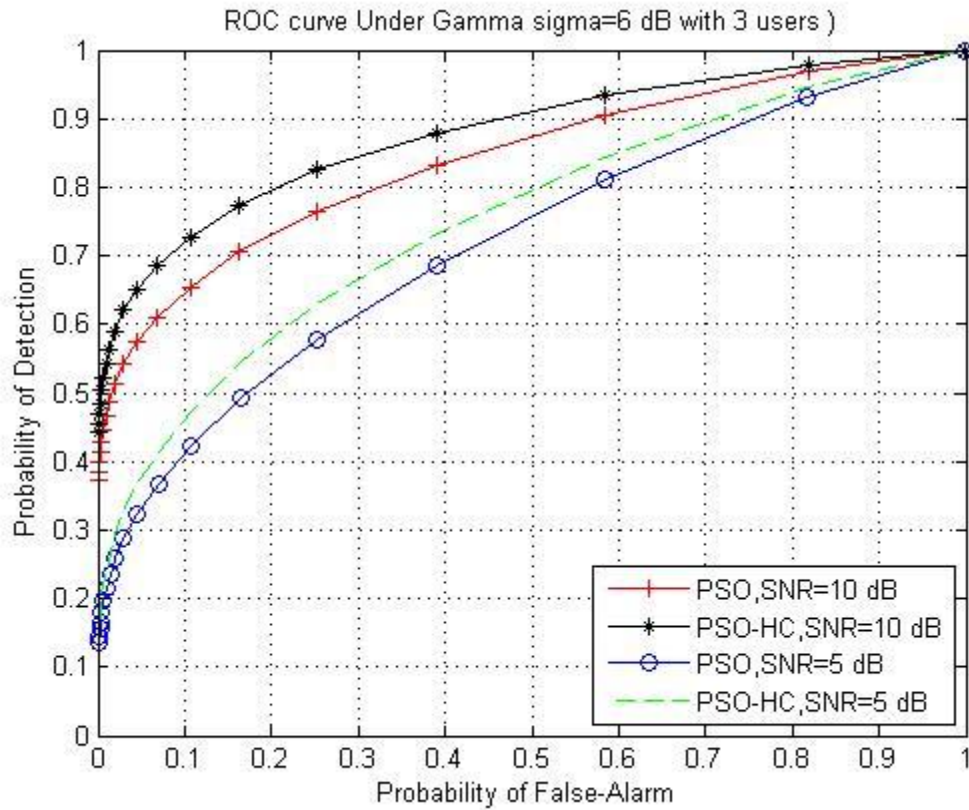


Figure 4-8: ROC curves for ED under Gamma channel with three cooperating SUs and  $\sigma_{dB} = 6$  dB using PSO and PSO-HC

Figure 4.8 represents the ROC curves of three cooperating SUs for ED using PSO algorithm and PSO-HC hybrid under Gamma channel with  $\sigma_{dB} = 6$  dB and SNRs of 5 dB and 10 dB across different probability of false alarm values. When the probability of false alarm is 0.1, the probabilities of detection for PSO-HC hybrid at SNRs of 5 dB and 10 dB are 0.47 and 0.72, respectively. For PSO, the probabilities of detection at SNRs of 5 dB and 10 dB are 0.41 and 0.65, respectively.

### 4.3.6 Nakagami – Lognormal Composite Fading Channel

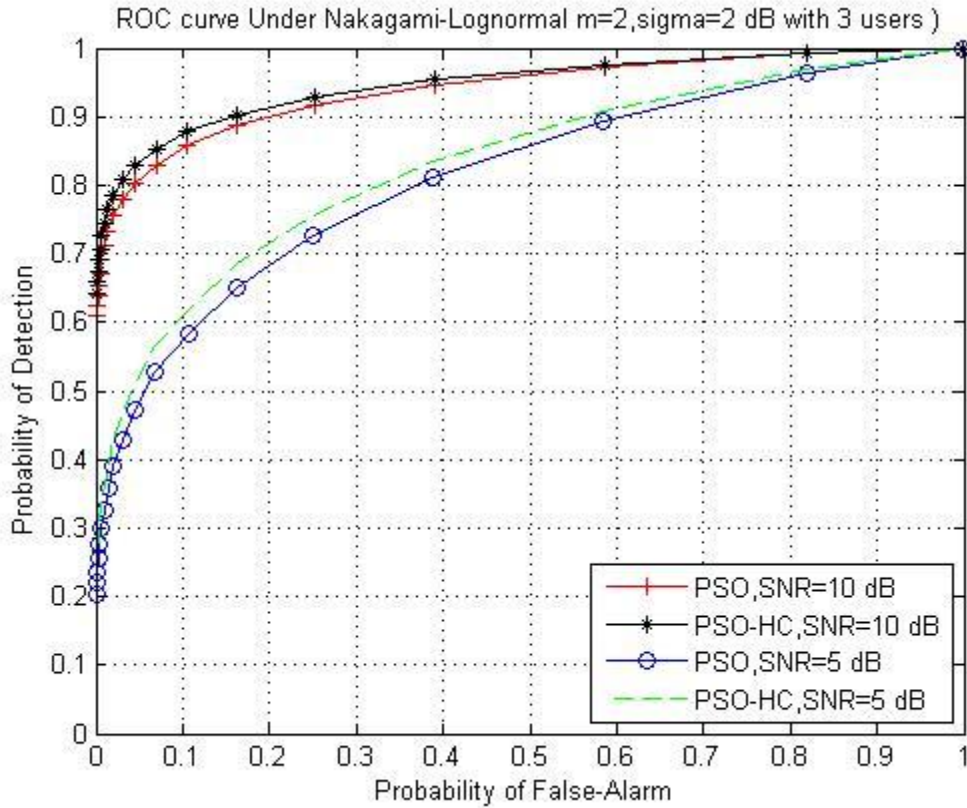


Figure 4-9: ROC curves for ED under Nakagami-Lognormal channel with three cooperating SUs,  $m = 2$  and  $\sigma_{dB} = 2$  dB using PSO and PSO-HC

The ROC curves of three cooperating SUs for ED using PSO algorithm and PSO-HC hybrid under Nakagami-Lognormal channel with  $m = 2$ ,  $\sigma_{dB} = 2$  dB and SNRs of 5 dB and 10 dB across different probability of false alarm values are represented in Figure 4.9. When the probability of false alarm is 0.1, the probabilities of detection using PSO algorithm and PSO-HC hybrid are 0.86 and 0.88 respectively at SNR of 10 dB. For SNR of 5 dB, the probabilities of detection are 0.57 and 0.61 for PSO algorithm and PSO-HC hybrid, respectively.

### 4.3.7 Nakagami – Gamma Composite Fading Channel

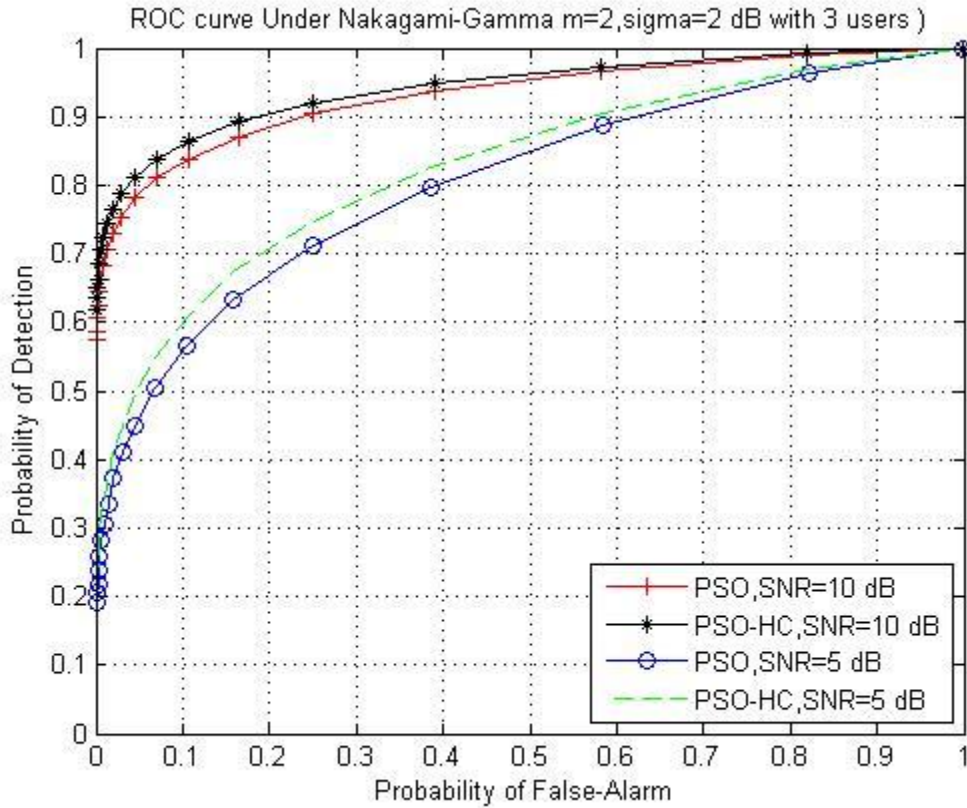


Figure 4-10: ROC curves for ED under Nakagami-Gamma channel with three cooperating SUs,  $m = 2$  and  $\sigma_{dB} = 2$  dB using PSO and PSO-HC

The ROC curves of three cooperating SUs for ED using PSO algorithm and PSO-HC hybrid under Nakagami-Gamma channel with  $m = 2$ ,  $\sigma_{dB} = 2$  dB and SNRs of 5 dB and 10 dB across different probability of false alarm values are represented in Figure 4.10. When the probability of false alarm is 0.1, the probabilities of detection using PSO algorithm and PSO-HC hybrid are 0.83 and 0.86 respectively at SNR of 10 dB. For SNR of 5 dB, the probabilities of detection are 0.56 and 0.60 for PSO algorithm and PSO-HC hybrid, respectively.

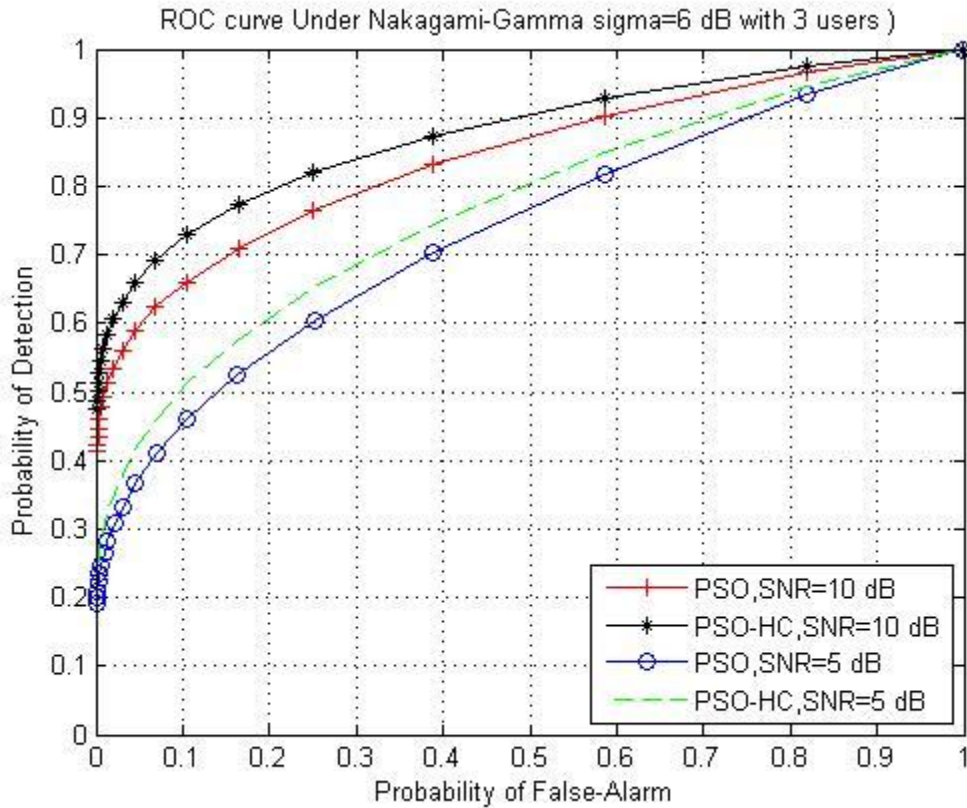


Figure 4-11: ROC curves for ED under Nakagami-Gamma channel with three cooperating SUs,  $m = 2$  and  $\sigma_{dB} = 6$  dB using PSO and PSO-HC

The ROC curves of three cooperating SUs for ED using PSO algorithm and PSO-HC hybrid under Nakagami-Gamma channel with  $m = 2$ ,  $\sigma_{dB} = 6$  dB and SNRs of 5 dB and 10 dB across different probability of false alarm values are represented in Figure 4.11. When the probability of false alarm is 0.1, the probabilities of detection using PSO algorithm and PSO-HC hybrid are 0.73 and 0.65 respectively at SNR of 10 dB. For SNR of 5 dB, the probabilities of detection are 0.46 and 0.51 for PSO algorithm and PSO-HC hybrid, respectively.



#### 4.4 Simulation Results for PSO-HC Fixed Pf

The energy detector performance is simulated for three cooperating SUs ( $M = 3$ ) with various channels including AWGN, Rayleigh, Nakagami, Gamma, Lognormal, Nakagami-Lognormal composite and Nakagami-Gamma composite using ROC curves. The time-bandwidth product is taken as  $m = 5$ , hence the number of samples become  $N = 10$ . The fixed false alarm probability is set at 0.1. PSO-HC hybrid is applied among cooperating users to improve the detection performance. The PSO parameters are taken as: the number of particles  $S = 60$ , the inertia weight  $\omega = 1$ , the cognitive coefficient  $c_1 = 2$ , the social coefficient  $c_2 = 2$  and the maximum number of iterations  $t = 30$ . The threshold at the fusion center is calculated from (3.11). PSO-HC hybrid is applied among cooperating SUs to improve the detection performance. The performance of PSO and PSO-HC hybrid techniques are compared to each other. The results are produced using 1000 Monte-Carlo simulations.

#### 4.4.1 AWGN Channel

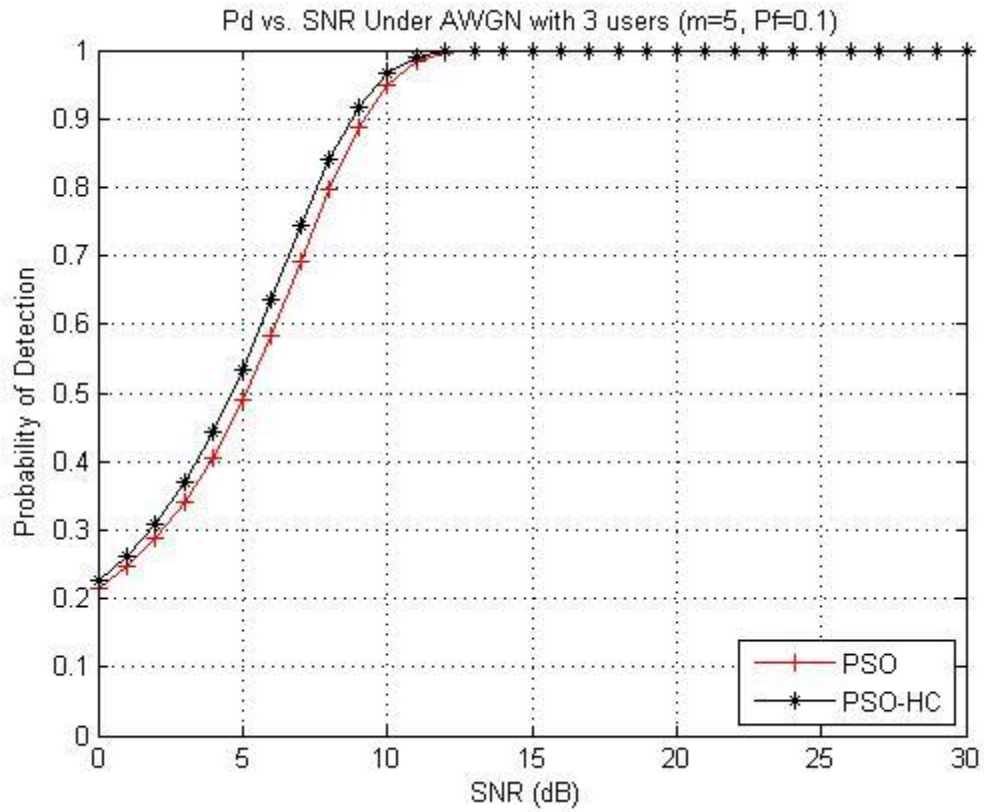


Figure 4-12: Probability of detection vs. SNR curves for ED under AWGN channel with three cooperating SUs and false alarm probability of 0.1 using PSO and PSO-HC

The performance of detection probabilities are compared between PSO and PSO-HC algorithms. Both ROC curves are plotted in Figure 4.12 each with three cooperating SUs under AWGN channel for different SNR from [0-30] dB. When the SNR is 10 dB, the probabilities of detection using PSO algorithm and PSO-HC hybrid are 0.95 and 0.98 respectively.

#### 4.4.2 Rayleigh Fading Channel

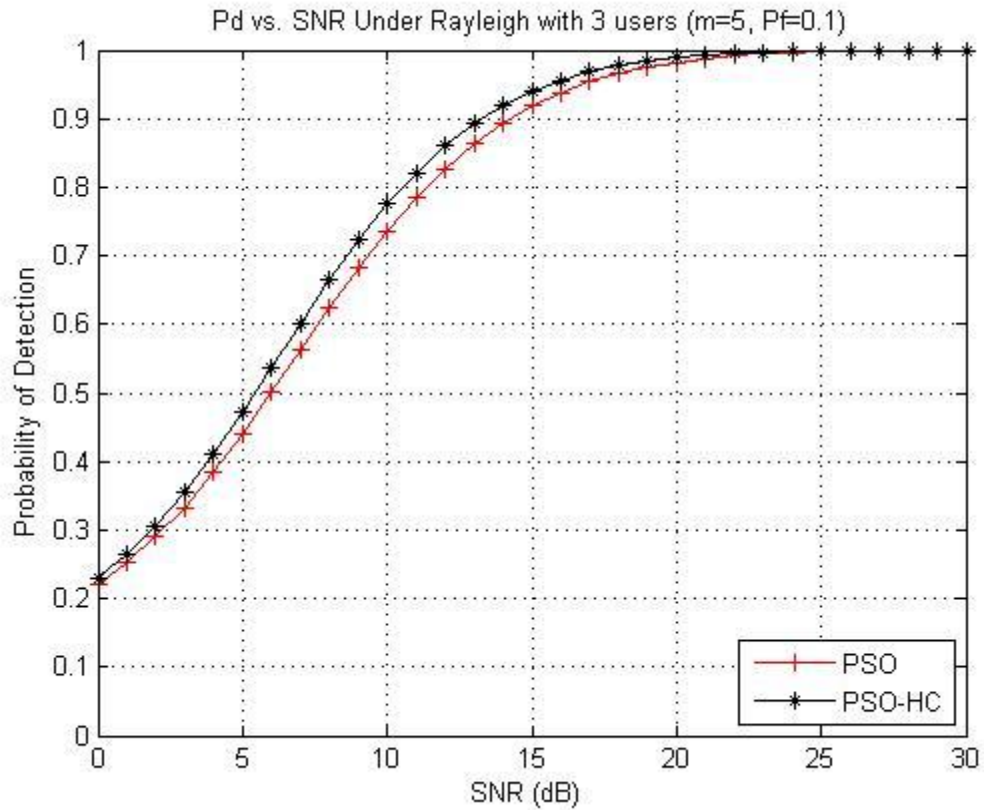


Figure 4-13: Probability of detection vs. SNR curves for ED under Rayleigh channel with three cooperating SUs and false alarm probability of 0.1 using PSO and PSO-HC

The performance of detection probabilities are compared between PSO and PSO-HC algorithms. Both ROC curves are plotted in Figure 4.13 each with three cooperating SUs under Rayleigh channel for different SNR from [0-30] dB. When the SNR is 10 dB, the probabilities of detection using PSO algorithm and PSO-HC hybrid are 0.73 and 0.78 respectively.

### 4.4.3 Nakagami Fading Channel

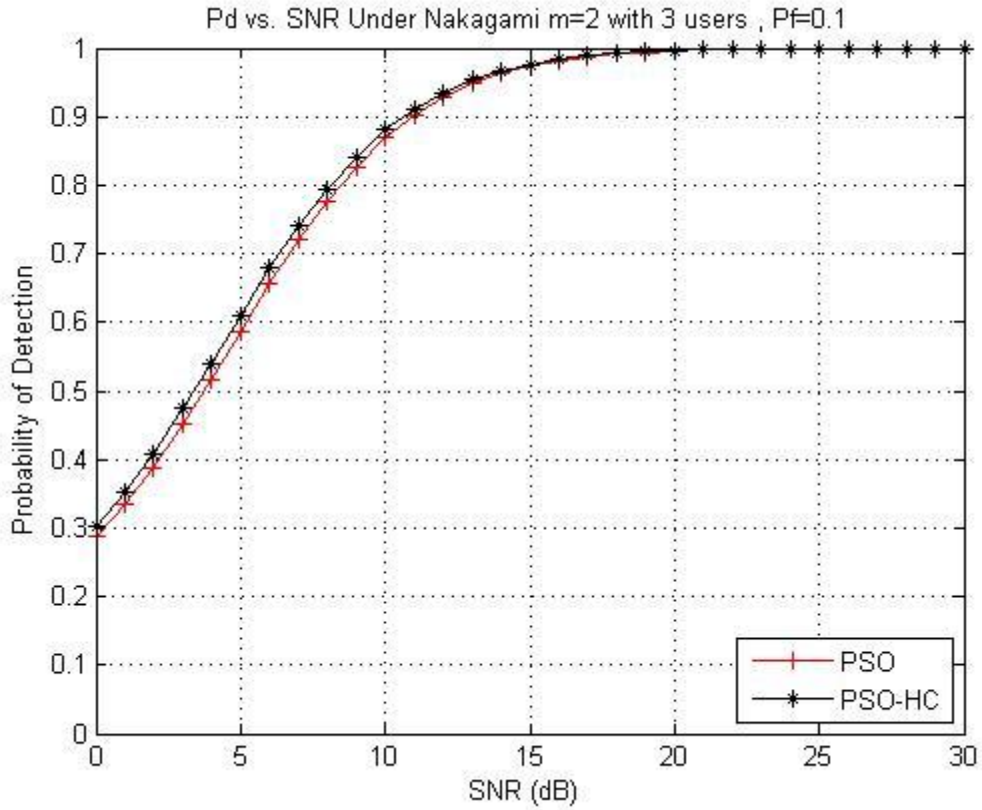
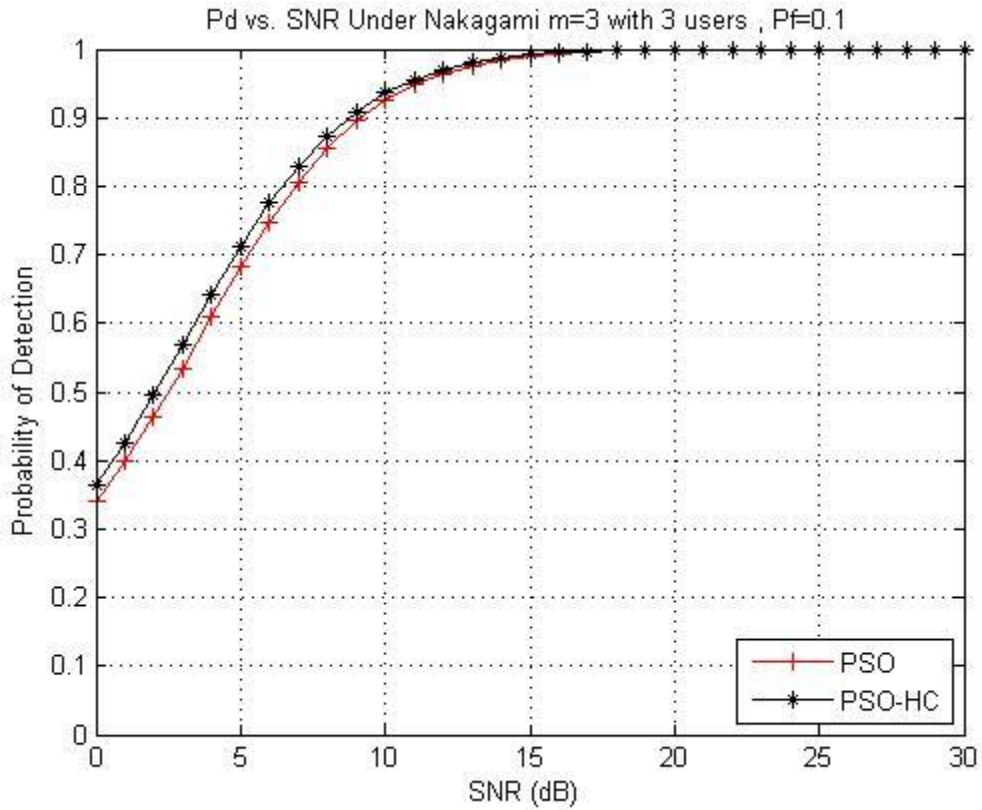


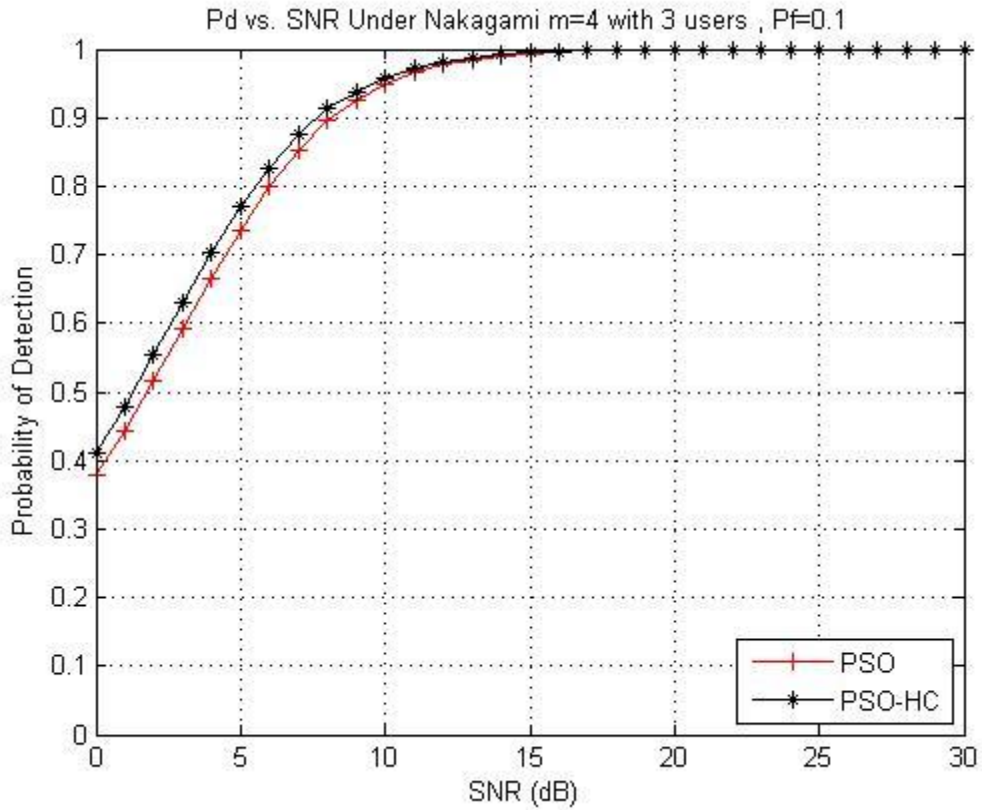
Figure 4-14: Probability of detection vs. SNR curves for ED under Nakagami channel with three cooperating SUs,  $m=2$  and false alarm probability of 0.1 using PSO and PSO-HC

Figure 4.14 represents the ED performance of three cooperating SUs for using PSO algorithm and PSO-HC hybrid under Nakagami channel with  $m = 2$  for different SNR from [0-30] dB. When the SNR is 10 dB, the probabilities of detection using PSO algorithm and PSO-HC hybrid are 0.87 and 0.88 respectively.



**Figure 4-15: Probability of detection vs. SNR curves for ED under Nakagami channel with three cooperating SUs,  $m = 3$  and false alarm probability of 0.1 using PSO and PSO-HC**

Figure 4.15 represents the ED performance of three cooperating SUs for using PSO algorithm and PSO-HC hybrid under Nakagami channel with  $m = 3$  for different SNR from [0-30] dB. When the SNR is 10 dB, the probabilities of detection using PSO algorithm and PSO-HC hybrid are 0.93 and 0.94 respectively.



**Figure 4-16: Probability of detection vs. SNR curves for ED under Nakagami channel with three cooperating SUs,  $m = 4$  and false alarm probability of 0.1 using PSO and PSO-HC**

Figure 4.16 represents the ED performance of three cooperating SUs for using PSO algorithm and PSO-HC hybrid under Nakagami channel with  $m = 4$  for different SNR from [0-30] dB. When the SNR is 10 dB, the probabilities of detection using PSO algorithm and PSO-HC hybrid are 0.95 and 0.96 respectively.

#### 4.4.4 Lognormal Shadowing Channel

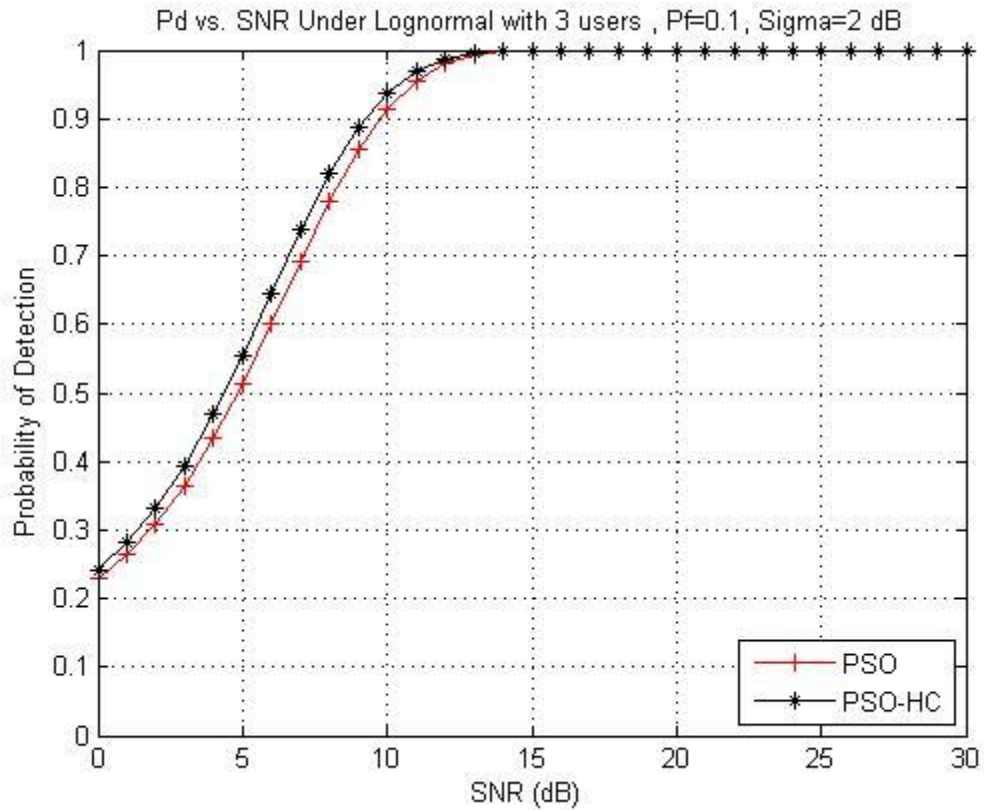


Figure 4-17: Probability of detection vs. SNR curves for ED under Lognormal channel with three cooperating SUs,  $\sigma_{dB} = 2$  dB and false alarm probability of 0.1 using PSO and PSO-HC

The ED performance of three cooperating SUs for using PSO algorithm and PSO-HC hybrid under Lognormal channel with  $\sigma_{dB} = 2$  dB for different SNR from [0-30] dB is shown in Figure 4.17. When the SNR is 10 dB, the probabilities of detection using PSO algorithm and PSO-HC hybrid are 0.91 and 0.94 respectively.

#### 4.4.5 Gamma Fading Channel

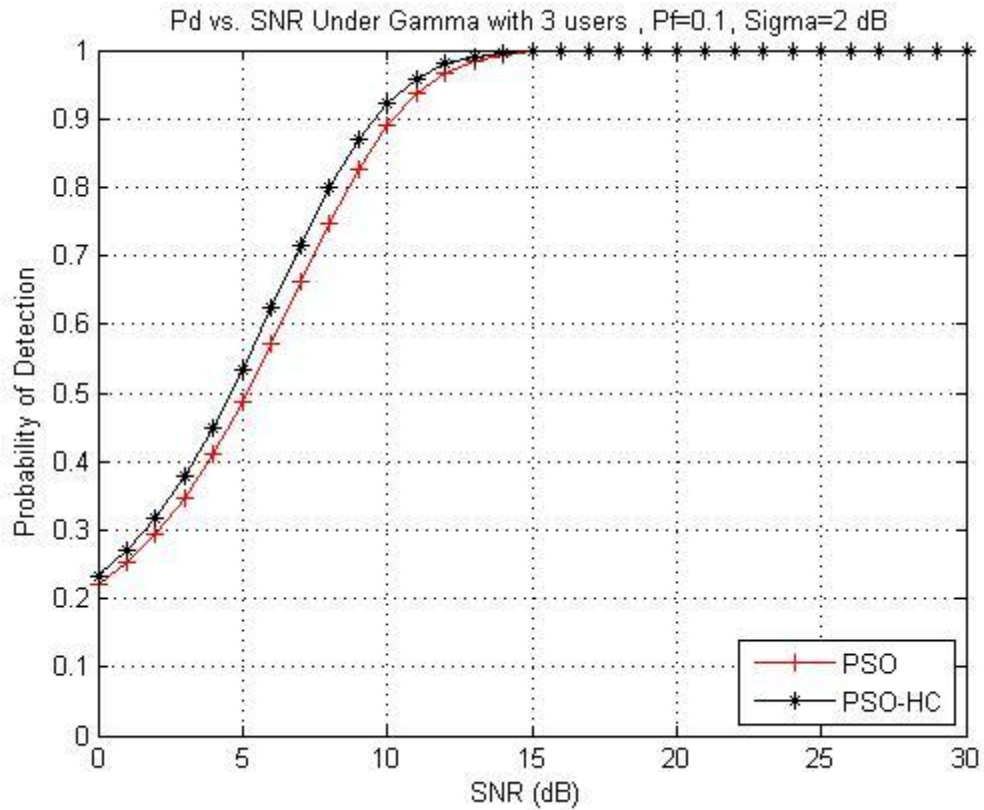
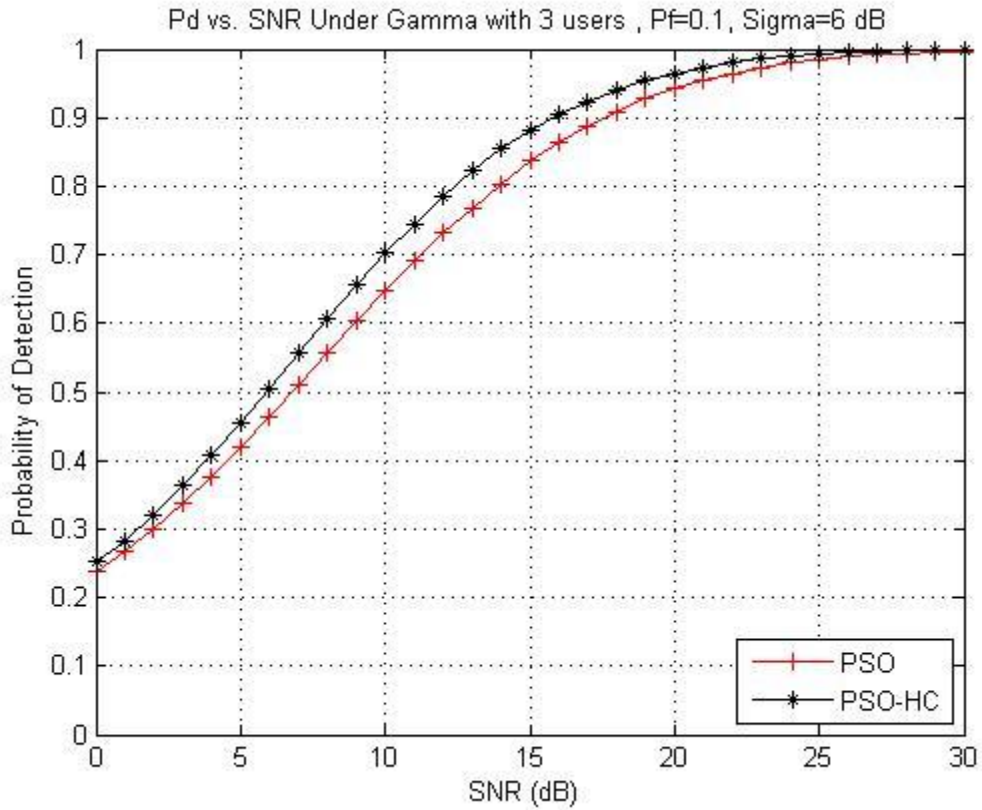


Figure 4-18: Probability of detection vs. SNR curves for ED under Gamma channel with three cooperating SUs,  $\sigma_{dB}=2$  dB and false alarm probability of 0.1 using PSO and PSO-HC

The ED performance of three cooperating SUs for using PSO algorithm and PSO-HC hybrid under Gamma channel with  $\sigma_{dB} = 2$  dB for different SNR from [0-30] dB is shown in Figure 4.18. When the SNR is 10 dB, the probabilities of detection using PSO algorithm and PSO-HC hybrid are 0.89 and 0.93 respectively.





**Figure 4-19: Probability of detection vs. SNR curves for ED under Gamma channel with three cooperating SUs,  $\sigma_{dB} = 6$  dB and false alarm probability of 0.1 using PSO and PSO-HC**

The ED performance of three cooperating SUs for using PSO algorithm and PSO-HC hybrid under Gamma channel with  $\sigma_{dB} = 6$  dB for different SNR from [0-30] dB is shown in Figure 4.19. When the SNR is 10 dB, the probabilities of detection using PSO algorithm and PSO-HC hybrid are 0.65 and 0.70 respectively.

#### 4.4.6 Nakagami – Lognormal Composite Fading Channel

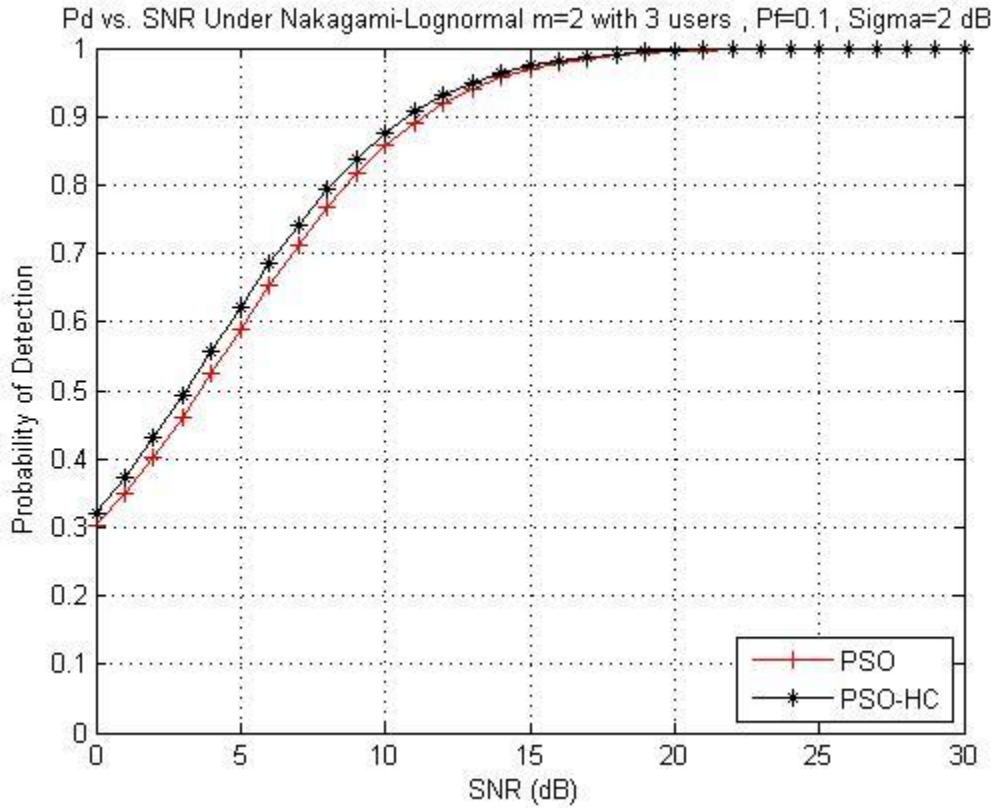


Figure 4-20: Probability of detection vs. SNR curves for ED under Nakagami-Lognormal channel with three cooperating SUs,  $m=2$ ,  $\sigma_{dB}=2$  dB and false alarm probability of 0.1 using PSO and PSO-HC

The ED performance of three cooperating SUs for using PSO algorithm and PSO-HC hybrid under Nakagami-Lognormal channel with  $m = 2$  and  $\sigma_{dB} = 2$  dB for different SNR from [0-30] dB is shown in Figure 4.20. When the SNR is 10 dB, the probabilities of detection using PSO algorithm and PSO-HC hybrid are 0.86 and 0.88 respectively.

#### 4.4.7 Nakagami – Gamma Composite Fading Channel

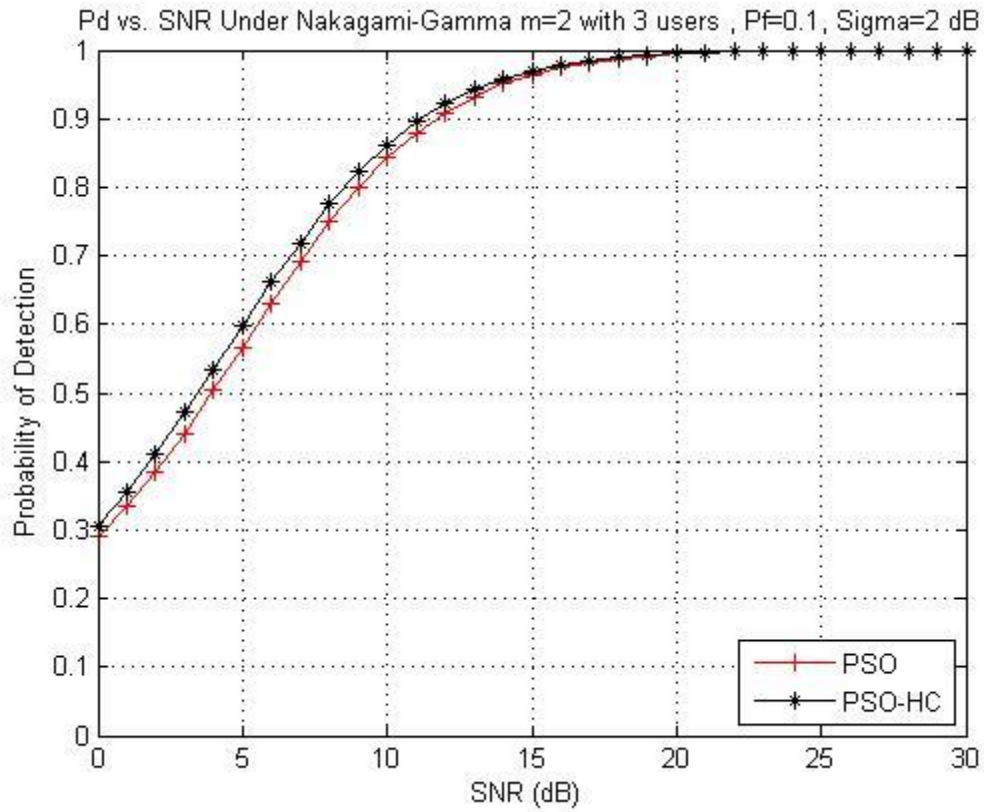
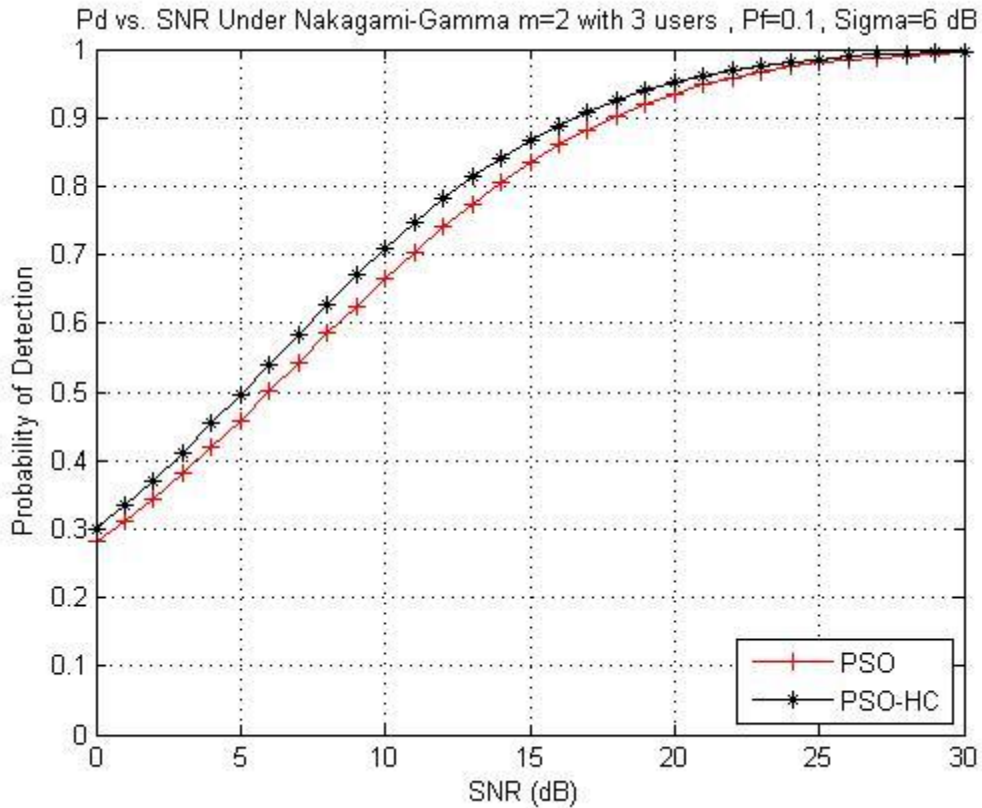


Figure 4-21: Probability of detection vs. SNR curves for ED under Nakagami-Gamma channel with three cooperating SUs,  $m=2$ ,  $\sigma_{dB}=2$  dB and false alarm probability of 0.1 using PSO and PSO-HC

Figure 4.21 shows the ED performance of three cooperating SUs for using PSO algorithm and PSO-HC hybrid under Nakagami-Gamma channel with  $m = 2$  and  $\sigma_{dB} = 2$  dB for different SNR from [0-30] dB. When the SNR is 10 dB, the probabilities of detection using PSO algorithm and PSO-HC hybrid are 0.85 and 0.86 respectively.



**Figure 4-22: Probability of detection vs. SNR curves for ED under Nakagami-Gamma channel with three cooperating SUs,  $m=2$ ,  $\sigma_{dB}=6$  dB and false alarm probability of 0.1 using PSO and PSO-HC**

Figure 4.22 shows the ED performance of three cooperating SUs for using PSO algorithm and PSO-HC hybrid under Nakagami-Gamma channel with  $m = 2$  and  $\sigma_{dB} = 6$  dB for different SNR from [0-30] dB. When the SNR is 10 dB, the probabilities of detection using PSO algorithm and PSO-HC hybrid are 0.67 and 0.71 respectively.

## 4.5 Simulation Results for PSO-HC Fixed SNR

The performance analysis of detection probability is summarized for single SU in Table 4.1, four cooperating SUs using OR, AND and Majority rules in Table 4.2, three cooperating SUs using PSO in Table 4.3 and three cooperating SUs using PSO-HC hybrid in Table 4.4.

**Table 4.1: performance analysis of detection probability summary for single SU**

SNR (dB)	AWGN	Rayleigh	Nakagami ( $m=3$ )	Lognormal ( $\sigma_{dB}=2$ dB)	Gamma ( $\sigma_{dB}=2$ dB)	Nakagami-Lognormal ( $m=2, \sigma_{dB}=2$ dB)	Nakagami-Gamma ( $m=2, \sigma_{dB}=2$ dB)
5	0.50	0.40	0.70	0.10	0.45	0.6	0.45
10	0.94	0.7	0.92	0.6	0.88	0.83	0.81

**Table 4.2: performance analysis of detection probability summary for four cooperating SUs using OR, AND and Majority rules**

SNR (dB)	AWGN	Rayleigh	Nakagami ( $m=2$ )	Lognormal ( $\sigma_{dB}=2$ dB)	Gamma ( $\sigma_{dB}=2$ dB)	Nakagami-Lognormal ( $m=2, \sigma_{dB}=2$ dB)	Nakagami-Gamma ( $m=2, \sigma_{dB}=2$ dB)
OR	0.9998	0.98	0.95	0.9992	0.9984	0.955	0.95
AND	0.60	0.20	0.61	0.50	0.40	0.58	0.52
Majority	0.993	0.84	0.87	0.982	0.271	0.88	0.86

**Table 4.3: performance analysis of detection probability summary for three cooperating SUs using PSO**

SNR (dB)	AWGN	Rayleigh	Nakagami ( $m=2$ )	Lognormal ( $\sigma_{dB}=2$ dB)	Gamma ( $\sigma_{dB}=6$ dB)	Nakagami-Lognormal ( $m=2, \sigma_{dB}=2$ dB)	Nakagami-Gamma ( $m=2, \sigma_{dB}=6$ dB)
5	0.49	0.43	0.49	0.50	0.41	0.57	0.46
10	0.96	0.72	0.86	0.91	0.65	0.86	0.65

**Table 4.4: performance analysis of detection probability summary for three cooperating SUs using PSO-HC hybrid**

SNR (dB)	AWGN	Rayleigh	Nakagami ( $m=2$ )	Lognormal ( $\sigma_{dB} = 2$ dB)	Gamma ( $\sigma_{dB} = 6$ dB)	Nakagami-Lognormal ( $m=2, \sigma_{dB} = 2$ dB)	Nakagami-Gamma ( $m=2, \sigma_{dB}=6$ dB)
5	0.51	0.46	0.51	0.55	0.47	0.61	0.51
10	0.97	0.80	0.87	0.94	0.72	0.88	0.73

## CHAPTER 5

### CONCLUSION

#### 5.1 Conclusion

CR technology makes efficient use of the radio spectrum by using the spectrum in an opportunistic manner. Also PSO is an efficient optimization method to solve problems. This thesis proposes a new PSO-HC hybrid method where it combines PSO algorithm and HC algorithm. PSO-HC hybrid is implemented in CR networks to improve the detection probability performance using energy detection.

Simulation results show the performance of PSO-HC hybrid across different fading channels. PSO-HC hybrid is compared to the conventional PSO. In non-fading/ low fading channels, the performance improves a little over the conventional PSO. This can be seen in AWGN channel and Nakagami fading channel with higher fading parameter  $m$  results. On the other hand, in deep fading channels, the performance improves a greatly over the conventional PSO. This can be seen in results of Rayleigh channel and Nakagami-Gamma fading channel with higher spread. PSO-HC hybrid performs well in deep fading channels and it is easy to implement especially when the time is limited.

## 5.2 Future Work

The energy detector performance is simulated for using various channels including AWGN, Rayleigh, Nakagami, Gamma, Lognormal, Nakagami-Lognormal composite and Nakagami-Gamma composite using ROC and complementary ROC curves. This work can be extended by implementing double threshold in energy detector where two thresholds are used to determine the PU signal presence. This method shows improvement in energy detection performance over the energy detection performance when using single threshold method. Also, in our work we have considered flat fading channels for the various fading channels used. The work can also be extended to frequency selective fading environments to see how it affects the detection performance of the energy detector. The signals processed through energy detector are assumed to be i.i.d where the ED is optimal is this case. However, the ED is not optimal for correlated signals. To solve this problem, one can use other detection methods e.g., maximum eigenvalue detection where it uses the maximum eigenvalue of a sample covariance matrix of the received signal as test statistics. This method gives better detection performance than ED method when signals are correlated.



## References

- [1] Ghasemi, A. and Sousa, E.S., "Collaborative Spectrum Sensing for Opportunistic Access in Fading Environments," *First IEEE International Symposium on New Frontiers in Dynamic Spectrum Access Networks, 2005 (DySPAN 2005)*, IEEE, pp. 131–136, 2005.
- [2] Umar, R. and Sheikh, A.; , "Cognitive Radio Oriented Wireless Networks: Challenges and Solutions," *International Conference on Multimedia Computing and Systems (ICMCS)*, IEEE. , pp. 1- 6, 2012
- [3] Ma, J., Zhao, G. and Li, Y., "Soft Combination and Detection for Cooperative Spectrum Sensing in Cognitive Radio Networks," *Communications, IEEE Transactions on*, vol.7, no.11, pp. 4502- 4507, Nov 2008.
- [4] Zeng, Y., Koh, C.L. and Liang, Y.C., "Maximum Eigenvalue Detection: Theory and Application," *International Conference on Communications ICC '08. IEEE*, pp. 1-5, 2008.
- [5] Zeng, Y. and Liang, Y.;; "Maximum to Minimum Eigenvalue Detection for Cognitive Radio," *The 18<sup>th</sup> Annual IEEE International Symposium on Personal, Indoor and Mobile Radio Communications (PIMRC'07)* , pp. 1- 5, 2007
- [6] Quan, Z., Shellhammer, S. and Zhang, W.;; "Spectrum Sensing by Cognitive Radio at Very Low SNR," *Global Telecommunication Conference (GLOBECOM 2009)*, IEEE, pp. 1- 6, 2009
- [7] Cabric, D., Tkachenko, A. and Brodersen, R.;; "Experimental Study of Spectrum Sensing Based on Energy Detection and Network Cooperation," *Online* , pp. 1- 8
- [8] Chen, R., Park, J. and Bian, K.;; "Robust Distributed Spectrum Sensing in Cognitive Radio Networks," *The 27<sup>th</sup> Conference on Computer Communications (INFOCOM)*, IEEE , pp. 1- 9, 2008
- [9] Krishnamoorthy, A.N., Pasupathy, A.S. and Mani, M. , "Optimization of Threshold for Energy Based Spectrum sensing Using Differential Equation," *Wireless Engineering and Technology* , pp. 130- 135, 2011.
- [10] Xiang, M.;; "On Optimization of Distributed Detection Systems under Neyman-Pearson Criterion," *9<sup>th</sup> International Conference on Information Fusion, IEEE*, pp. 1- 6, 2006

- [11] Zhao, Q. and Sadler, B.M., "A Survey of Dynamic Spectrum Access," *IEEE Signal Processing Magazine*, pp. 79- 89, May 2007.
- [12] Cabric, D., Mishra, S.M. and Brodersen, R.W., "Implementation Issues in Spectrum Sensing for Cognitive Radios," *Berkeley Wireless Research Center*, University of California, Berkeley.
- [13] Umar, R. and Sheikh, A.U.H., "A Comparative Study of Spectrum Awareness Techniques for Cognitive Radio Oriented Networks," *Physical Communication, ELSEVIER*, vol.9, pp.148-170, December 2013.
- [14] Ma, J., Li, G. Y. and Hwang, B., "Signal Processing in Cognitive Radio," *Proceedings of the IEEE*, vol.97, no.5, pp. 805- 823, May 2009.
- [15] Zeng, Y., Liang, Y.C. and Hoang, T., "A Review on Spectrum Sensing for Cognitive Radio: Challenges and Solutions," *EURASIP Journal on Advances in Signal Processing*, pp. 1- 15, 2010.
- [16] Alamos,L.; , "Learning with Neyman –Pearson and Min-Max Criteria," *National Laboratory* , pp. 1- 14, 2002
- [17] Chen, B. and Willett, P.;, "On the Optimality of the Likelihood-Ratio Test for Local Sensor Decision Rules in the Presence of Nonideal Channels," *IEEE Transactions on Information Theory* , vol.51, no.2, pp. 693- 699, 2005
- [18] Quan, Z., Cui, S. and Sayed, A.H., "Optimal Linear Cooperation for Spectrum Sensing in Cognitive Radio Networks," *Signal Processing, IEEE Selected Topics in*, vol.2, no.1, pp. 28- 39, Feb 2008.
- [19] Digham, F.F., Alouini, M.S. and Simon, M.K., "On the Energy Detection of Unknown Signals Over Fading Channels," *Communications, IEEE Transactions on* , vol.55, no.1, pp. 21- 24, Jan 2007.
- [20] Rasheed, H. and Rajatheva, N., "Spectrum Sensing for Cognitive Vehicular over Composite Fading," *International Journal of Vehicular Technology*, pp. 1- 9, 2011.
- [21] Lee, E. A. and Messerschmitt, D.G., "Digital Communication" Springer.
- [22] Yucek, T and Arslan, H., "A Survey of Spectrum Sensing Algorithms for Cognitive Radio Applications," *IEEE Communications Surveys & Tutorials*, vol.11, no.1, pp. 116- 130, 1<sup>st</sup> Quarter 2009.

- [23] Erceg, V., "An Empirically based Path Loss Model for Wireless Channels in Suburban Environments," *IEEE Journal on Selected Areas in Communications*, vol.17, no.7, pp. 1205- 1211, Jul 2009.
- [24] Cabric, D., Tkachenko, A. and Brodersen, R. W., "Experimental Study of Spectrum Sensing Based on Energy Detection and Network Cooperation," *Berkely Wireless Research Center*.
- [25] Cheng, Q., Chen, B. and Varshney, P., "Detection Performance Limits for Distributed Sensor Networks in the Presence of Nonideal Channels," *IEEE Transactions on Wireless Communications* , vol.5, no11, pp. 1- 6, November 2006
- [26] Atapattu, S., Tellambura, C. and Jiang, H., "Performance of Energy Detector over Channels with both Multipath Fading and Shadowing," *IEEE Transactions on Wireless Communications* , vol.9, no.12, pp. 3662- 3670, December 2010
- [27] Al-Hussaini, E., Al-Bassiouni, A. and Mourad, H., "Composite Macroscopic and Microscopic Diversity of Sectorized Macrocellular and Microcellular Mobile Radio Systems Employing RAKE Receiver Over Nakagami Fading Plus Lognormal Shadowing Channel," *Wireless Personal Communications, Springer*, pp. 309- 328, 2002
- [28] Hearth, S. and Rajatheva, N., "Analysis of Equal Gain Combining in Energy Detection for Cognitive Radio over Nakagami Channels," *Global Telecommunication Conference (GLOBECOM 2008), IEEE*, pp. 1- 5, 2008
- [29] Atapattu, S., Tellambura, C. and Jiang, H., "Representation of Composite Fading and Shadowing Distributions by using Mixtures of Gamma Distributions," *Wireless Communications and Networking Conference (WCNC), IEEE*, pp. 1- 5, 2010
- [30] Shi, Q., "On The Performance of Energy Detection For spectrum Sensing in Cognitive Radio Over Nakagami-Lognormal Composite Channels," *IEEE China Summit & International Conference on Signal and Information Processing (ChinaSIP), IEEE* , pp. 566- 569, 2013
- [31] Kaligineedi, P. and Bhargava, K., "Distributed Detection of Primary Signals in Fading Channels for Cognitve Radio Networks," *IEEE GLOBECOM Global Telecommunications Conference, IEEE* , pp. 1-5, 2008

- [32] Derakhtion, M., Izedi, F and Sheikhi, A.;, "Cooperative Wideband Spectrum Sensing For Cognitive Radio Networks in Fading Channels ," *IET Signal Process* , vol.6, no.3, pp. 227- 238, 2012
- [33] Rasheed, H, Haroon, F. and Rayatheva, N.;, " Performance Analysis of Rice-Lognormal Channel Model for Spectrum Sensing," *International Conference on Electrical Engineering/Electronics Computer Telecommunications and Information Technology (ECTI-CON), IEEE* , pp. 420-424, May 2010.
- [34] Olabiyi, O. and Annamalabi, A.;, "Further Results On The Performance of Energy Detector Over Generalized Fading Channels," *IEEE 22<sup>nd</sup> International Symposium, Indoor and Mobile Radio Communications* , pp. 604- 608, 2011
- [35] Rasheed, H, Haroon, F. and Adachi, F.;, "On The Energy Detection Over spectrum Sensing in Cognitive Radio Over Generalized-K (KG) Fading," *14th International Multitopic Conference (INMIC), IEEE* , pp. 367- 371, 2011
- [36] Yao, Y. and Sheikh, A.;, "Cochannel Interference Modeling and performance Analysis of Microcell Systems for Wireless Personal Communications," *Can. J. Elect. and comp. Eng.* , vol.19, no.1, pp. 27- 35, 1994
- [37] Li, G., Cano, A. and Zhu, S., "High- Diversity Cooperative Spectrum Sensing in Cognitive Radio Networks," *Global Telecommunications Conference (GLOBECOM 2010), IEEE* , pp. 1- 5, 2010
- [38] Zheng, S., Lou, C. and Young, X.;, "Cooperative Spectrum Sensing Using Particle Swarm Optimization," *Electronics Letters* , vol.46, no.22, pp. 1- 2, 28<sup>th</sup> October 2010
- [39] Patel, A. and Trivedi, A.;, " Particle Swarm Optimization Based Multiuser Detector for Multicarrier CDMA Communications," *International Conference of Computational Intelligence and Communication Networks* , pp. 534- 538, 2010
- [40] Wimalajeewa, T and Jayameera, S.;, " Particle Swarm Optimization for Constrained Optimization: Optimal Power Sheduling for Correlated Data Fusion in Wireless Sensor Networks," *18<sup>th</sup> Annual IEEE International Symposium on Personal, Indoor and Mobile Radio Communications (PIMRC07)* , pp. 1- 5, 2007
- [41] Krusienski, D and Jenkirs, W.;, "Design And Performance of Adaptive Systems Based on Structured Stochastic Optimization Strategies," *IEEE Circuits and Systems Magazine*, pp. 8- 20, 2005

- [42] Onwnalu, J. and Durlofsky, L.; "Application of A Particle Swarm Optimization Algorithm for Determining Optimum Well Location and Type," *Computational Geosciences, Springer* , vol.14, iss.1, pp. 183-198, January 2010
- [43] Shi, Y. and Eberhart, R.;, "A Modified Particle Swarm Optimizer," *The 1998 IEEE International Conference on Evolutionary Computation Proceedings, IEEE World Congress on Computational Intelligence, IEEE* , pp. 69- 73, 1998
- [44] Kennedy, J. and Eberhart;, " Particle Swarm Optimization," *IEEE International Conference on Neural Networks Proceedings, IEEE* , vol.4, pp. 1942- 1948, 1995
- [45] Campona, E., Fasano, G. and Peri, D.;, " Particle Swarm Optimization: Efficient Globally Convergent Modifications," *European Conference on Computational Mechanics, Solids, Structures Coupled Problems in Engineering* , pp. 1- 18, June 2006
- [46] Shi, Y. and Russel, C.;, "Comparison Between Genetic Algorithms and Particle Swarm Optimization," *Evolutionary Programming VII, Lecture Notes in Computer Science, Springer vol. 1447*, pp. 611- 616, 1998.
- [47] Shi, Y. and Russel, C.;, "Empirical Study on Particle Swarm Optimization ," *Proceedings of the 1999 Congress on Evolutionary Computation (CEC 99), IEEE* , vol.3, pp. 1945- 1950, 1999
- [48] Angeline, J.;, "Evolutionary Optimization Versus Particle Swarm Optimization: Philosophy and Performance Differences," *Evolutionary Programming VII, Lecture Notes in Computer Science, Springer vol. 1447* , pp. 601- 610
- [49] Poli, R., Kennedy, J. and Blackwell, T.;, " Particle Swarm Optimization: An Overview," *Swarm Intelligence, Springer* , pp. 33- 57, August 2007
- [50] Blondin, J.;, "On Particle Swarm Optimization: A Tutorial ," pp. 1- 5, September 2009
- [51] Trelea, I.;, "The Particle Swarm Optimization Algorithm: Convergence Analysis and Parameter Selection," *Information Processing Letters 85, ELSEVIER* , pp. 317- 325, 2003
- [52] Yang, C. and Simon, D.;, "A New Particle Swarm Optimization Technique," *18th International Conference on Systems Engineering (ICSEng), IEEE* , pp. 1- 6, 2005
- [53] Abdelsalam, H. and Al-Shaar, A.;, "An Enhanced Binary Particle Swarm Optimization Algorithm for Channel Assignment in Cognitive Radio

Networks," *Proceedings of international Conference on Modeling Identification and Control (ICMIC)* , pp. 221- 226, 2013

- [54] Zhang, J., Zhou, Z. and Ye, Y.;; "Cognitive Radio Adaption Decision Engine Based on Binary Quantum-Behaved Particle Swarm Optimization," *6<sup>th</sup> International ICST Conference on Communications and Networking in China (CHINACOM)* , pp. 221- 225, 2011
- [55] Min, J., Qun, W. and Xuemai, G.;; "An Adaptive Particle Swarm Optimization Algorithm for Multiuser Cognitive Radio System," *Cross Strait Quad Regional Radio Science and Wireless Technology Conference* , pp. 1028- 1031, 2011
- [56] El-Khamy, S., Aboul-Dahab, M. and Attia, M.;; "A Hybrid of Particle Swarm Optimization and Genetic Algorithm for Multicarrier Cognitive Radio," *26<sup>th</sup> International Radio Science Conference (NRSC2008)* , pp. 1- 7, 2009
- [57] Niknam, T.;; "A New Fuzzy Adaptive Hybrid Particle Swarm Optimization Algorithm for Non-Linear, Non-Smooth and non Convex Economic Dispatch Problem," *Applied Energy, ELSEVIER*, vol.87, iss.1, pp. 327- 339, January 2010
- [58] Krusienski, D. and Jenkins, W.;; "A Modified Particle Swarm Optimization Algorithm for Adaptive Filtering," *International Symposium on Circuits and Systems (ISCAS 2006), IEEE* , pp. 137- 140, 2006
- [59] Eberhart, R. and Shi, Y.;; " Particle Swarm Optimization: Developments, Applications and Resources," *Proceedings of the 2001 Congress on Evolutionary Computation, IEEE*, vol.1 , pp. 81- 86, 2001
- [60] Chen, P.;; " Particle Swarm Optimization for Power Dispatch with Pumped Hydro," *Proceedings of the 2001 Congress on Evolutionary Computation, IEEE* , vol.1, pp. 131- 144, 2001
- [61] Zhan, Z., Zhang, J. and Li,Y.;; "Adaptive Particle Swarm Optimization," *IEEE Transactions on Systems, Man and Cybernetics- Part B : Cybernetics* , vol.39, no.06, pp. 1362- 1381, December 2009
- [62] Park, J., Jeong, Y. and Shin, J.;; "An Improved Particle Swarm Optimization for Non Convex Economic Dispatch Problems," *IEEE Transactions on Power Systems* , vol.25, no.01, pp. 156- 166, February 2010
- [63] Mohammed, F. and Deriche, M.;; "A Two Threshold Cooperative Spectrum Sensing Algorithm Using Swarm Intelligence," *13<sup>th</sup> International Symposium on Communications and Information Technologies, IEEE* , pp. 1- 5, 2013

- [64] Xu, H. and Zhou, H.; "Cognitive Radio Decision Engine Using Hybrid Binary Particle Swarm Optimization," *13th International Symposium on Communications and Information Technologies (ISCIT)* , *IEEE* , pp. 59- 62, 2013
- [65] Vo, T., Lee, B. and Kim, H.; "Optimizing Maximum Velocity of Fish Robot Using Hill Climbing Algorithm and Genetic Algorithm," *10<sup>th</sup> International Conference on Control, Automation, Robotics and Vision, IEEE* , pp. 1- 6, 2013
- [66] Karagiannidis, G., Sagiias, N and Tsiftsis, T.; , "Closed-Form Statistics For The Sum of Squared Nakagami-m Variates and Its Applications," *IEEE Transactions on Communications* , vol.54, no.8, pp. 1353- 1359, August 2002
- [67] Chen, Y. and Tellambura, C.;, "Distribution Functions of Selection Combiner Output in Equally Correlated Rayleigh, Rician and Nakagami-m Fading Channels," *IEEE Transactions on Communications* , vol.52, no.11, pp. 1948-1953, November 2004
- [68] Rashid, R., Baguda, Y. and Fisal, N.;, "Optimizing Achievable Throughput for Cognitive Radio Network Using Swarm Intelligence," *17<sup>th</sup> Asia Pacific Conference on Communications (APCC), IEEE* , pp. 354- 358, 2011
- [69] Quan, Z., Cui, S. and Sayed, A.;, "Optimal Multiband Joint Detection for Spectrum Sensing in Cognitive Radio Networks," *Transactions on Signal Processing, IEEE* , vol.57, iss.3, pp. 1- 12, March 2009
- [70] Russell, S.and Norvig, P.;, "Artificial Intelligence: A Modern Approach," *Prentice Hall*, 2<sup>nd</sup> edition, pp. 111–114, 2003

## **Vitae**

Name : Ali Abdullah Al-Saihati

Nationality : Saudi

Date of Birth : 3/10/1985

Email : alialsaihati@yahoo.com

Address : Saihat- King Abdul Aziz St.

Academic Background : BS in EE from KFUPM